HYDROGEL BASED INSOLES FOR DIABETIC FEET

Rathnayake Mudiyanselage Ruwan Chaminda Udayanandana

(178039F)

Degree of Master of Philosophy

Department of Electronic and Telecommunication Engineering

University of Moratuwa

Sri Lanka

March 2022

HYDROGEL BASED INSOLES FOR DIABETIC FEET

Rathnayake Mudiyanselage Ruwan Chaminda Udayanandana

(178039F)

Thesis submitted in partial fulfilment of the requirements for the degree of Master of Philosophy

Department of Electronic and Telecommunication Engineering

University of Moratuwa

Sri Lanka

March 2022

Declaration

I declare that this is my own research work and this report does not incorporate without acknowledgment any material previously published submitted for a Degree or Diploma in any other university or institute of higher learning and to the best of my knowledge and belief it does not contain any material previously published or written by another person except where the acknowledgment is made in the text.

Signature: UOM Verified Signature Date: 20/01/2022

The candidate, whose signature appears above, carried out research for the MPhil dissertation under my supervision

Name of the supervisor: Dr. Thilini Gunasekara

Signature of the supervisor: … UOM Verified Signature Date:08/02/2022

Name of the supervisor: Dr. Pujitha Silva

Signature of the supervisor: . UOM Verified Signature Date:08/02.2022

Contributions by others to the thesis

My supervisors Dr. Pujitha Silva and Dr. Thilini Gunasekara, have given the necessary advice, reviewed this thesis, and provided editorial suggestions.

Ms. Chathurani Dias has assisted with getting pressure insole readings.

Acknowledgment

I acknowledge with gratitude to my supervisors Dr. Pujitha Silva and Dr. Thilini Gunasekara who went beyond to make sure that this thesis was always on the right track. Their advice and valuable feedback helped me make this research a success.

I would also like to thank, National science foundation (NSF) for providing funding for this research under the grant number RPHS/2016/DTM 02, and Dr. Anjula de Silva provided great support in providing necessary funding and advice as principal investigator of NSF funding, the top-up funding provided under the SRC grant number SRC/TP/2017/04 for one year was immense support to the continuation of the research works. Further thanking goes to the Electronic and Telecommunication Engineering department and head of departments Prof. Rohan Munasinghe and Dr. Nuwan Dayananda for approving documentation works and providing working space with a computing facility.

I gratefully acknowledge the Chemical and Process Engineering Department heads Dr. (Mrs) S.H.P. Gunawardena and Prof. S. Walpalage for providing chemical synthesis facilities. The Technical officers Mrs.I.K.Athukorala, W.S.M de Silva and Lab attendants Mr.H.L.G.S Peiris and Mr.D.S. Dayananda provided immense support during the synthesis process. The Materials science and engineering departments provided chemical analysis testing facilities and I would like to thank the head of the department Mr V.S.C.Weragoda for giving fast approval for using the testing facility. Special thanks go to Dr. Pujitha Silva, Director, Center for Biomedical Innovation (CEBI), the University of Moratuwa for proving Tactilus pressure insole to test pressure distribution effectiveness.

I am grateful to Prof. Ruwan Gopura and Dr. Himan Punchihewa heads of the Mechanical Engineering department for the permission given to use mechanical testing facilities and help given by Ms.T.L.K. Kumari, Technical Officer, and W.L. Kumara, Lab attendant to operate the universal testing machine.

I sincerely thank my family for the support and continuous encouragement.

Abstract

This research considered an extensive study of double network poly (acrylic acid) and single network polyacrylamide hydrogel as an insole material for the diabetic foot by testing on compression strength, stress relaxation, compression fatigue, shear stress, and shock absorption properties. The previous studies on hydrogel fatigue were mainly focused on fatigue fracture in tension and crack propagation. This study focuses on the mechanical behaviour of hydrogels under diabetic foot-specific loading conditions. The expected testing conditions include minimum 20 000 fatigue cycles under maximum compression stress of 250 kPa at a 200 mm/ min strain rate.

The hydrogel synthesis and testing started with double network poly (acrylic acid) hydrogel. The developed double network poly (acrylic acid) hydrogel displayed fatigue properties up to 3000 loading cycles at maximum stress of 390±30 kPa. Further, maximum average shear stress and shear modulus of 80 kPa and 140 kPa respectively were observed at 84% strain before fracture.

Developed Single network polyacrylamide hydrogel displayed good fatigue properties up to 13,000 loading cycles at maximum stress of 520±50 kPa and 200 mm/min crosshead speed. When the maximum stress condition was reduced to 350±50 kPa, the maximum number of loading-unloading cycles was increased up to 20 000 indicating a single network polyacrylamide hydrogel capable of withstanding more than 20 000 cycles at 250 kPa.

Hydrogels showed superior recoverable and viscoelastic properties when compared with available insole materials. The developed finite element model was validated with pressure insole test data and used to investigate the pressure distribution properties and to optimize the thickness suitable for insole applications

The additional properties of a hydrogel such as high thermal capacity and structural similarity to soft tissues are seen as added advantages when compared to other insole materials to prevent re-ulceration.

Keywords

Hydrogel synthesis, Material characterization, Pressure insole, Finite Element Analysis,

Table of Contents

List of Figures

List of Tables

List of Abbreviations

Abbreviation	Description
AA	Acrylic Acid
AAm	Acrylamide
ATL	Achilles tendon lengthening
BM	Body mass
BMI	Body mass index
CL	Crosslink
DFU	Diabetic foot ulcer
DN	Double network
EVA	Ethylene vinyl acetate
FEA	Finite element analysis
I	Initiator
KPS	Potassium persulfate
M	Mole weight in g/ mol
MBA	N,N'-Methylenebisacrylamide
PAA	Polyacrylic acid
PAAm	Polyacrylamide
PNIPAAm	Poly (N-isopropyl acrylamide)
PU Gel	Polyurethane gel
SN	Single network
SW	Swelling percentage
TCC	Total contact cast

Chapter 1

INTRODUCTION

Foot ulcers are a major problem worldwide caused by the complication of diabetes mellitus. High morbidity, costs, and mortality are associated with foot ulceration [1] [2] [3]. Globally, an estimated 463 million adults were living with diabetes in 2019 and the diabetic population is expected to rise to 700 million by 2045 [4] [5]. The recurrence rates of healed ulcers are between 30% and 40% in the first year [6] [7]. Prevention and proper treatment of these ulcers are therefore of high priority.

When a healthy person feels a high-pressure point or pain on the foot planter, naturally the weight on the foot is shifted to a different position to reduce the pressure on the painful area. Diabetic patients with peripheral neuropathy cannot feel the soreness due to atrophied nerve endings. This can give rise to pressure points and eventually wounds that heal badly [8] [9]. If these high pressures under the foot are not adequately reduced, or "offloaded," ulcers may occur or present ulcers may not heal [10].

Abnormal plantar pressure distributions are mainly caused by rheumatoid foot pain and diabetic ulceration [11] [12]. These painful foot-related diseases can be successfully relieved or resolved by distributing elevated pressures with the use of a proper foot insole [12] [13]. The type of insole best suited to achieve this is still an area of development [14].

Four main techniques are used in clinical practice for the reduction of mechanical pressure, ulcer prevention, and ulcer healing [15]. They include, "casting, footwear (shoes, insoles, socks, insole plugs, metatarsal bar), Surgical offloading (Achilles tendon lengthening (ATL), silicone injections, metatarsal head resection, an external fixation) and other offloading techniques (bed rest, crutches/canes/wheelchairs, bracing, non-removable walkers, offloading dressings, felted foam/padding, callus debridement, walking exercise, and gait modification)" [15, p. 100].

There are different types of orthotic insoles designed for diabetic foot ulcer patients. The orthosis should have the capability to distribute force in a larger area to reduce peak pressure most effectively on the plantar foot. The orthosis is expected to confirm with the arch of the foot and is rigid enough to support the foot under body weight [16].

The effectiveness of different materials used for these insoles has been researched [17] [18]. EVA (ethylene-vinyl acetate) foam, Plastazote (Polyethylene) foam, soft PVC, flexible polyurethane foam, polyurethane gel, and medical-grade silicone gel are the most commonly used insole materials [15]. The choice of material is based on personal experience, cost, and availability. According to Campbell, Newell, and McLure [19], "The ideal insole material would progressively deform throughout the full range of load to accommodate the shape of the bony prominence and transfer a portion of the load to other less prominent regions of the foot" [19, p.51].

The shear or friction forces play a critical role when prescribing foot orthosis for a diabetic patient with ulcer formation risk [16]. According to the study of Curryer and Lemaire [17], the gel materials perform better than the foam materials at reducing shear forces. The material behaviour similar to soft tissue works as a better-replacing material for diabetic patients with thin fat pads [20].

Applications of hydrogels vary from contact lenses, hygiene products, agricultural applications, and wound dressings to many other simple and sophisticated products. The load-bearing capacity is not a major concern in many of these products. Nevertheless, tough hydrogels developed in recent years have not been investigated thoroughly for mechanical strength limitations and fatigue properties.

Hydrogels were considered the first biomaterial used in the human body due to their structural similarity with soft tissue. They have a polymeric three-dimensional structure filled with water [21] [22]. Hydrogels closely simulate natural living tissue, more than any other class of synthetic biomaterials due to their high water content (50–90%), porosity, soft consistency, shock absorption, stimuli-responsiveness, and low

sliding friction [23] [24]. Besides, from the diabetic foot ulcer management aspect, hydrogel hydrates the wound by promoting autolytic debridement.

Recent studies found that a moist environment and the ability to interact with the wound helped improve healing and reduced the risk of infection and pain [25] [26] [27]. The ability to absorb contaminated exudate results in the isolation of bacteria within hydrogel and high water content allows transmission of oxygen to the wound [28]. Hydrogels have a marked cooling and soothing effect on the skin, which is valuable in painful wounds [29]. The physical consistencies of the hydrogel are much similar to the human fat pad as that capable of acting as a layer of artificial fat pad to protect bony prominences [30].

The Finite element method (FEM) can be used for predicting the stress distributions in the foot–insole interface if the complex geometry and material conditions of the foot and insole are properly modelled. The FEM can be used for comparing the effects of pressure distributions for different insole conditions by varying the material property, foot geometry, and loading condition. The finite element method has been employed previously in many foot-related biomechanics studies [9] [31] [32]. The peculiar behaviour known as poroviscoelasticy has to be considered when modelling hydrogel. This can be considered as a combination of the viscoelastic behaviour of the polymeric network and the poroelastic behaviour caused by the water movement within the hydrogel [33].

In this work, polyacrylic acid (PAA) and polyacrylamide (PAAm) based hydrogels were developed with a better pressure-relieving ability for diabetic insoles. The composition variations (monomer concentration, crosslinker percentage, initiator percentage, swelling percentage) The processing paramerters (sterring speed, the mixing temperature and oven temperature during synthesis) and the testing parameters (compression ratio, strain rate in compression, and the number of cycles compressed) were identified as hydrogels' property changing parameters.

In this thesis, the main concerns will be to synthesize and mechanical characterization of PAA and PAAm hydrogels under loading conditions of the foot

and to optimize the mechanical properties under the constraints of low cost and simple processing so that it can be used in the diabetic insole applications which were not tested and thoroughly studied by any of the researchers based on literature review. Finally, the mechanical and pressure distribution properties were compared with available insole materials for effectiveness by using finite element analysis and pressure insole readings.

1.1 Motivation

Orthotic insoles are commonly used in the treatment of diabetic feet to prevent ulcerations. Choosing suitable insole material is important for effective foot orthotic treatment. The softer gel materials allow the foot to sink further into the material, thus increasing the force-bearing area of the foot [34]. Hydrogel has a specific relaxation property that cannot be found in either pure solid or pure liquid due to its liquid-filled porous structure. The key research question is what mechanical properties would decide the suitability and limitations of the hydrogel as a diabetic insole material.

The poor mechanical property was one of the main reasons for underutilizing the hydrogel for important applications. The conventional hydrogel has low fracture toughness, brittleness, and has low extension under the applied force. The research gap includes the lack of experimental test results on hydrogels under different loading conditions of the foot such as compression fatigue, shear, stress relaxation, and shock absorption properties. The inherent moisture surface and drying of hydrogel with time are some of the drawbacks that need to be addressed when using hydrogel as an insole material for diabetic patients.

1.2 Aim

- Systematic design of hydrogel-based insole material for diabetic foot based on experimental studies and finite element analysis models.

1.3 Objectives

Objective 1: To optimize hydrogel composition for the desired mechanical properties of the diabetic insole by synthesizing hydrogel with different chemical compositions.

Objective 2: Material characterization of hydrogel for strength, physical and chemical stability, and repeatable use.

- Systematically evaluating their mechanical properties.
- Optimized samples are tested for stress relaxation, creep, shear, and fatigue.
- Testing samples under different swelling percentages, temperature values, thicknesses, and strain rates.

Objective 3: Finite element analysis and pressure insole testing to ensure that desired pressure relief is possible.

- Development of finite element model of the hydrogel.
- Observe pressure distribution under constant load.

1.4 Thesis overview

To address the above aims and objectives, this thesis is divided into the following main chapters.

Chapter 2 Literature review

In this chapter, the mechanism of soft tissue damage in the diabetic foot, pressure and stresses acting on foot plantar, methods available to relieve foot pressure, the effectiveness of diabetic insoles, mechanical testing of insole materials, different types of hydrogels and their properties, and finite element model development of hydrogel were reviewed. The critical analysis of the literature elaborates ulcers recurred in patients, even if they wore therapeutic footwear. The main factors affecting the ulcer

recurrence were identified and the alternative material with special properties suitable for the diabetic foot was identified as hydrogels.

Chapter 3 Materials and Methods

This research was conducted under three approaches. The first approach was to test the commercially available insole materials and to gain a comprehensive insight into their properties. The second approach was to develop fundamental hydrogel products. Thus, poly (acrylic acid) (PAA) based double network (DN) hydrogel and single network (SN) polyacrylamide (PAAm) were synthesized, optimized and the mechanical properties were tested for compression, stress relaxation, hardness, and rebound resilience. In addition to that, hydrogel samples were subjected to shear and compression fatigue tests. As the last approach, developed and optimized hydrogel was tested under different thickness, friction conditions, and adding polyethylene glycol (PEG) as a plasticizer to improve softness suitable for the diabetic foot.

Chapter 4 Results and Discussion

The test results and discussion of available insole materials, PAA hydrogels, and PAAm hydrogels were covered under this section. The limitations of SN PAA and DN PAAm hydrogels under the loading conditions of diabetic foot was assessed and compared with available insole materials. In addition to mechanical tests, finite element analysis and pressure insole results were used to decide on the pressure distribution ability of hydrogels.

Chapter 5 Conclusion

This chapter concludes the thesis with a summary of major findings from this thesis and suggestions for future work.

Chapter 2

LITERATURE REVIEW

2.1 Tissue damage due to repetitive load

The plantar soft tissue is located beneath the bones of the foot. The main function of this is to distribute vertical and shear loads during walking. The heel pad consists of organized fibrous compartments retaining body fat. The deep macro-chamber and superficial micro-chamber are two layers in the fat pad. In people with diabetes, increased macro-chambers stiffness causes the easy stress transfer from the calcaneus to the skin but decreased micro-chambers stiffness may cause diminished cushioning capacities in diabetic heels [35]. As a result, the process of ulceration in diabetic feet may start in deeper plantar soft tissue [36].

The different properties of the plantar soft tissue of diabetic and non-diabetic were studied to understand the possible mechanism of ulcer formation. Soft tissue properties indicate the presence of diabetes [37]. The change in properties like thinner soft tissue can be due to diabetes or aging so that when considering mechanical properties, the age, the tissue state is in whether living or cadaveric, diabetic status must be considered [38]. The epidermal layer of plantar skin shows thickening in people with pure diabetes [39] but thinning in diabetes complicated by foot ulceration or sensory peripheral neuropathy. A 15% reduction in average epidermal thickness of plantar skin was visible in people with diabetic foot ulceration [40]. Based on mechanical compression properties, diabetic tissue showed significantly higher modulus (1146.7 kPa) compared to non-diabetic tissue (593.0 kPa) but the change in energy loss was not significant in diabetic and non-diabetic tissues (68.5 vs. 67.9%) [41]. In contrast, some researchers stated an increase in energy loss in diabetic soft tissue [35], an increase in peak shear stress by 52–62%, increase in final shear modulus by 47% in diabetic tissue [42].

2.2 Foot pressure

According to Fernández-Seguín et al [43], "The pes cavus foot showed a significant reduction in their weight-bearing area (neutral feet: 165.04 ± 20.68 cm^2; pes cavus: 118.26± 30.31 cm^2); $p<0.001$ and significantly increased pressures under all zones of the forefoot except the fifth metatarsal (metatarsal pressure: in neutral feet 503.8 ±9.32 kPa; in pes cavus 656.12± 22.39 kPa; $p<0.001$)" [43, p.789].

An upper limit or threshold plantar pressure value (207 kPa) was established by Owing et al [44] for the prevention of ulcer recurrence. This study was conducted on a group of 49 patients with diabetes and neuropathy. In the same study, the mean barefoot plantar peak pressure measured with the EmedÒ platform was 566 kPa.

The test results for barefoot walking showed the peak pressure for patients with a history of diabetic foot ulcer and diabetic neuropathy patients as 738.6 ±322.3 kPa and 568.0 ±123.8 kPa, respectively with p= 0.2075. The peak shear stress values for the same patient groups were 135.3 6 ± 60.6 kPa, 86.4 ± 30.3 kPa, respectively with p=0.0465 [45].

The shear and pressure data collected on healthy individuals by Stucke et al [46] showed the peak pressures measured to be 362 ± 106 kPa in the heel and 527 ± 123 kPa in the forefoot. Similarly, the average peak shear values were higher in the forefoot than heel but the peak pressure locations and peak shear locations were not similar. The highest shear stress of 37 .7±7.6 kPa occurred in the forefoot directed anteriorly and the heel peak shear stress of 21.2 5 kPa occurred in the posterior direction.

2.3 Methods available to relieve foot pressure

The methods used to offload the foot include bed rest, wheelchair, crutch-assisted gait, total contact casts (TCC), felted foam, half shoes, surgical offloading, therapeutic shoes, and removable cast walkers [47]. TCC is considered the "gold standard" in achieving pressure redistribution because of the close fit of the cast material to the plantar surface of the foot. This increases the plantar weight-bearing surface area to help distribute the plantar pressure. TCC is quite effective in treating the majority of

noninfected, nonischemic plantar diabetic foot wounds, with healing rates ranging from 72% to 100% over 5 to 7 weeks. But Wu et al [47] argue that "TCC application is time-consuming and often associated with a learning curve. Most centres do not have a physician or cast technician available with adequate training or experience to apply a TCC safely. Impaired activities of daily living, such as difficulty sleeping comfortably, and bathing difficulties while trying to avoid getting the cast wet are some other difficulties faced by patients" [47, p.426].

Certain designs of TCCs may also cause postural instability [48] and alter gait parameters [49]. Patients are often resistant to cast applications or removable cast walkers (RCWs) due to the extra costs associated. Clinicians, therefore, have to use alternative methods such as insoles that are less costly and effective.

2.4 The effectiveness of Insoles for diabetic foot

Many specially designed therapeutic footwear or orthoses are currently used to reduce the high plantar pressure in diabetic patients [9]. According to the study of Bus et al. [50], custom-made insoles were more effective in reducing peak pressure compared to flat insoles, but with considerable variability between individuals. During balanced standing, the heel region experiences the highest plantar pressure [31]. This can redistribute to the mid-foot region with the use of a custom-made insole [9].

In general, custom moulded, thicker, and softer orthoses have been shown to reduce the peak plantar pressure and redistribute it in a more uniform pattern but Cheung and Zhang [31] argues that the insole's custom-moulded shape is more important in reducing peak plantar pressure than the stiffness of the material from which it is made. The custom-moulded insole has 40% less maximum pressure compared to the flat insole with similar thickness and material [51]. But Mills et al [52] argue that soft-flat insoles are more comfortable than all contoured insoles. Increasing thickness beyond around 0.75 cm is ineffective and a range between 0.5 and 0.75 cm is more suitable [51]

The diabetic patient-specific orthotic developed with metatarsal bar based on plantar pressure data showed a 58% reduction in peak pressure compared to the flat insole (50 Shore A EVA). The insole with a metatarsal bar reduces pressures up to 29 kPa under the metatarsal heads. The average pressures were reduced to 219 kPa at the 1st metatarsal region and 208 kPa at the 2nd to 4th metatarsal areas. The flat insole showed an average and maximum peak stress of 240 kPa and 325 kPa respectively [53].

The type of orthosis and the material are some of the factors that should be considered when prescribing the insoles to prevent complications due to pressure redistribution. For example, the semi-rigid material customized insole is prescribed for diabetic patients with neuropathic ulcers, whereas a softer insole is required for elderly patients with thin fat pads [31].

For a diabetic foot, the expected minimum reduction in peak pressure is 30% during walking or the peak pressure should be less than 200 kPa when measured with a calibrated pressure measuring system with a sensor size of 2 cm^2 [54]

The shear force acting on the foot plantar is an important factor in preventing foot ulcer formation in diabetic patients. Pollard et al [55] found that Plastazote® reduced the peak longitudinal shear force by 30-50%. The effectiveness of five different materials (three foam materials and two gel materials) in reducing plantar shear force was tested by Curryer and Lemaire [17]. The gel materials showed better shear force reduction compared to foam materials. The braking and propulsive impulses were the main two parameters considered in this test. The percent reduction in shear forces in each material is listed in Table 2.1. The gel materials (Soft Shear and Conformagel®) can perform better in shear than foam materials (Plastazote, Spenco, and PPT) because the top layer of gel can glide relative to the bottom layer. This behaviour can be defined as a ball-bearing effect [17] [56].

Table 2.1: Comparison of the percent reduction in shear force in foam and gel insole materials.

Material	Description	Shear force reduction (%)	
		Braking	Propulsion
Plastazote®	Expanded closed-cell polyethylene foam	6.0	7.0
Spenco®	Neoprene rubber foam with nylon cover	10.0	6.0
PPT®	Open-cell urethane foam	11.5	6.5
Soft Shear®	Medical grade silicone gel (fabric cover both sides)	21.0	13.0
Conformagel®	Hydrogel wound dressing	28.0	16.0

Source: adapted from [17]

2.5 Insole materials

Polyethylene (PE) foam, silicone rubber, and ethyl vinyl acetate (EVA) are the most common insole materials due to their availability with different thicknesses, hardness, and densities. Latex foam, Dynafoam®, Plastazote®(closed-cell polyethylene foam), Orthofelt®, PPT®, Spenco®, and Molo®, insole materials were tested by Leber and Evanski [57]. The plantar pressure was measured by using Harris and Beath footprinting techniques. They observed an average pressure of 398.15 kPa in patients with forefoot plantar area pain. Plastazote, Spenco, and PPT showed the highest reduction in plantar pressure of 53%, 53%, and 51% respectively. Tong and Ng [58] tested four types of 6.4 mm thick materials for plantar pressure (slow recovery Poron, Poron, Poron + soft Plastazote, and Poron + firm Plastazote). Poron + firm Plastazote showed as the most effective material by reducing mean peak pressure by 27%. Plastazote insoles can achieve approximately 32-48% pressure reduction after contoured to the shape of the foot due to an increase in the surface area [59]. The custom insoles were made from 1.27 cm Plastazote with a Shore A value of 35 [60].

Seven types of EVA and polyethylene foam materials with Shore A hardness ranging from 15 to 58 tested by Lo et al [61] found the highest compressive stress of 1139 kPa was withstood by the highest hardness material and the lowest hardness EVA sample had the minimum compression stress (98 kPa). The coefficient of friction

without sock varies from 0.32 to 0.54 and the shear angle from 3.76º to 15.26º and the coefficient of friction varies from 0.22 to 0.39 and the shear angle varies from 3.7º to 12.43º with the sock.

Very recently, researchers have experimented on using hydrogel insoles for diabetic patients with foot-related issues. Patwa et al [62] investigated the polyvinyl alcohol/carboxymethyl cellulose (PVA/CMC) based magnetic hydrogels prepared by physical crosslinking as an alternative for diabetic shoe inserts. The master of applied science thesis of Kermen [63] experimented on PVA hydrogel which is reinforced by bacterial cellulose (BC) natural nanofibers (PVA-BC). The most important test, compression fatigue, had not been conducted in all of these researches.

2.6 Properties of diabetic insole materials and testing

Durability under cyclic loading, resilience, compressive stiffness, insole-skin friction, shear modulus, pressure distribution, water vapour permeability, perspiration resistance, and thermal comfort properties are generally taken as the key requirements for the evaluation and selection of suitable materials for orthotic insoles [61]. The comfort perception of the insole is affected by the design, contour, and hardness of the insole material. The comfort is inversely related to the hardness of the material [52]. A performance index was developed by Lo et al [61] by combining the above-mentioned properties for accommodation, cushioning, and control.

2.6.1 Resilience

Resilience is the ratio between the energy released after impact to the impact energy applied. This is measured through the ratio between the heights of the pendulum returned after impact to the height of the pendulum released. The test standards for rubber are DIN 53512 or ISO 4662 and the test piece size is 50 mm × 50 mm × 12.5 mm length, width, and thickness respectively. [64] The test arrangement used by Lo et al [61] measured the impact force reduction by implementing loadcell under the test material after dropping the ball bearing at a height of 400 mm. The EVA polymers with a density of 290 kg/ m^3, a hardness of 65 Shore A, and a thickness of 12 mm had

a resilience of 41% [65]. The lowest resilience of 8% to 20% was shown by Polyurethane with hardness varying from 15 to 35 Asker C when compared with EVA, Polyethylene, and Latex foam materials [64].

2.6.2 Fatigue resistance

The compression fatigue resistance test simulates the cyclic compression forces exerted during walking. Peaks of the vertical forces occur when the heel strikes the ground and during the propulsion phase. Tong et al [66] considered the walking frequency was approximately 1 step per second and vertical peak pressures vary between 200 kPa to 500 kPa in the cyclic compression test conducted on three different types of diabetic insoles. The compression fatigue test conducted by Fauli et al [64], for diabetic insole material selection, used 100,000 compression cycles, with maximum stress of 700 kPa and a frequency of 1Hz. The thickness of the sample was measured 30 min after the end of the fatigue test.

2.6.3 Shear

Seven types of insole materials were tested for insole-skin friction, and shear properties by Lo et al. [61]. Materials with high frictional force on the foot plantar resulted in a high shearing load [18]. The dynamic coefficients of friction and the shear angles of the insole-sock interface are lower than those of the insole-skin interface. Hence, diabetic patients are recommended to wear socks because the dynamic friction coefficient and the shear angle between the insole and sock are lower than those of the insole and foot plantar. [61]

The thermal changes in the foot of diabetes and peripheral neuropathy patient have an association with shear stress applied on plantar during walking [67]. Keeping a lower temperature on the plantar surface can reduce reulceration [68]. Wrobel et al [69] developed an insole to reduce shear stress on the foot. This dynamic foot orthoses (DFO) has a free-floating distal segment to reduce sliding friction at the metatarsal heads. Frictional resistance was reduced first at foot plantar skin by using neoprene rubber top cover with 4-way stretch darlex® (Richardson Products Incorporated,

Frankfort, IL, USA) multi-directional stretch fabric on both sides and second deep tissue shear reduction by using a silicone layer that slides on EVA base material lined with ballistic nylon. This insole is capable of reducing the temperature at forefoot and midfoot increase by 64.1% and 48% respectively compared to standard insoles.

2.6.4 Optimum stiffness of insole material

The effectiveness of insoles is strongly dependent on the stiffness of the material used. At low load, the optimum distribution of loads achieves at low stiffness. At a higher load, a material achieves optimum cushioning with higher stiffness. As a result, people with higher BM or BMI have to use stiffer insole materials to minimize plantar pressure. This behaviour is shown in Table 2.2. The increase in load indicates an increase in stiffness to achieve the minimum peak pressure (Table 2.3). An 80 kg person developed minimum dynamic peak pressure of 383 kPa with a material having Shore A hardness 10±1. Pressure on foot plantar can be reduced on standing and walking by at least 16 and 19% respectively by optimizing the stiffness of cushioning materials. The optimum stiffness is not affected by the cushioning material's thickness [34].

Table 2.2: The relationship of tested insole materials between hardness and stiffness

Material type	Shore A Hardness	Minimum peak stress at 50% compression strain (kPa)	
		Static	Dynamic
1	2±1	25±1	36±2
2	3 ±2	36±2	51±2
3	10±1	99±2	155±4
4	14±1	149±4	227±4
5	18±2	185±3	276±3

Source: adapted from [34]

Table 2.3: Variation of peak pressure for gradually increasing the external load on heel model and polyurethane foam material under static loading.

Net force range on single heel area (N)	Minimum peak pressure range (kPa)	Material type with minimum peak pressure
0-110	0-40	1
110-290	40-140	2
290-365	140-175	3
365-530	175-250	4
530-550	250-270	5

Source: adapted from [34]

2.7 The temperature inside the shoe

The lowest and highest temperatures inside a shoe were 15.9˚C in winter and 37.5˚C in summer respectively [70]. A higher foot temperature (32-35ºC) could be observed in patients with diabetic neuropathy compared to patients without neuropathy (27-30ºC) [71] [72]. This temperature rise is due to enzymatic autolysis and inflammation of tissues as a result of repetitive stress on the foot.

Foot temperature changes cannot be found in different locations of the foot and change in vertical pressure has no effect on temperature change but temperature increase can be observed during walking [73]. After 5 min walking, the temperature increases by an average of 9.1ºC under the hallux [74].

2.8 Hydrogel

Highly tough hydrogels have been developed with different approaches. Double network (DN) hydrogels, sliding-ring hydrogels, nanocomposite hydrogels, macromolecular microsphere composite hydrogels, physical interaction enhanced hydrogels, and tetra-PEG hydrogels are some of them. Among them, DN hydrogels have been demonstrated to achieve extremely high mechanical strength (fracture

compressive stress of 17.2 MPa and strain of 92%, fracture tensile stress of 1–10 MPa, and strain of 1000–2000%) [23]

The first DN hydrogel was developed by Gong et al [75] in 2003. This consists of a two-step sequential free-radical polymerization method. The first network consisted of poly(2-acrylamido-2-methyl propane sulfonic acid) (PAMPS) and the second network was polyacrylamide (PAAm). Since then, different DN gels, including microgel-reinforced DN gel [76], inverse DN gel, void-DN gel, jellyfish DN gel, polysaccharide-based hybrid DN gels, and lamellar bilayers DN gels have been developed by different methods. All of these DN hydrogels have shown stiffness (elastic modulus) of 0.1–1.0 MPa [77].

"The networks of DN gels can be cross-linked by physical noncovalent or chemical covalent bonds, chemically cross-linked polymer networks are generally stronger than physically cross-linked ones, but chemically linked network makes the gels very difficult to be repaired or recovered from damages and fatigues, due to irreversible, permanent bond breaking. According to the research of Gong et al. [75], the following results can be highlighted. The mechanical strength of the DN gel is affected by the first and second network cross-linking density; A dramatic increase in mechanical strength occurs when the first network is highly cross-linked and the second one is loosely cross-linked; If the first network cross-linking density keeps at 4 mol% and changes that of the second network from 0 to 0.1, 0.5, 1.0, and 2.0 mol %, all the DN gels showed similar elastic modulus, regardless of the cross-linking density of the second network; When the second network has a crosslinking density of 0-0.1 mol%, the highest fracture strength and strain are obtained.

Table 2.4 shows some examples of a highly cross-linked first network and loosely crosslinked second network DN gels [75]. The DN gel consisting of poly (acrylic acid) (PAA) as the first network and PAAm as the second network has fracture stress 21 times higher than that of the PAA single network gel." [73, pp. 1156-1157]

Table 2.4**:** Compression properties of hydrogels at room temperature

First network	Second network	Water content (wt-%)	Fracture Stress (MPa)	Fracture Strain (%)	$\sigma_{max}^{DN}/\sigma_{max}^{SN}$
PAA-1-4[a]	-	99	0.1	65	-
	PAA-1-0.1	95	0.7	77	7
	PAAm-1-0.1	89	2.1	95	21
PAAm-1-1	-	93	0.7	98	-
	PAAm-1-0.1	92	5.4	92	7.7

[a] P-x-y: P, x, and y represent the abbreviated polymer name, molar monomer ratio, and the crosslinker ratio in mol-% from the monomer, respectively. Source: adapted from [75].

"There was a limited study on fatigue and shear properties of hydrogels. Recently more attention has been given to the study on the fatigue fracture of hydrogel under cyclic tensile load [78] [79] [80]. Most of these reported hydrogels are polyacrylamide-based. Compression fatigue testing has been conducted for the application of nucleus pulposus replacement [81] [82]. The maximum strain in these compression tests has been reported in the range of 15% -25%.

Shear strength is another important parameter to be considered in biomedical applications. Direct shear testing [83] and mechanical lap testing [84] are the two main methods used for the shear testing of hydrogels.

Even though few researchers have tested hydrogel for rebound resilience [85] no studies were found for double network DN PAA hydrogels for rebound resilience and had done a comparison with other insole materials with similar hardness" [86, p. 1101].

2.8.1 Poly (Acrylic Acid) (PAA) Hydrogels.

PAA hydrogel has high absorptivity and biocompatible properties. Due to this special structure, PAA was used in applications such as wound dressings, filtration, hygiene products, medical waste solidification, and cosmetics [87] [88] [89]. The studied properties of PAA hydrogel were, swelling [90] [91], diffusion [92], Physico-chemical [93], and mechanical properties [94]. The main concern in this type of

hydrogel is its poor mechanical properties and the large volume change during swelling [95] [96].

The compression properties of different types of hydrogels tested by Gong et al [75] showed that SN PAA with 1M PAA and 4 mol% MBA showed fracture stress of 0.1MPa at fracture strain of 65%and swelling water content of 99%. When the second network of 1M AA and 0.1 mol% MBA was added, this DN PAA increased fracture stress up to 0.7 MPa at a fracture strain of 77% and swelling water content of 95%.

PAA hydrogels with superior mechanical properties were prepared based on a single network (SN) structure with dual cross-linking. The network consists of covalently cross-linked PAA chains enabled by MBA and ionic cross-links enabled by Fe^{3+} irons from $Fe(NO_3)_3 \cdot 9H_2O$ [87]. The high material cost of $Fe(NO_3)_3 \cdot 9H_2O$ and longer stirring time (12 h) were the main drawbacks of this method. The fracture stress decreases gradually with the increase of the water content of the hydrogel.

The polymerization of acrylic acid monomer could be started with free radicals created by an initiator such as KPS (Figure 2.1). Next, the PAA monomers are propagated in the presence of SO_4^- (Figure 2.2). PAA hydrogels are obtained by polymerization of the acrylic acid monomer and a crosslinker as shown in Figure 2.3.

$$K_2S_2O_8 \longrightarrow 2K^+ + S_2O_8^{2-}$$

$$S_2O_8^{2-} \longrightarrow 2SO_4^-$$

Figure 2.1**:** Free radicals created by dissolving KPS in water

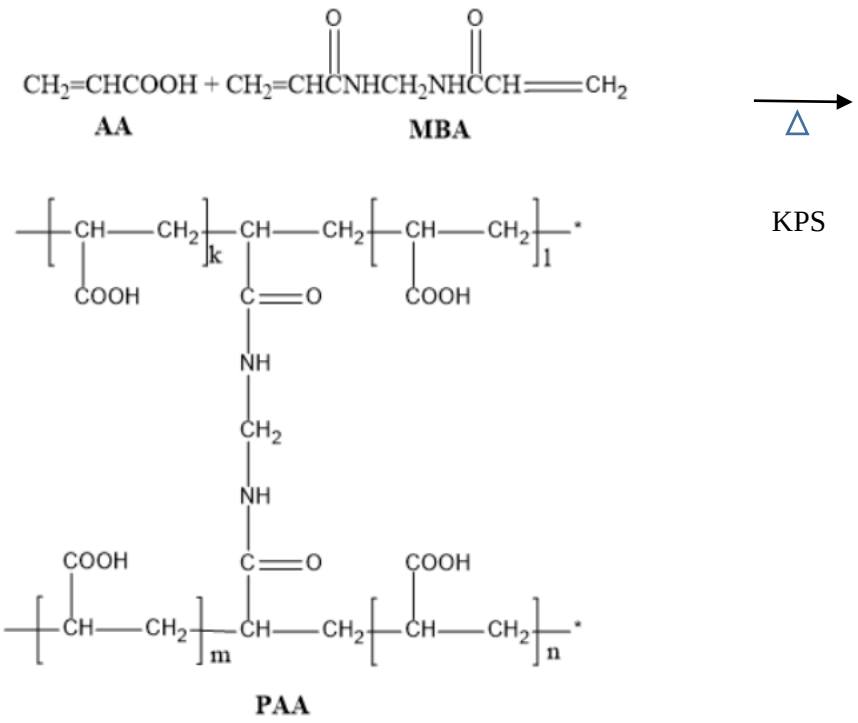

Figure 2.2: Free radical polymerization of acrylic acid and cross-linking with MBA

2.8.2 Polyacrylamide hydrogel

One of the most commonly used hydrogels is polyacrylamide (PAAm) due to its easy synthesis and availability. Polyacrylamide was first synthesized by C. Moureu in 1893 but its commercial usage was started in 1954 [97].AAm is biodegradable and soluble in water, ethanol, and acetone [98].

PAAm is a hydrophilic polymer for the preparation of hydrogels [99]. The basic chemical formula of AAm is CH_2=CH-$CONH_2$. The common method for the synthesis of PAAm hydrogels is covalently crosslinked free radical polymerization. The aqueous solution of acrylamide was initiated by either ammonium persulfate or potassium persulfate and free radical polymerization of AAm was initiated in the presence of SO_4^- (Figure 2.4). The presence of MBA results in the formation of PAAm crosslinked

hydrogels. The crosslinker is capable of connecting to the growing polymer chain of AAm due to the identical reactive ends of Bis and AAm (Figure 2.5)

"PAAm is a key component in several recently developed tough hydrogels. Ronken et al [100] showed PAMPS/ PAAm compositions with lower water content result in stiffness parameters closer to cartilage and Wang et al [101] synthesized extremely stretchable and tough hydrogels by mixing two types of crosslinked polymers: ironically crosslinked alginate and covalently cross-linked polyacrylamide" **[**100, p.533]**.**

Orakdogen and Okay [102] prepared PAAm hydrogels from AAm monomer and MBA crosslinker. They used three monomer concentrations of 3, 5, and 7 w/v %. This is approximately equal to 0.4 M, 0.7M, and 1M solution of AAm. The MBA concentration was varied between 0.2 mol% and 1.8 mol% for each concentration of AAm. The increase in elastic modulus was visible with the increase in MBA concentration in all three monomer concentrations. The highest elastic modulus was shown by the gel with a 1M AAm concentration. The minimum requirements of MBA for the onset of gelation were 0.03, 0.19, and 0.55 mol% for AAm concentrations of 7, 5, and 3 w/v% respectively. So that the higher concentration of AAm solution has a lower threshold concentration of MBA. The fraction of effective cross-link form is less than 20% and it further decreases below 1% with the decrease in monomer concentration. This is due to cyclization and multiple crosslinking reactions with the reduction of monomer concentration. [103]

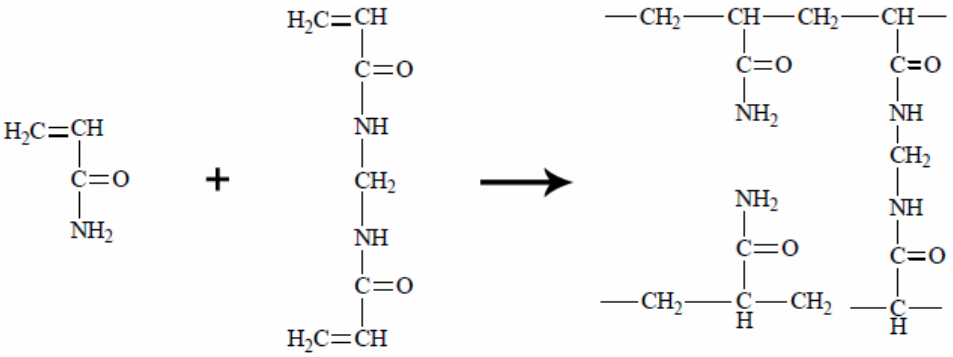

Acrylamide N,N’-methylene-bis(acrylamide) Representative element of crosslinked polyacrylamide

Figure 2.3: Basic reaction of acrylamide cross-linking with bis crosslinker

2.8.2.1 Safety

Acrylamide in the monomer state is considered to be a neurotoxicant at low levels. Acute exposure to acrylamide through inhalation could cause central and peripheral nervous system damage and effects such as drowsiness, fatigue, and hallucinations. The contact with skin would irritate and be considered a probable carcinogen in humans [104]. The synthesized polymers were dialyzed against distilled water for 4 days to remove the unreacted monomers [105].

2.8.3 Effect of synthesis temperature

The elevated synthesis temperature lowers the degree of polymerization [106] and shortens the polymer chains than those that were prepared at lower temperatures. The few cross-linking junctions in the short polymer chain resulted in a loose network due to much freedom to move by chains. In contrast, long polymer chains prepared at low temperatures are less flexible due to many cross-linking junctions on the chain [107].

2.8.4 Swelling properties of hydrogels

The swelling percentage (SW) of the hydrogel is an important parameter that affects mechanical properties. SW is calculated by (2.1).

$$SW = \frac{W_s - W_d}{W_d} \times 100\% \quad (2.1)$$

Where W_s and W_d are swelling and dry weights of hydrogel respectively. The swelling behaviour of PAA tested by Mannadova et al [90] showed an increase in the degree of swelling with the increase of the pH value of the swelling solution.

The cross-linking density is an important factor in deciding the swelling ratio of hydrogels [108]. The swelling capacity increases with increasing cross-linker (MBA) content to a maximum value, and then decreases when the MBA content further increases [109]. This behaviour is due to the higher restriction with the increase in MBA content [87]. 2-hydroxyethyl methacrylate (HEMA)–acrylic acid (AA) comonomer gel tested by Johnson et al. stated the unswollen hydrogels are highly entangled and resistant to deformation. During the swelling process, the polymer structure becomes disentangled by the influx of water. Decay in stiffness can be observed with swelling due to this reason [110].

Flory–Rehner's theory [111] is applied for analysis in swelling of non-ionic hydrogels. Hydrogels swelling equilibrium is attained through the balance of enthalpic mixing. The entropy change from polymer-solvent mixing is positive and promotes swelling. The elastic force imposed by the network structure leads to contraction. This theory can be expressed by using the Gibbs free energy equation shown in (2.2)

$$\Delta G = \Delta G_{el} + \Delta G_{mix} \quad (2.2)$$

Where $\Delta G_{el}$and ΔG_{mix} are free energy of elastic reactive forces and free energy of polymer and solvent mixing respectively.

2.8.5 Drying of hydrogels

Hydrogels contain more than 90% of water and the volume is 20 times larger than dried condition. Much labour, equipment, and time are required for the drying process. When the hydrogels were dried at 110˚C or higher for 30 to 40 h while flowing air, cracking and distortion occur on most of the gels. The uneven drying was the main cause of cracking. As a solution, porous particles such as activated clay or alumina clay were used during the drying process. One option was to dry the hydrogel at 50˚C in an oven for 24 h [105]. The next method suggested was to start from the lowest temperature 50˚C or lower which can evaporate the water in the hydrogel to a high temperature that does not deteriorate the hydrogel (less than 250˚C). It was not recommended to increase temperature suddenly without a sufficient amount of humidity in the drying chamber. The amount of water vapour humidity in the chamber should reduce gradually. The amount of water vapour that evaporates from the surface of the hydrogel and the amount transmitted from the gel interior have to be balanced to prevent cracking. When the powdered or granular porous material is applied to the surface of the hydrogel, the vapour generated from the hydrogel is first absorbed by the porous material by keeping constant humidity on the surface [112].

2.8.6 Crosslinking density, monomer, and initiator concentrations

The crosslinking density of hydrogels has a greater impact on the mechanical strength of the hydrogels. The young's modulus of a 2-hydroxyethyl methacrylate (HEMA)–acrylic acid (AA) comonomer gel hydrogel increase with crosslinking density up to a maximum value, after that decay in Young's modulus can be observed. This could be due to further exposure to UV forms ozone that can create oxygen radicals. The oxygen radical is capable of breaking bonds [110]. Yazici and Okay [113] prepared PAA hydrogels at different crosslinked polymer volume fractions. It showed that the effective cross-link density increases with the initial monomer concentration and decreases the swelling capacity.

About 7000 monomers can be positioned between two crosslinks of PAAm hydrogels [79] [78]. Polyacrylamide –Alginate hydrogel prepared by Fitzgerald et al

[114] showed a decrease in modulus when radical initiator (Ammonium persulfate (APS)) content was increased. Poor gelation occurred below 0.17 wt.% (0.0037 mol%) initiator. The reason for this behaviour is, chain length becomes shorter when there is an excess of radical initiators. This leads to early termination and shorter chains that provide less stiffness. Longer chains assist in resisting applied load. The entanglement ability of longer chains is higher and gives more resistance to the applied load.

The elastic modulus increase by 415% when the monomer concentration increases from 2M to 4M. On the other hand, when increasing the monomer concentration, the hydrogel inhomogeneity increases due to an increase in the viscosity of the solution. The increase in MBA concentration increases elastic modulus [114]. The acrylamide-only hydrogels also showed similar behaviour. The monomer concentration has a higher effect than the MBA concentration to increase modulus [115].

2.8.7 Spatial inhomogeneity

The concentration fluctuations of gel can be classified into two categories; time dependant liquidlike fluctuations and time-independent solidlike fluctuations. Inhomogeneous crosslink density distribution known as spacial gel inhomogeneity can be seen in hydrogels [116]. The main reasons for spatial inhomogeneity are different reactivates of the functional groups, cyclization, multiple crosslinking, and microgel formation [103]. As a result, the optical clarity and strength of the gel reduce. In general, gel inhomogeneity reduces with the introduction of ionic units and increases with crosslink density [117]. The initial monomer concentration of PAAm hydrogel affects the degree of inhomogeneity [118]. When the monomer concentration is increased, the effective crosslinking density also increases, as a result, spatial inhomogeneity increases. The concentration differences between loosely and densely crosslinked can be reduced by decreasing the degree of swelling after preparing gels. The spatial inhomogeneity of PAA hydrogels was investigated by Yazici and Okay [113] by using light scattering measurements. The maximum degree of spatial inhomogeneity of PAA hydrogels was shown at critical monomer concentration.

2.8.8 Fatigue properties

The ability to withstand a large number of compressive cycles is the main requirement of insole materials. Hydrogel with both covalent and ironic cross-links shows better fatigue properties. Some of the hydrogels are self-recovery. However, self-recovery hydrogels are also susceptible to fatigue fracture [80]. These hydrogels contain covalent polymer networks and reversible noncovalent networks.

Two types of samples were used for fatigue tests; uncut samples and precut samples. The irreversible changes that happen in mechanical properties during uncut sample testing were defined as fatigue damage. For example the reduction in elastic modulus with the number of fatigue cycles. The gradual extension of the crack during the precut test is called the fatigue fracture. Polyacrylamide [78], poly(2-acrylamido-2-methyl propane sulfonic acid)-polyacrylamide (PAMPS/PAAM) [119] , and alginate-polyacrylamide [79], poly (vinyl alcohol) (PVA) - polyacrylamide (PAAm) [80] were some of the hydrogels tested for fatigue fracture. Among these hydrogels, alginate-PAAm and PAAm-PVA can be considered as self-recovery hydrogels.

The parameters related to fatigue damage include the change in elastic modulus with the number of cycles [75], the stress-strain hysteresis loop changes, fracture stress, and recovery efficiency. During the deformation of the self-recovery hydrogel, the covalent network provides the elasticity needed for recovery. The reversible physical bond break during deformation dissipates energy, toughens the material, and reforms upon unloading. The stress-strain behaviour of PAAm/ PVA hydrogel remains unchanged after five thousand tensile loading cycles under maximum stress of 10 kPa [80]. When a sample is subjected to cyclic stretches over thousands of cycles, internal damage build-up until a steady-state is reached. When a cut sample is under cyclic loading, the crack propagates with the cyclic loading if the maximum load applied is above a certain value.

The gradual softening of hydrogel under cyclic load was explained by the Mullins effect. The large hysteresis or energy dissipation in fully chemical crosslinked double network hydrogel is due to the partial fracture of covalent bonds [120]. However, the

hysteresis in the hydrogel is different from that in rubber. The hysteresis of the tough hydrogel can be modelled by modifying the free energy function with additional damage variables. For example, Zhang et al [121] expressed a coupled cohesive-zone and Mullins-effect model to predict fracture energies and crack-tip fields of tough gels.

2.8.9 Toughness, Energy density, and Energy release rate

The toughness (fracture energy) was measured by Zang et al. [119] in PAMPS/PAAm hydrogels using a pure shear test. The test was conducted in a sealed acrylic chamber to prevent drying. The energy release rate (G) was defined in (2.3) [122].

$$G = HW(\lambda) \tag{2.3}$$

Where H was the undeformed thickness of the sample and W(λ) was the energy density (energy per volume) of the sample. W(λ) was obtained by the area below the stress-strain curve of the sample. The toughness was defined as the critical energy release rate when the crack propagates. The fatigue threshold toughness of single network PAAm hydrogels was about 53 J/m^2 [79]. This value was much lower than the fracture energy of around 10 000 J/m^2 under static loading conditions.

In PAMPS/ PAAm double network hydrogels, the PAAm network with low density crosslinking showed a threshold of around 400 J/m^{2,} and the PAAm network with high-density crosslinking showed around 200 J/m^2. The effective energy release rates of uncut samples were tested at the 2000th fatigue cycle for comparison purposes [123].

The fatigue fracture in elastomers is described in the Lake-Thomas model [124]. According to that, fracture propagation does not occur below the critical level of strain. When a chain in the hydrogel network is pulled closer to the breaking point, the entire chain is pulled to the same level. The Lake-Thomas model estimates the threshold for fracture by the chemical energy in a unit area of a single layer of chains. Because when the network breaks at a single point, the energy in the entire chain similarly dissipates energy.

2.8.10 Shear testing

The hydrogel was shear tested for different load-bearing applications such as the replacement of cartilage and diseased or damaged tissues. Poly(vinyl alcohol) (PVA) hydrogels tested by Stammen et al. [83] showed a shear tangent modulus between 0.1 and 0.4 MPa. These results were strain magnitude dependant. No statistically significant difference in shear tangent modulus could be found for samples with a swelling percentage of 75% and 80%. The tested sample was 6 mm in diameter and 6 mm in thickness. The samples were bonded to Plexiglas slides by using cyanoacrylate adhesives. The lap shear testing was conducted and shear modulus (G) was calculated according to (2.4), where $F_{parallel}$ is the load applied on moving plate, A is the cross-sectional area of the sample, ΔL is the recorded displacement and L is the initial thickness of the sample

$$G = \frac{\tau}{\gamma} = \frac{F_{parallel}}{A[\tan^{-1}(\Delta L/L)]} \quad (2.4)$$

The rheology method was used by many researchers to assess the properties of hydrogels. Degree of crosslinking, structural homogeneity, and molecular weight. The main rheological testing method used to characterize hydrogel is small-amplitude oscillatory shear (SAOS). During this test, small-amplitude torsional oscillation generates shear in the sample [125]. The tested equilibrium shear modulus (G_e) for five types of hydrogels was: agarose 1200 Pa; collagen 120 Pa; fibrin 160 Pa methylcellulose 340 Pa [126]. Yeung et al [127] tested the PAAm hydrogel with AAm concentration vary from 3% to 12% w/v and MBA 0.05 to 0.6% w/v. The results showed that shear modulus varies in the range from 10 Pa to 50 kPa. The highest shear modulus of 55.292 kPa was shown with 12% w/v AAm and 0.6 % w/v MBA concentration.

2.8.11 Stress relaxation

Stress relaxation can be defined as a time-dependent decrease in stress under constant strain. The crosslink link (MBA) concentration in PAAm-Alginate hydrogel changes the stress relaxation behaviour. The viscoelastic stress relaxation response can

be increased by decreasing the MBA concentration [114], Single network hydrogels such as PAAm with covalent bonds are capable of recovery after deformation as long as the bonds are not broken. Hydrogels with only ironic bonds such as alginate undergo permanent deformation. When these two networks are combined, each network behaves differently to dissipate energy from the applied load. First, the covalent network stretches. Next, the alginate physical bonds break and reform under deformation [128]. The acrylamide network moves more freely in the hydrogels with a lower degree of covalent crosslinking. [129]

2.8.12 Biocompatible, biodegradable properties and safety

Biocompatibility is defined as "the ability of a material to perform with an appropriate host response in a specific application" by Williams [130] and "property of any medical material that is used in contact with a living body" by Ikada [131]. The toxic chemical used in the synthesis process of synthetic hydrogels presents a challenge in biocompatibility. The unreacted monomers, initiators, crosslinkers are toxic to tissues or encapsulated cells. The various purification methods such as solvent washing or swelling for a longer period in a large solvent container have to be conducted to remove hazardous chemicals. [132]

The biodegradability of the hydrogel is another factor to be considered. The rate of degradation and breakdown of the network is considered in designing biodegradable hydrogels. Some tissue engineering applications may not require complete degradation such as corneal and cartilage replacement. The incorporation of cleavable groups into the polymer network of crosslinks can be considered to make degradable hydrogels. Biodegradation is achieved through a biological process such as enzymatic digestion [133].

Poly(2-hydroxyethyl methacrylate) (PHEMA) [134], poly(vinyl alcohol) (PVA) [135], poly(ethylene glycol) (PEG) [136], hyaluronic acid and natural materials [137] are some of the biocompatible hydrogels used in tissue engineering applications. PAAm and PAA hydrogels were used as biomaterial after thorough washing. Acrylamide/ crotonic acid and acrylamide/ itaconic acid copolymer hydrogels

biocompatible with rats implanted for 10 weeks [138]. Polyacrylamide-chitosan hydrogels have shown biocompatibility with no cytotoxicity and were a possible candidate for controlled delivery of antibiotics. This hydrogel was washed extensively with distilled water to remove any unreacted chemicals. Before the application, the hydrogels were washed three times with sterile phosphate-buffered saline and UV light was applied for 30 min [139].

2.8.13 Mechanical behaviour of hydrogels

The basic properties of hydrogels such as stiffness and fracture strength can be calculated from a stress-strain curve. Constitutive models of stress-strain curves are used for characterizing the behaviour of materials. The mathematical representation of the physical behaviour of the material is defined as a constitutive model. Common three types of materials stress-strain curves under quasi-static loading are shown in Figure. 2.6. The hydrogel exhibit nonlinear elastic or hyperelastic behaviour similar to soft biological tissues (Figure 2.6(c)) [140]. The nonlinear constitutive models are expressed as a function of change in internal energy per change in strains [141].

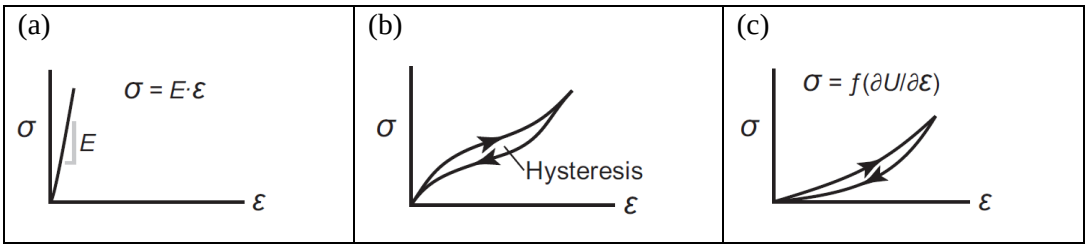

Figure 2.4: Common behaviour of stress-strain curves for quasi-static loading and relevant constitutive models. (a) Linear elastic (e.g. polymers) (b) Nonlinear elastic or hyperelastic (e.g. elastomers) (c) nonlinear elastic or hyperelastic (e.g. soft biological tissue and hydrogels)

The theories applied for small deformations do not apply to the large deformation of the hydrogel. The large deformations change the structure of hydrogel considerably [142]. In most gels, the fracture behaviour depends on the strain rate but the deformation properties such as stiffness and elastic modulus do not depend on the strain rate [109] [143]. Crack after a time delay in a three-point bending test under constant load was due to the activation energy for crack nucleation. High activation

energy leads to a longer time delay [144]. The mechanical properties of hydrogels can be improved by modifying the microstructures [145].

2.8.14 Viscoelastic and Poroelastic properties

Viscoelasticity and poroelasticity are time-dependent behaviours in polymer gels. Poroelasticity results from the migration of a liquid [146], while rearrangements of polymer chains and reversible crosslinks contribute to the viscoelasticity of the gel [147] [148]. Another perspective of viscoelastic behaviour was described as the behaviour of an elastic solid network surrounded by an aqueous solution [129]. Some researchers considered only the viscoelastic property in modelling hydrogels. Wang et al [129] proposed a method capable of separating viscoelasticity and poroelasticity gels by using an unconfined parallel-plate stress relaxation test. They developed a theory on the poroviscoelasticity of hydrogel based on the theory of linear poroviscoelasticity by Biot [149] and the non-linear field theories of hydrogels [150] [148]. The large deformation viscoelasticity model for the type of DN hydrogels was presented by Mao et al [151]. This consists of a covalently-crosslinked polyacrylamide network with long chains, and an ionically-crosslinked alginate network with short chains. Wang and Hong [150] formulated a unified theoretical framework for the transient behaviour of polymeric gels to account for both solvent migration and viscoelastic deformation.

Viscous material behaviour can be expressed as shown in (2.5) based on Newton's law. Where η is viscosity, σ is the stress and ε is deformation strain.

$$\sigma(t) = \eta \times \frac{d}{dt}\varepsilon(t) \tag{2.5}$$

2.8.15 Characterization of stress relaxation behaviour using Prony model

Hydrogel's stress relaxation behaviour is modelled as a linear viscoelastic material. The Prony series is used to represent linear viscoelastic relaxation [152]. The common model for viscoelasticity is represented by springs and dashpots in various configurations. The Prony series model is composed of a free spring and a finite series

of Maxwell elements in parallel. Each Maxwell element is an individual spring and dashpot in series (Figure 2.7)

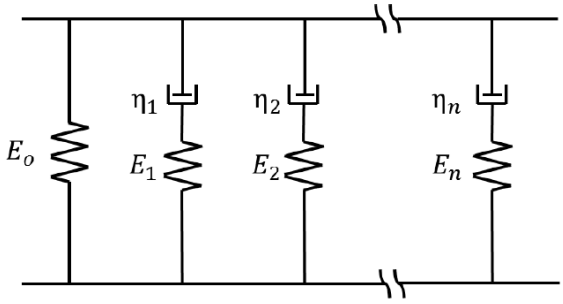

Figure 2.5: Prony series for modelling viscoelastic behaviour

The effective relaxation module, E(t), is expressed by the (2.6) [152]. Where E_∞ is the long-term elastic modulus and the n, g_i, and τ_i are material constants of the Prony series parameter.

$$E(t) = \frac{E_\infty}{1-\sum_{i=1}^{n} g_i}\left[1 - \sum_{i=1}^{n} g_i\left(1 - e^{-t/\tau_i}\right)\right] \quad (2.6)$$

2.8.16 Effect of temperature

The temperature-sensitive hydrogel undergoes a phase transition in which discontinuous volume change occurs in a narrow range of temperature [153]. Poly (N-isopropyl acrylamide) (PNIPAAm) hydrogel can change the volume at a temperature close to 32°C, which is known as lower critical solution temperature (LCST) [154].

The slight increase in the swelling ratio can be visible with the increase in temperature in PAAm hydrogels. But in PNIPAAm hydrogels, the swelling ratio decreases with the increase of temperature. The elastic modulus of PAAm hydrogel [155] and poly (N,N-dimethylacrylamide-co-methacrylic acid) hydrogels [156] decrease as the temperature increase. But in PNIPAAm hydrogels, reduction in elastic modulus from 25°C to 30°C temperature and increase in elastic modulus from 30°C to 40°C temperature were observed. Above LCST, the collapsed PNIPAAm chains improve the mechanical properties of the hydrogel [155]. Fatigue and fracture shear studies conducted by Zang et al [123] showed that poly(N -isopropylacrylamide)

(NIPA) hydrogel fracture energy, maximum critical stretch, and maximum nominal stress increases with temperature increase from 31ºC to 39ºC.

2.9 Finite element analysis

The finite element analyses (FEA) enable efficient parametric evaluations for different insole shapes and material modifications, without needing to fabricate and test orthoses in a series of patient trials. Researchers [9] [157] [31] have used FEA to study what effects orthotic thickness and stiffness have on plantar soft tissue and plantar pressure distribution. ABAQUS FEA software was used by most of the researchers [31] [158] for the analysis of foot insole interaction. Some researchers have used ANSYS software [159]. Maas et al [160] have described the advantages of using FEBIO open-source FEA software recently designed specifically for analysis in computational solid biomechanics.

2.9.1 Finite element model generation

Castro et al [161] presented a comparison between the performances of two Finite Element (FE) solvers for the modelling of the poroelastic behaviour of highly hydrated collagen hydrogels. The Neo-Hookean hyperelastic model was used. V-Biomech has shown its potential for the validation of biomechanical characterization of soft tissues, while Abaqus' versatility is useful for the modelling and analysis of tissue engineering applications, the development of visco-hyperelastic numerical material used experimental tests such as compression, creep, and stress relaxation [162] and to develop the initial hyperelastic material model such as Ogden hyperfoam material model [163].

The uniaxial compression of hydrogel was performed using viscoelastic and poroelastic material models. The commercial software package Abaqus was used by Forte et al to model gelatine gels [164]. The deformation of elastic structure and flow of the liquid through the porous structure of hydrogel is considered for the rate-dependant and rate-independent behaviour. The rate-independent behaviour of the solid network of hydrogel seemingly follows the Ogden hyperelastic model [164].

The Ogden hyperelastic model strain energy potential W is defined in (2.7). Where N, the order of the model varies from 1 to 3. λ_i is the principle stretches, μ and α are material parameters, the units of μ is pressure and α is a dimensionless quantity. D is an incompressible parameter used to indicate volume change. Second term W_{volume} accounts for the volume change of the material.

$$W = \sum_{i=1}^{N} \frac{\mu_i}{\alpha_i}\left(\lambda_1^{\alpha_i} + \lambda_1^{\alpha_i} + \lambda_1^{\alpha_i} - 3\right) + W_{volume} \quad (2.7)$$

The Ogden model is implemented in most commercial finite element packages. The model works reasonably accurately for high strains. The Ogden model reduces to the Neo-Hookean model when α =2 [165]. If N = 2, $\alpha_1 = 2$, and $\alpha_2 = -2$, the Ogden model reduces to a Mooney–Rivlin model [166].

Chapter 3

MATERIALS AND METHODS

3.1 Materials

All the chemicals used were analytical grade. Acrylic acid (AA) - 99.5% (Daejung,), Acrylamide (AAm) - 98% (Sigma Aldrich), N, N′-methylene-bisacrylamide (MBA) 99 % (Sigma Aldrich) and potassium persulfate (KPS) - 95 % (Duksan) used on synthesis of hydrogels. Additionally, polyethylene glycol (PEG) (Sigma Aldrich) (M=2700-3000 g/mol) was used as a plasticizer (Table 3.1). All the chemicals were used as received unless otherwise noted. The initial composition was chosen according to literature, ensuring that the mechanical properties (compression strength and stiffness), were in line with the desired properties for foot insole applications.

Table 3.1: Material used for the synthesis of hydrogels

Material	Abbreviation	Purity (%)	Source
Acrylic acid	AA	99.5	Daejung Chemicals and Metals Co. Ltd
Acrylamide	AAm	98	Sigma Aldrich (SA)
N, N′-methylene-bisacrylamide	MBA	99	SA
Potassium persulfate	KPS	95	Duksan Pure Chemicals Pvt. Ltd
Polyethylene glycol)	PEG	-	SA

3.2 Poly(Acrylic acid) hydrogels

During the development of DN PAA hydrogels, the crosslinker mole percentage was changed in the first network relative to monomer concentration. The crosslinker mol % of the first network solution was locked based on the results and subsequently, the crosslinker percentage of the second network was optimized from 1 to 0.1 mol % (Table 3.2).

The chemical compositions shown in Table 3.1 were used to prepare the samples and each sample was triplicated. The best sample selected from Table 3.2, based on the compression test, was used for other mechanical tests. “The first network of 1M 10 ml AA solution was prepared by mixing 0.7 ml of acrylic acid in 9.3 ml of deionized water. Next 4 mol% of MBA was added as crosslinker (CL) and 0.2 mol% of KPS was added as the initiator (I). The mixture was stirred at speed of 250 rpm and temperature of 50˚C with a magnetic stirrer for 15 min (Figure 3.1 (a))” [86, p. 1101]. The mixture was transferred into cylindrical plastic containers of 35 mm internal diameter (Figure 3.1 (b)) and heated at 70°C for one hour. After drying the samples, the second crosslinking solution with 1M AA, 0.1 mol% MBA, and 0.2 mol% KPS were prepared and the samples were swelled for 24 h in the solution.

The swollen samples were placed in the oven (Mammert universal oven UT 110) at 70°C for 1 h to develop the DN hydrogels. The DN PAA hydrogel samples were swelled for 48 h in deionized water to remove any unreacted molecules. Next, the samples with 3, 4, and 5 mol % CL were fully dried (Figure 3.1(c)) and swelled (Figure 3.1(d)) to the average swelling percentage of 75±5% before testing (Figure 3.1(e)). The best crosslink percentage of the first network was selected based on stiffness, fracture strength, less stickiness, easy removal from the mould, and cost of the materials. The sample nomenclature was developed as follows: composition with 1M AA and 4 mol% CL in the first network and 1M AA and 0.1 mol% CL in the second network was referred to as 1MAA 4CL /1MAA 0.1CL.

Table 3.2**:** DN PAA Hydrogel synthesis chemical compositions

First network			Second network		
AA (M)	MBA (mol-%)	KPS (mol-%)	AA (M)	MBA (mol-%)	KPS (mol-%)
1	2	0.2	1	0.1	0.2
1	3	0.2	1	0.1	0.2
1	4	0.2	1	0.1	0.2
1	5	0.2	1	0.1	0.2
1	6	0.2	1	0.1	0.2

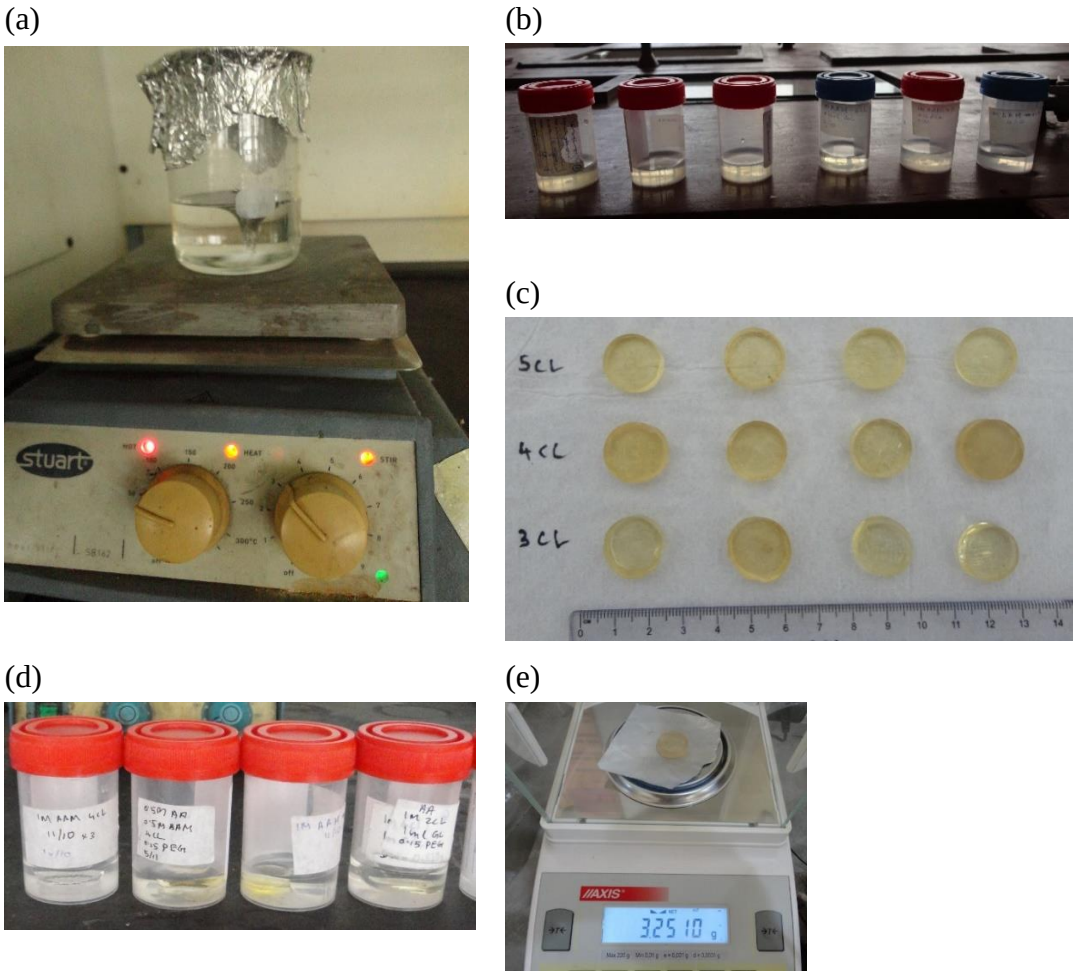

Figure 3.1: (a) Stirring of hydrogel precursor solution on a hot plate at 40˚C. (b) 10 ml of hydrogel precursor solution in plastic containers. (c) Dried hydrogel samples (d) Dry hydrogel samples are kept in distilled water to swell to the desired amount. (e) Swollen sample weight measure before testing the hydrogels.

3.3 Polyacrylamide hydrogels

The SN PAAm hydrogel was synthesized by keeping monomer and initiator concentration constant at 1M and 0.2 mol% respectively and using 1 mol% and 2 mol% crosslink concentrations.

The single network of 1M AAm 10 ml solution was prepared by mixing 0.725 g of AAm in 10 ml of deionized water. 1 mol% of the MBA was added to the solution as crosslinker (CL) and 0.2 mol% of KPS was added as an initiator (I). All the chemical compositions used for initial sample preparation are given in Table 3.3. The mixture was stirred with a magnetic stirrer for 15 min and transferred into cylindrical plastic containers of 35 mm internal diameter. All the containers were filled with 10 ml of mixture to achieve the minimum thickness requirement of 5±1 mm in the final sample and kept inside the oven at 70˚C for one hour.

The synthesized polyacrylamide (PAAm) hydrogel samples were swelled for 48 h in a deionized water container to remove any unreacted molecules. The samples were fully dried to measure dry weight and the dried samples were swelled to 60% swelling before testing. This composition with 1M AAm and 1 mol% CL is referred to as 1M AAm 1CL [167].

Table 3.3: PAAm with different MBA composition

AAm (M)	MBA (mol-%)	KPS (mol-%)
1	1	0.2
1	0.8	0.2
1	0.5	0.2

3.4 Improve softening and nonstick properties

Polyethylene glycol (PEG) 0.05, 0.1, and 0.15 mol-% were added to SN PAAm hydrogels as shown in Table 3.4. The initial PEG composition was based on literature [168] and the suitable range was selected based on the mechanical test results ensuring that the mechanical properties (stiffness and fatigue strength), were in line with the desired properties for foot insole applications. The triplicated samples were first tested

for stress vs strain behaviour and selected the composition that gives the desired stiffness of 200 kPa at 0.5 strain. Next, the selected composition was tested for fatigue behaviour under maximum stress of 400 kPa and strain rate of 200 mm/min.

Table 3.4: PAAm chemical composition with the addition of PEG

AAm (M)	MBA (mol-%)	KPS (mol-%)	PEG (mol-%)
1	1	0.2	0.05
1	1	0.2	0.10
1	1	0.2	0.15

3.5 Calculation of swelling properties

The percent mass swelling was determined by using the equation (3.1).

$$\%\, Swelling = \frac{(M_s - M_d)}{M_d} \times 100\% \qquad (3.1)$$

where M_d and M_s are the dry mass and swollen mass of the sample respectively.

The test samples with desired swelling percentages were obtained by keeping a dried hydrogel sample and calculating (M_s-M_d) amount of distilled water in a sealed container for 24 h.

3.6 Hydrogel insole development

The optimum composition of DN PAA and SN PAAm hydrogel was identified as 1MAA 4CL- 1MAA 0.1CL and 1M AAm 1CL respectively. Using this composition, hydrogel insoles were developed by using a mould as shown in Figure 3.2(a) and the developed hydrogel insole is shown in Figure 3.2 (b). As a solution for the shrinking of the hydrogel insole, a large sheet of hydrogel was moulded (Figure 3.2 (c) and (d)). The desired shape was cut from the sheet of the hydrogel for testing. The strength of the hydrogel sheet was further improved by reinforcing it with cotton mesh.

(a) (b)

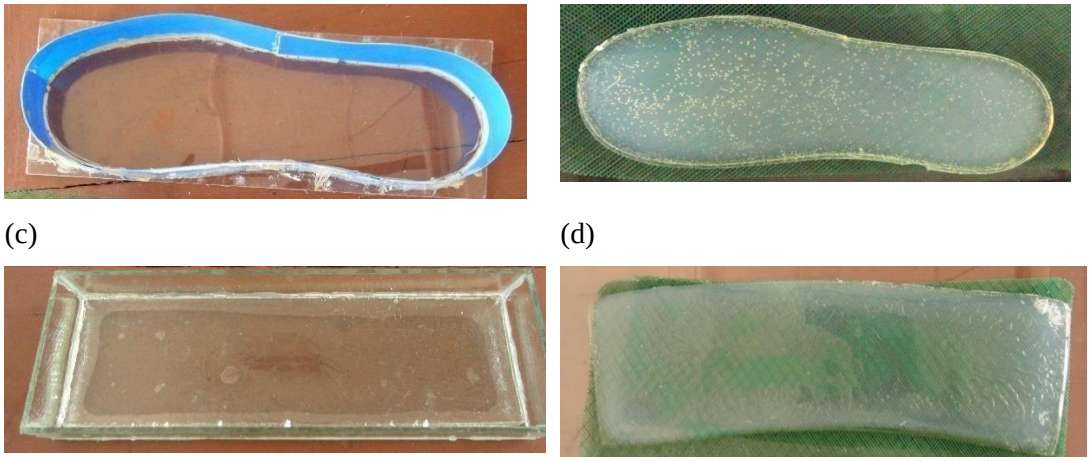

(c) (d)

Figure 3.2: Hydrogel insole development (a) Insole mold (b) Hydrogel insole prepared by using a mold. (c) Glass mold is used for making hydrogel sheets. (d) Sheet of hydrogel

3.7 Mechanical Characterization

"Mainly compression, creep, stress relaxation, fatigue, shear and rebound resilience tests were conducted. All hydrogel samples were triplicated and average stress-strain behaviour was considered for calculations.

The mechanical tests were conducted on a Testometric M350-10 AT universal material testing machine (Rochdale, England, +/-0.5% down to $1/1000^{th}$) at ambient temperature (30°C), with different crosshead speeds (1, 5, 10, 20, and 100 mm/min). The graphs of force vs displacement and force vs time at constant displacement (stress relaxation) were generated. The weight, diameter, and thickness of the samples were measured before and after the test. The stress (σ) was calculated by using the equation (3.2)

$$\sigma = F/\pi r^2 \qquad (3.2)$$

Where F is the applied load and r is the original radius of the specimen. The strain (ε) was calculated from the ratio of change of the thickness (t) and the initial gauge thickness (t_0) of the measured sample (equation (3.3))

$$\varepsilon = t/t_0 \qquad (3.3)$$

The modulus (stiffness) is the change in stress (σ_2 - σ_1) divided by the change in strain (ε_2-ε_1). In this research, the modulus was calculated from the slope (derivative) of the stress-strain curve due to the non-linear behaviour of hydrogels (3.4)" [86, p. 1102]

$$\text{Modulus (Stiffness)} = (\sigma_2 - \sigma_1) / (\varepsilon_2 - \varepsilon_1) = d\sigma/d\varepsilon \qquad (3.4)$$

The test samples with the correct swelling percentage for all the mechanical tests were prepared by measuring the dry weight of the samples and then keeping them inside the sealed containers for 24 hrs with a measured amount of distilled water required for the desired swelling percentage. The correct swelling percentage was calculated based on swelling weight and dry weight and the applicable maximum force was calculated based on maximum stress and the sample contact area before starting the mechanical tests.

3.7.1 Compression test

The general test setup used for compression testing is shown in Figure 3.3(a) and Figure 3.3(b). Dry and swollen sample weights were measured and the mass swelling percentage was calculated before the test. The weight of the sample was measured after the test to calculate any water loss during the test. Initial compression tests were conducted at 10 mm/min crosshead speed and 80% swelling percentage for PAA and 60% swelling percentage for PAAm hydrogels. The DN PAA hydrogel samples in Table 3.1 and Table 3.2 were compressed until the break, cracks appear, or up to 80% strain. The chemical composition with the highest compression strength was selected for the next modification in the composition and finally, the optimum composition was used for other testing methods. The compression strengths were measured at different crosslink percentages, swelling percentages, and crosshead speeds. The sample was kept in a moisturized container to minimize dehydration during the test (Figure 3.3(b)). Water droplets were sprayed on the inner surface of the container to maintain the humidity. All the samples were weighed before and after the test. Test conditions and parameters include; crosshead speeds 10 -200 mm/ min, sample diameter 20±0.4 mm, thickness 5±0.3 mm, 50-120±5% swelling.

(a)

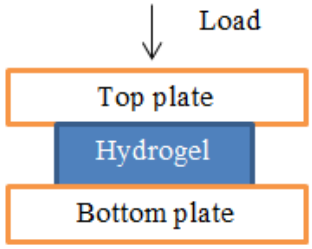

(b)

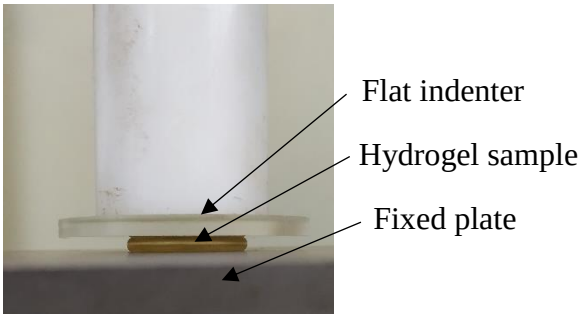

Figure 3.3**:** (a)Schematic diagram of the hydrogel compression test. (b) Test arrangement for compression, stress relaxation, creep, and fatigue tests

3.7.2 Criteria for selecting the best composition

According to the research conducted by Chatzistergos et al on the effectiveness of pressure distribution ability of insole materials with different stiffness showed that optimum stiffness range was between 71 kPa and 551 kPa at 50% strain. The studies conducted by Tang et al [66] showed that when wearing EVA insoles, the maximum peak pressure was 255 kPa with 35 Shore A. By considering these results, the minimum stress for force calculation in fatigue testing was set to 350 kPa.

3.7.3 Effect of crosslink percentage

Set of AA triplicated samples with composition 1MAA XCl/1M 0.1 CL where X varies from 2 to 6 and swelling of 80±5% shown in Table 3.1 were tested at 10 mm/min crosshead speed. The samples were compressed up to 80% of strain until breaking. And maximum compressive strength was recorded. The sample with the highest compressive strength and desired stiffness was selected as the optimum crosslink percentage.

3.7.4 Effect of strain rate

The hydrogel samples with the best chemical composition were triplicated and compressed at 10, 20, 50, 100, and 200 mm/min crosshead speeds. By considering average values, the variation of stress with strain was plotted in the same graph.

3.7.5 Effect of swelling percentage

Triplicated hydrogel samples with optimum chemical compositions were swelled to 40, 60, 80, 100, and 120 swelling percentages and tested at 100 mm/min crosshead speed.

3.7.6 Effect of temperature on hydrogel behaviour.

The compression behaviour of DN PAA and SN 1M AAm 1CL hydrogel was tested at 20˚C, 30˚C, and 40˚C. The samples were kept inside a heat-resistant container to minimize heat loss (Figure 3.4 (a)). First, the set of triplicated samples was kept inside a refrigerator for one hour in sealed containers. Another set of sealed triplicated samples was heated inside the oven at 60˚C for 30 min. Next, a set of triplicated samples was kept at room temperature (30˚C). All the samples were measured for temperature (Figure 3.4(b)), weight, diameter, and thickness before and after the test. Average values were considered for calculations.

(a) (b)

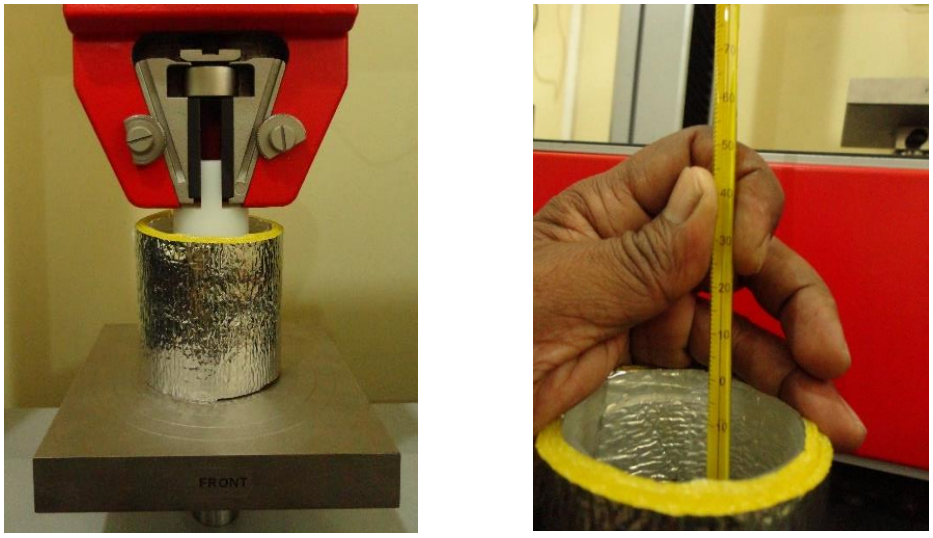

Figure 3.4: compression testing hydrogel samples at 20°C and 40°C *(a)* Test arrangement with heat resistant material wrapped around the container *(b)*. Measuring temperature before and after testing.

3.7.7 Available insole materials

Polyurethane (PU) gel and Ethylene-vinyl acetate (EVA) samples (Figure 3.5(b) and (c)) were selected as available insole materials. PU samples were cut from PU gel insole (SIDAS - 18 rue Léon Béridot - 38509 Voiron – FRANCE) (Figure 3.5(a)). These samples were subjected to compression, stress relaxation, and rebound resilience tests.

(a) (b) (c)

Figure 3.5: (a) PU gel insole (b) Pu gel sample prepared for testing: Diameter =23.5 mm, Thickness=4 mm. (c) EVA sample: Dameter= 24 mm, Thickness 4 mm

3.7.8 Stress relaxation

The same test setup shown in Figure 3.3 was used. The test was conducted using a step compression method. Samples were kept in constant displacement and variation of force with time was observed. The stress relaxation test for PAAm hydrogel was conducted in two different ways. First, the sample was compressed with a preload speed of 10 mm/min and held at constant strain for 300 s. During the second method, the samples were compressed up to maximum stress of 250 kPa, and the strain was kept constant for the 60s and then release for 40s. This cycle was repeated five times.

3.7.9 Creep

Variation of displacement with time under constant force was observed. Samples were compressed at 10 mm/min preload speed until reaching 200 kPa for 60 s interval and 40 s release up to a total of 300 s.

3.7.10 Shear

Shear properties of hydrogel were tested by bonding the hydrogel sample onto two metal plates as shown in Figure 3.6. First, two sandpapers were bonded to the metal plates and the next hydrogel samples were bonded to sandpapers by using Cyanoacrylate glue. Torsional and horizontal compression effects incurred during loading were neglected, and the shear modulus (G) was calculated by using the equation (3.5), where τ, γ, F_s, A, and d were shear stress, shear strain, recorded load, cross-sectional area, and recorded displacement of the sample respectively.

$$G = \frac{\tau}{\gamma} = \frac{{}^{F_s}/_{A}}{{}^{d}/_{t_0}} \tag{3.5}$$

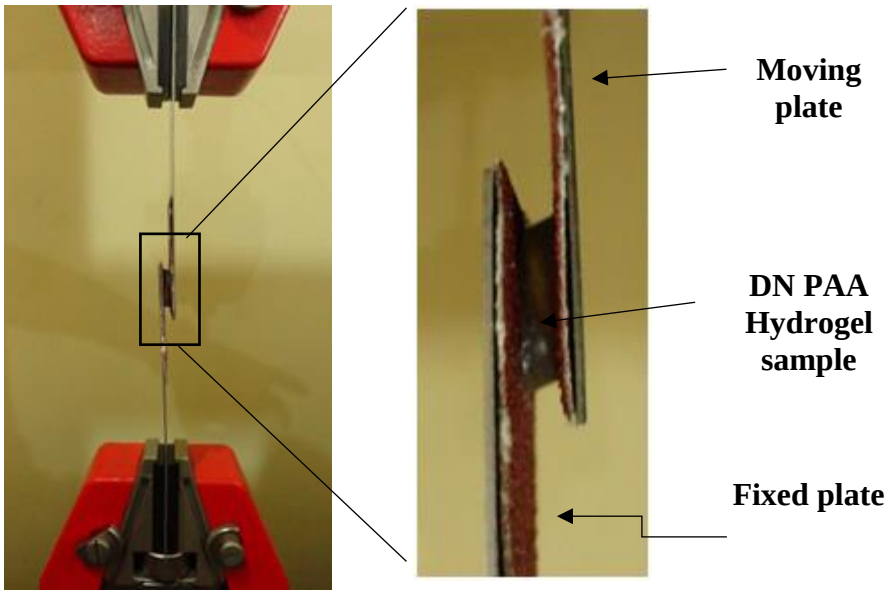

Figure 3.6: Shear testing

3.7.11 Rebound Resilience and hardness

Rebound resilience is defined as the ratio of the energy returned to the energy applied to a test piece as the result of a single impact of a striker terminated by a

suitable indenter [84]. Figure 3.7 shows the rebound resilience tester (Precision scientific equipment corp., New Delhi, India) used and it contains a scale from 0 to 100. First, the thickness and hardness of all the samples were measured before starting the test (Table 3.5). The hardness of each sample was measured by using a portable Shore A hardness tester (0-100 HA) (Figure 3.8(a)) and thickness was measured by using a thickness gauge (H.W. Wallace & Co Limited, England, Resolution: 0.01 mm) (Figure 3.8 (b)). Next, a sample was kept at 0 level by holding from the pin of the vertical rod and the pendulum was lifted to 100 mark level and dropped onto the sample. This test was repeated three times on a single sample. The maximum rebound heights were recorded and the average value was considered for results.

Table 3.5: Samples used for rebound resilience testing

Material	Manufacturer	Thickness (mm)
EVA foam	DSI Samson Group, Colombo, Sri Lanka	4
EVA foam		5
EVA foam		6
EVA foam		10
Silicone	Oppo Medical Inc, USA.	5
PU gel	SIDAS, Voiron, France	4
PU gel		8
DN PAA hydrogel	-	5
DN PAA hydrogel	-	7
SN PAAm hydrogel	-	5
SN PAAm hydrogel	-	7.5

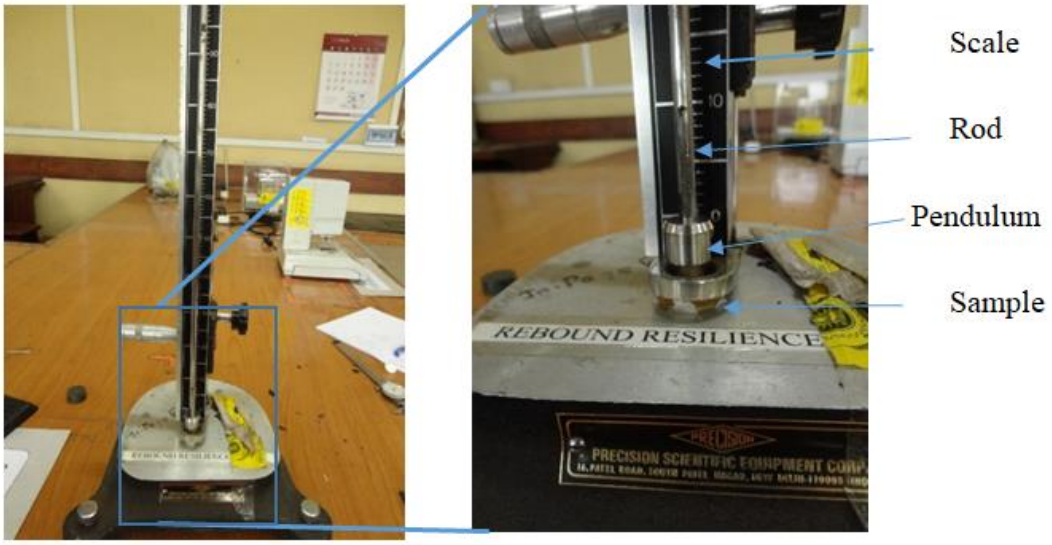

Figure 3.7: Rebound Resilience testing.

(a) **(b)**

Figure 3.8: (a)Hardness testing with portable Shore A hardness tester. (b) measuring insole thickness with Thickness gauge

3.7.12 Fatigue testing

The foot is most at risk for re-ulceration in the first 20-30 days after healing when patients start to resume full walking activities [53]. The number of steps walked by foot ulcer patient range between 1461-2154 [169] and the step cycle is approximately 1 Hz [170]. The peak pressure recorded after wearing an insole varies from 200 kPa to 500 kPa [66] but the peak pressure has to keep below 200 kPa to prevent re-ulceration [54].

By considering the above factors, machine limitations, and safety, the minimum number of loading-unloading cycles requirement was 20 000 cycles at a constant crosshead speed of 200 mm/min under maximum average stress of 200 kPa. A constant swelling percentage of 80% and 60% were kept for DN PAA and SN PAAm samples (Table 3.6).

Typically, during the loading-unloading cycle, the hydrogel samples were compressed to a pre-set maximum strain and then returned to the initial length. To examine the recovery of the hydrogel and to keep a constant swelling percentage, after every 1000 cycles, the samples were measured for weight, diameter, and thickness, relaxed for 10 min controlled times, and the cycle was restarted.

Table 3.6: Hydrogel samples used for fatigue testing

No	Sample	Swelling percentage (%)	Diameter (mm)	Thickness (mm)
1	1MAA 4CL/`1M AA-0.1CL	80±5	23±1	5±0.5
2	1M AAm-1CL	65±5	20±0.4	5±0.3
3	1M AAm 1CL 0.15PEG	65±5	20±0.4	5±0.3
4	1M AAm 2CL 0.15PEG	65±5	20±0.4	5±0.3

3.8 Pressure insole testing

To investigate, simulate and compare the effect of hydrogel and other insole materials on pressure redistribution under foot plantar, Tactilus® pressure-sensing insole (Sensor Products Inc., 300 Madison Ave STE 100, Madison, NJ 07940, United States) and the Tactilus 4.1 software were used for recording the pressure values. The pressure insole was placed in between bottom plate or insole material to observe the interface pressure between ground or insole and indenter (Figure 3.9(a))

The barefoot maximum stress on diabetic foot is 700 kPa. The load was applied by using stainless steel indenter as shown in Figure 3.9(a). The dimensions of the indenter were given in Figure 3.9 (b). First, the barefoot condition of the diabetic foot was simulated by applying a force that generates maximum peak stress of 700 kPa. Under the same load, the peak pressure reduction and the effectiveness of uniformly distributing plantar pressure by hydrogels and other insole materials were tested and compared.

(a) (b)

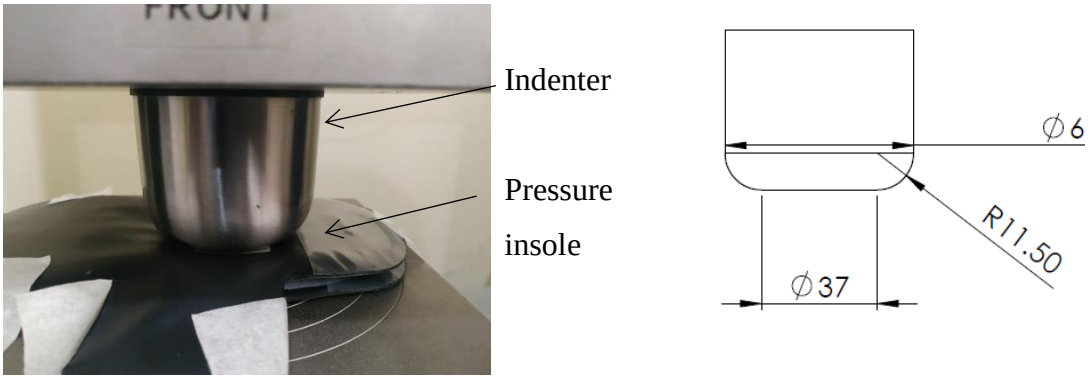

Figure 3.9: (a) Test arrangement for pressure insole readings. (b) Indenter dimensions

Chapter 4

RESULTS AND DISCUSSION

4.1 Existing insole materials

According to Figure 4.1 (a) and (b), SIDAS® PU gel and EVA samples respectively did not show any significant variation in stiffness with the crosshead speed of compression. The stiffness of these insole materials can be considered rate-independent in the tested strain rate range 10 mm/min to 100 mm/min. This behaviour complies with the results of Ross-Murphy et al [109] and van Vliet [143].

The closed-cell EVA material's elastic zone, a plateau region with stress increase slowly and densification region where stress increases rapidly as the closed cells compress and behave as solid material can be visible in strain ranges 0 to 0.1, 0.1 to 0.5, and above 0.5 respectively. At 100 mm/min crosshead speed and 0.5 strain, EVA and PU gel showed 140 kPa and 649 kPa respectively indicating high stiffness of PU gel insole and high softness of EVA material.

The minimum peak pressure at 50% strain for diabetic insole vary from 155±4 kPa to 350 ± 5 kPa for patient's body mass varies from 50 kg to 125 kg when the hardness of insole material changes from Shore 10A to 20A respectively (the detailed relationship can be found in Table 2.2 [34]. The tested EVA material satisfies this requirement but the PU gel was in a higher stiffness range.

(a) (b)

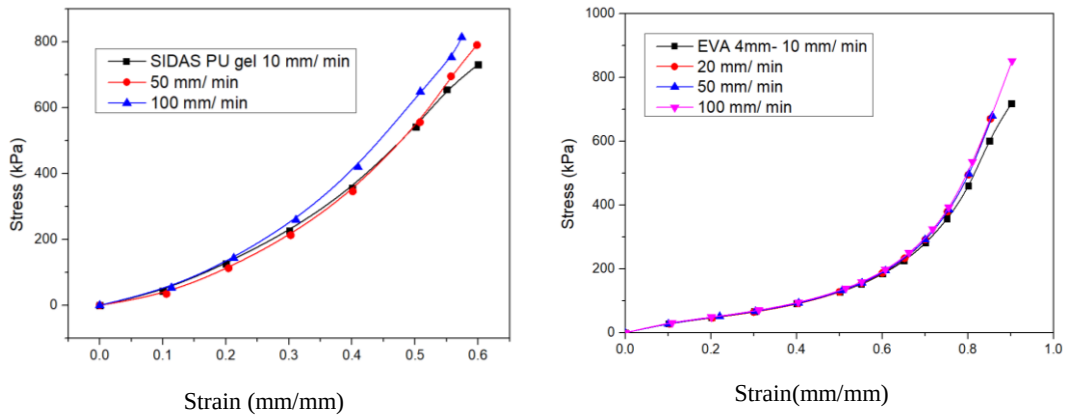

Figure 4.1: Variation of stress with the strain (a) 4 mm thick SIDAS® PU gel (b) 4 mm thick EVA

4.2 Double network polyacrylic acid (PAA) hydrogels[1]

4.2.1 Effect of crosslink percentage on compression behaviour

The PAA hydrogel with composition given in Table 3.1 was tested and stress vs strain and stiffness vs strain were plotted as shown in Figure 4.2 (a) and (b) respectively. DN PAA with crosslinker mol % varying between 2 and 6 was tested and from 2CL to 3CL, a considerable increase in stiffness was visible. The stiffness increased by 69% from 2CL to 3CL at 50 % strain. The increase in CL value has not contributed to a significant increase in stiffness (Table 4.1). This indicates the maximum number of crosslinks achieved at 3CL and further addition of CL has not contributed to property improvement. With the increase in CL mol%, a proportionate decrease in stickiness was observed. The 2CL and 3CL samples showed high stickiness and handling difficulty. By considering the above factors, 4CL composition was selected for further improvements and testing.

[1] Part of this results were published in R. Udayanandana, P. Silva, and T. Gunasekara, "Mechanical properties of double network poly (Acrylic Acid) based Hydrogels for potential use as a biomaterial," in *2019 41st Annual International Conference of the IEEE Engineering in Medicine and Biology Society (EMBC)*, Berlin, 2019, pp. 1101-1104.

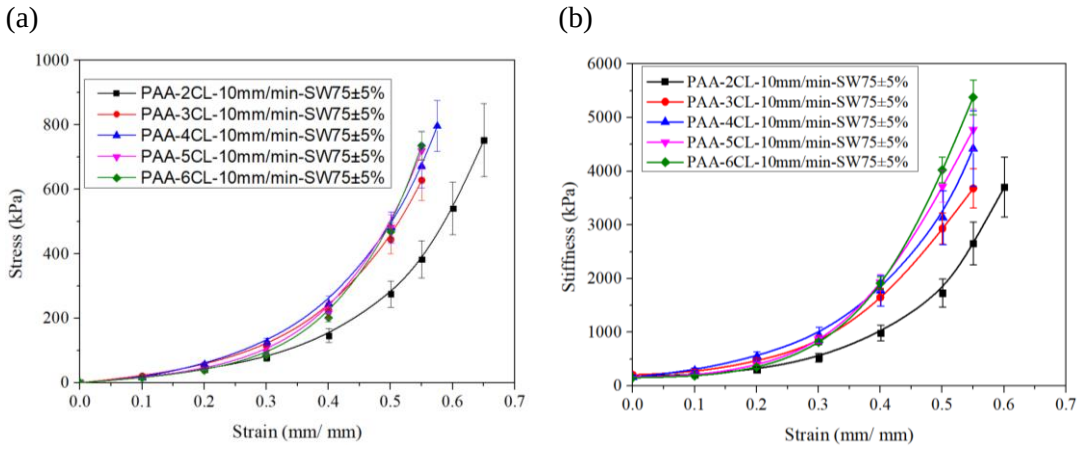

Figure 4.2: Compression of DN PAA hydrogel under CL mol% vary from 2 to 6 and swelling percentage of 75±5% (a) Variation of stress with strain at 10 mm/min cross-head speed (b) Variation of stiffness with strain at 10 mm/min cross-head speed.

Table 4.1: Variation of stiffness with CL mol% at 50% strain and 10 mm/min crosshead speed.

PAA CL mol%	Stress at 50% strain (kPa)	Stiffness at 50% strain (MPa)
2	275	1.730
3	445	2.931
4	500	3.255
5	483	3.716
6	468	4.024

4.2.2 Crosshead speed variation

A significant variation of stress cannot be observed with the variation of strain rate in PAA hydrogels (Figure 4.3). The stress values of 459 kPa, 462 kPa, 532 kPa, and 539 kPa at 50 % strain were shown by crosshead speeds of 10 mm/min, 50 mm/min, 100 mm/min, and 200 mm/min respectively (Table 4.2). According to Yang et al [171], when the strain rate is below 0.12 s^{-1} (crosshead speed: 36 mm/min), the modulus increases rapidly and when the strain rate is above 0.12 min^{-1}, the modulus remains almost constant. The fracture stress increases when the strain rate vary from 0.25 min^{-1} (crosshead speed: 1.25 mm/min) to 25 min^{-1} (125 mm/min) [164]. The mechanical behaviour of hydrogel depends on the solid matrix deformation and the movement of the fluid in and out of the pores during the deformation. When the speed of

compression is much higher than the speed of liquid transfer between pores, hydrogel behaves as an elastic material.

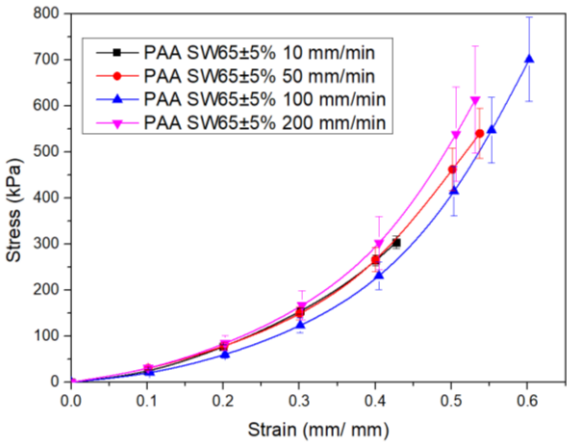

Figure 4.3: Variation of stress with the strain of PAA hydrogel at different strain rates of compression

Table 4.2: The crosshead speed and strain rate and stress at 50% strain

Crosshead speed (mm/min)	Strain rate (s^{-1})	Stress at 50% strain
10	0.03	459
50	0.17	462
100	0.33	532
200	0.67	539

4.2.3 Variation of mechanical properties with the swelling percentage

PAA hydrogel showed an inverse relationship between swelling percentage and stiffness (Figure 4.4). The expected stress at 0.5 strain was 220 kPa to 280 kPa when the load was applied between 300 N to 600 N [34]. The 80% and 120 % swollen samples show the stress of 355±16% kPa and 280±6% respectively. The 80% swollen samples were selected for further testing by considering the increased tendency of the material to fracture with the swelling percentage.

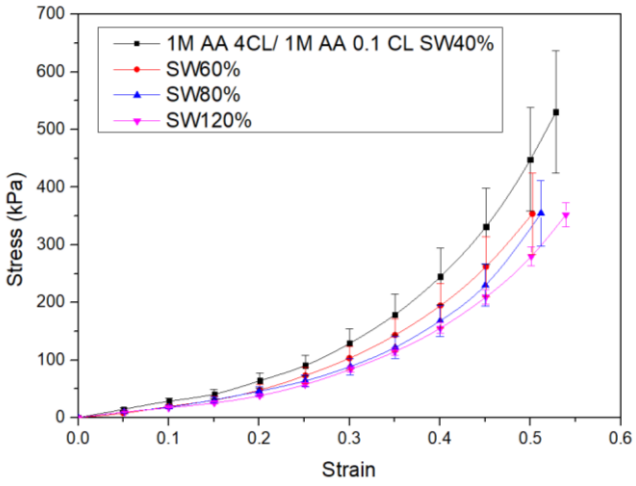

Figure 4.4: Variation of stress with the strain of PAA hydrogels under different swelling percentages.

4.2.4 Fatigue

The 1M-4CL/ 1M-0.1CL (PAA) sample was tested with 110 N maximum force and a test speed of 100 mm/min. The maximum force accounts for maximum stress of 365±11 kPa. At the end of 3000 cycles of the test period, two cracks were appearing in the sample (Figure 4.5 (b)). The strain-softening of the sample with the number of cycles is visible from Figure 4.5(a) by the movement of the hysteresis loop towards the right-hand side. After the completion of each 1000 loading cycle, there was only a 1% loss of total weight. This was due to water loss and the effect on mechanical properties was negligible. The endplates were completely dry before and after the test, indicating water loss occurs only by evaporation. The long-range movement of water in poroelastic behaviour was not visible during compression. The 60% swollen samples used in this test were considered to be the reason for this behaviour.

.(a) (b)

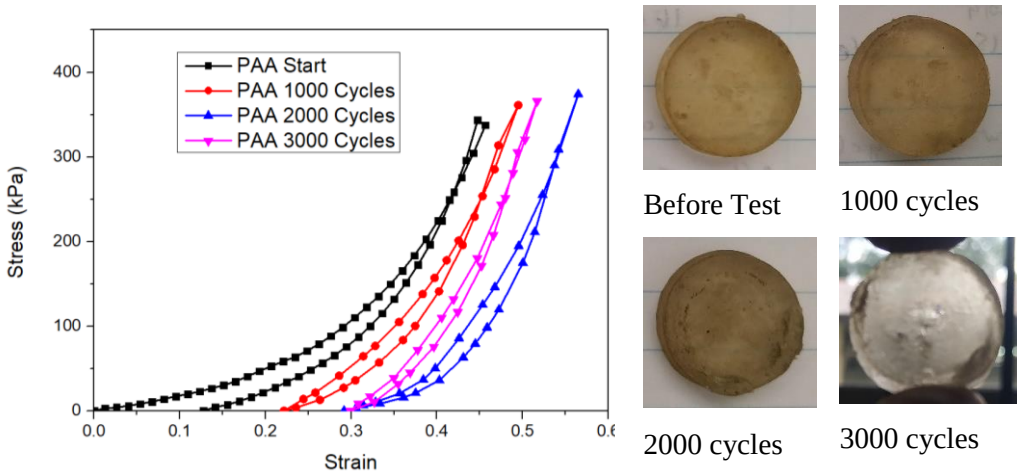

Figure 4.5: Compressive fatigue test of 1M AA 4CL/ 1M AA 0.1CL (PAA) at 80±5% swelling and 200 mm/min crosshead speed (a) Variation of stress with strain up to 3000 cycles (b) Hydrogel samples deformation and crack propagation with number of cycles

4.3 Single network polyacrylamide (SN PAAm) hydrogels[2]

4.3.1 Compression of PAAm hydrogels with different MBA compositions

PAAm hydrogels with different crosslinker mol% were tested as shown in Figure 4.6. When the MBA (CL) mol% was reduced, the stiffness reduces gradually (Figure 4.6 (b). The area between the loading and unloading curves shows an increase in energy loss with a reduction of MBA composition. The higher value of strain at the end of the loading curve when stress was zero indicates the lower recoverability rate at low CL mol% (Figure 4.6 (a)). By considering these factors and handling difficulty due to an increase in stickiness with lower CL mol %, 1 mol % CL was selected for further testing.

[2] Part of this results were explained in "R. Udayanandana, P. Silva, and T. Gunasekara, "Compression Fatigue and Stress Relaxation Properties of Single Network Polyacrylamide Hydrogels," in *2019 Moratuwa Engineering Research Conference (MERCon)*, Colombo, 2019, pp. 533-537."

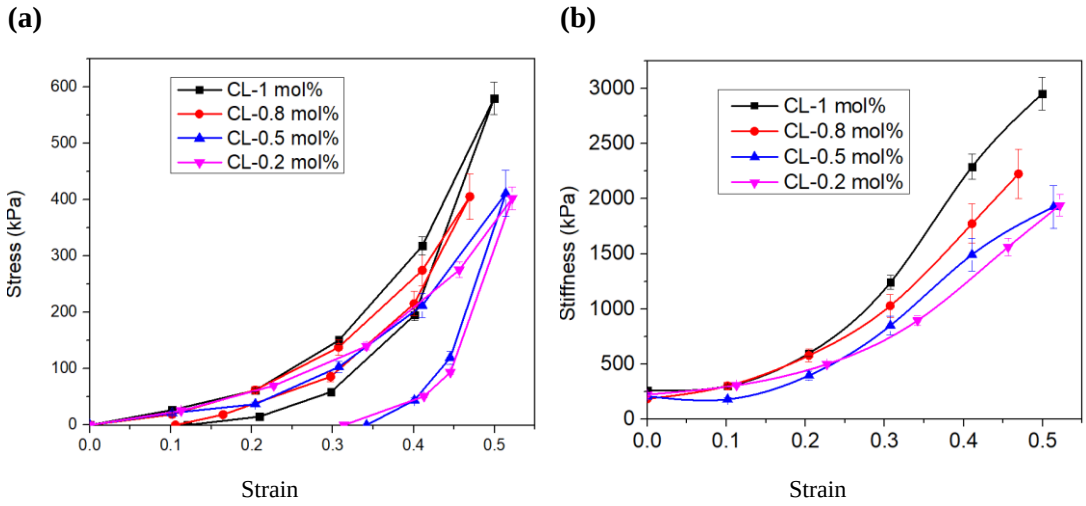

Figure 4.6: PAAm hydrogels with different CL mol %.(a) Variation of stress with strain for loading and unloading curves. (b) Variation of stiffness with strain for loading.

4.3.2 Compression strength

"Compression of a single network PAAm-1CL (1M AAm-1CL) sample until the fracture is shown in Figure 4.7(a) and Figure 4.7(b). The maximum compression stress of 946 kPa was observed at 59% strain under the 10 mm/min crosshead speed and 65% swelling. A similar composition of PAAm hydrogel tested by Gong et al [20] at 93% swelling and 97% fracture stain showed 700 kPa fracture stress. The modulus of toughness or strain energy density and energy release rate of the single network PAAm hydrogel during initial compression was calculated to be 136.6 kJ/ m^3 and 683 J/m^2 respectively based on the area under the stress-strain curve in Figure 4.7(a). The crack propagation rate vs energy release rate curve developed for PAAm hydrogel during extension by Tang et al [78] showed that above energy release rate threshold of 7 J/ m^2, crack propagation rate proportional to energy release rate. A similar curve for compression of PAAm hydrogel was not found in the literature.

The stiffness of the sample varied from 1 MPa to 3.7 MPa at 30% to 50% strain respectively. The maximum stiffness of 4.9 MPa was observed at 58% strain (Figure 4.7(b))" [167, p.534]. The stiffness values were higher than the recommended value of 155 kPa to 276 kPa at 50% strain for a diabetic foot [34].

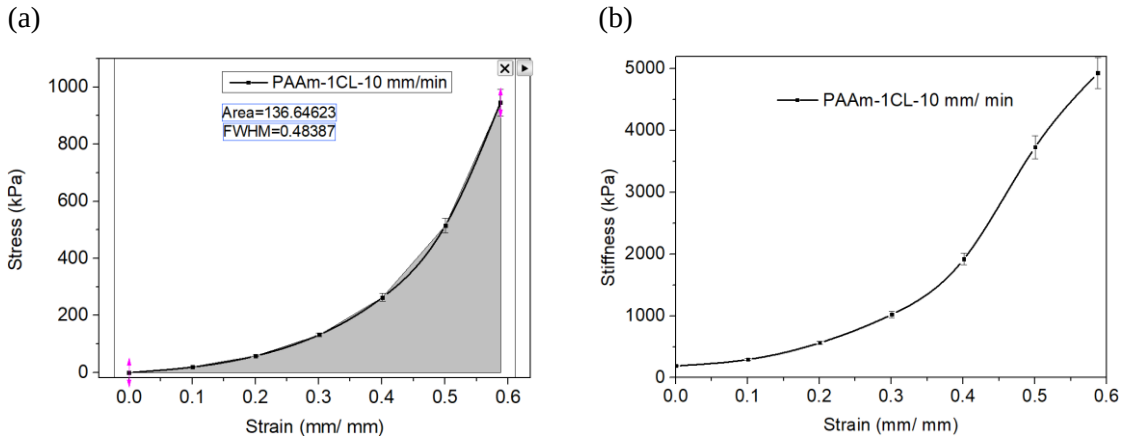

Figure 4.7: Compression strength of single network PAAm hydrogel- swelling of 65±5% and a crosshead speed of 10 mm/ min (a) Variation of stress with strain (b) Variation of stiffness with strain.

4.3.3 Compression at different swelling percentages

The compression of PAAm hydrogel at 60, 80, and 100 swelling percentages are shown in Figure 4.8. The average maximum compression strengths of 765±30% kPa, 661±20% kPa, and 335±30% kPa showed at 60%, 80%, and 100% swelling respectively indicating a reduction in compression strength with an increase in swelling percentage. Higher fatigue life is also expected when the swelling percentage is 60%-80% [78]. The stress values of 532 kPa, 479 kPa, and 335 kPa at 0.5 strain indicate the reduction in stiffness with the increase in swelling percentage.

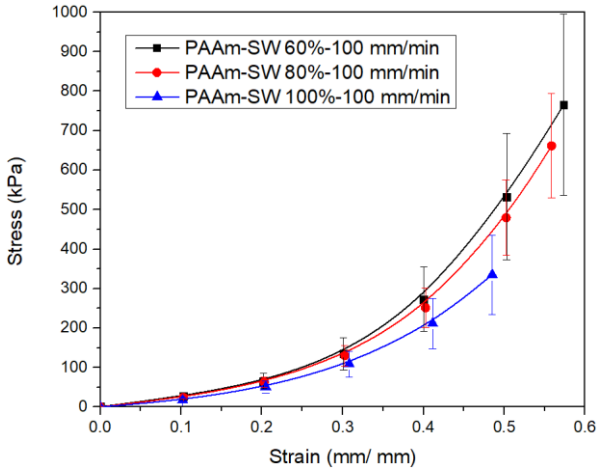

Figure 4.8: Variation of stress with strain for SN PAAm hydrogel at 60, 80, and 100 swelling percentages and 100 mm/ min strain rate.

4.3.4 Crosshead speed variation (Different strain rates)

According to Figure 4.9, PAAm, samples did not show any significant variation in stiffness with the strain rate of compression. Two possible reasons for this behaviour were identified. First, the selected strain rates during the test were in a higher range similar to strain rates in walking. According to Yang et al [171], the constant modulus could be observed at a strain rate above 0.12 s^{-1}(crosshead speed: 36 mm/min). Second, the nonlinear elastic behaviour is shown by PAAm hydrogels at selected compositions. A similar relationship for starch gel was shown by Gamonpilas, Charalambides, and Williams [172]. This can be considered as the nonlinear elastic behaviour of PAAm hydrogel due to insignificant variation of the stress-strain curve with crosshead speed. The PAAm hydrogels displayed elastic or viscoelastic behaviour depending on network crosslink density. Viscoelastic behaviour can be visible when the monomer concentration was less than a critical value or the monomer to crosslinker (M/C) ratio was more than some critical value. When the M/C ratio (by weight) was between 10 and 200, elastic behaviour can be expected [173]. The PAAm hydrogel used for the testing in Figure 4.9 has an M/C ratio of 46 and a monomer concentration of 7.2 % w/v indicating compliance with Zhang, Dauber, and Foegeding [173] test results. PAAm hydrogel displays viscoelastic property at a given M/C ratio of 37.5 with monomer concentration less than 2.4% w/v and constant monomer concentration of 5% w/v with M/C ratio higher than 200 [173]. The structural definition for this is the formation of an inhomogeneous network when monomer concentration is low at a given M/C ratio [174]. Consequently, the gel permeability is high and solvent flows within the matrix possible during deformation [175]. When the crosslinker concentration is low (high M/C ratio), the network chains are longer and more flexible to occur chain rearrangement during deformation with time, causing rate-dependent behaviour.

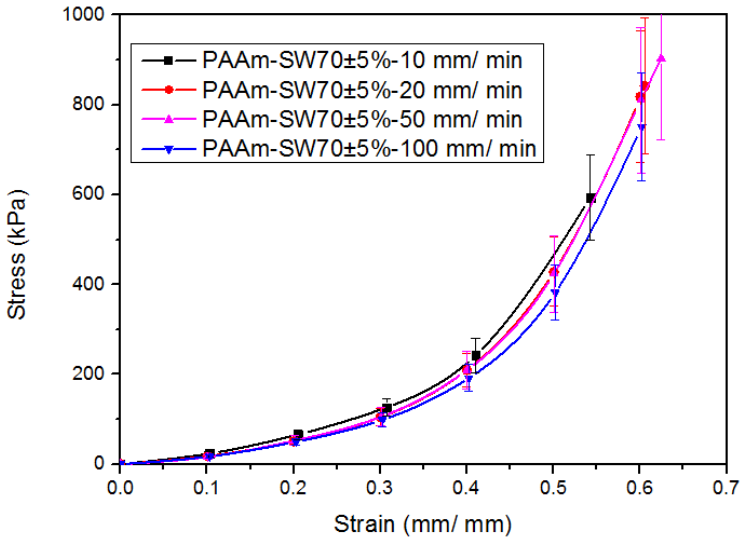

Figure 4.9: Compression of PAAm hydrogel at different crosshead speeds

4.3.5 Effect of thickness variation

As shown in Figure 4.10(a), the samples show a gradual increase in stiffness with reduction of thickness and the error percentage of the average value is higher when the thickness reduces. The stiffness of the diabetic insole material is expected to be in the range of 155 kPa to 276 kPa at 50% strain for minimum peak pressure development in foot plantar [34]. The 5 mm, 7 mm, and 9.5 mm thickness PAAm hydrogel samples tested under friction on surface contact showed the stress of 532 kPa, 336 kPa, and 218 kPa respectively at 50% strain (Table 4.3). Therefore, the 9.5 mm PAAm hydrogel sample showed the most suitable properties at 60% swelling when friction acting on the contact surfaces.

The frictionless condition testing showed that both 5 mm and 7 mm samples had the stress of 181 kPa and 171 kPa respectively at 50% strain (Figure 4.10(b) and Table 4.4). It can be concluded that the thickness dependant behaviour under friction is due to barrelling effect of the sample and the silicone oil applied on the surface of the gel sample showed a thickness-independent low stiffness value suitable as diabetic insole material.

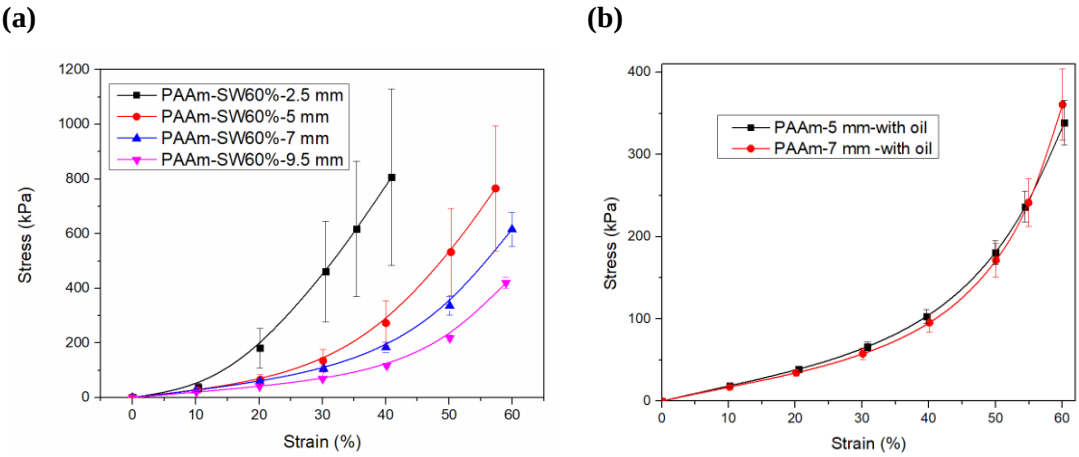

Figure 4.10: The variation of stress with strain for different thickness PAAm hydrogels (a) Without applying silicone oil on the sample surface. (b) After applying silicone oil on the sample surface.

Table 4.3: Stress at 50% strain for different thickness values of PAAm hydrogel tested without applying silicone oil on the sample surface.

Thickness	Stress at 50% strain
5	532±30%
7	336±10%
9.5	217±5%

Table 4.4: The stress at 0.5 strain at the frictionless condition for 5mm and 7 mm thickness

Thickness (mm)	Stress at 0.5 strain
5	180.8 ± 8%
7	171.4 ±12%

4.3.6 Creep

The PAAm hydrogel with three thickness values (5 mm, 7.5 mm, and 9.5 mm) was tested for three cycles of repeated creep at compression stress of 200 kPa for 60s interval and 40s release (Figure 4.11). The gradual increase in peak strain with the thickness could be observed in the results. This could be due to the increase in barrelling effect with thickness. A negligible increase in maximum strain in each cycle

could be observed as an indication of better recoverability of PAAm hydrogel at different thickness values (Table 4.5)

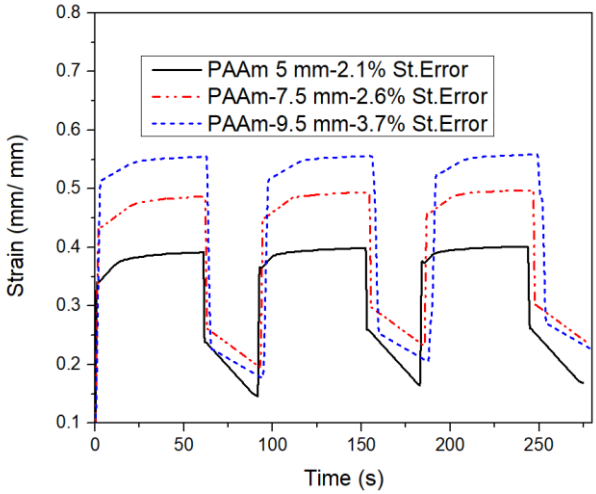

Figure 4.11: Repeated creep behaviour of PAAm hydrogels at 5 mm, 7.5 mm, and 9.5 mm

Table 4.5: Increase in the strain at each cycle of loading with 5 mm, 7.5 mm, and 9.5 mm thickness values.

Thickness (mm)	Increase in strain per cycle (%)
5.0	0.6
7.5	1.2
9.5	0.3

4.3.7 Stress relaxation

The stress relaxation behaviour for 5 mm, 7 mm, and 9.5 mm thickness values showed that the stress relaxation was independent of thickness variation during the first 300s but the peak pressure reduction with thickness was observed during the impulsive load application at the start of the first and second cycles (Figure 4.12). This behaviour was probably due to an increase in shock absorption ability with thickness.

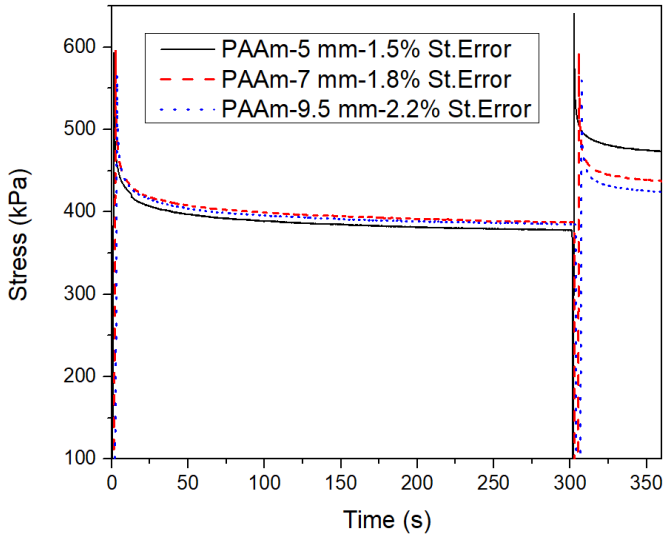

Figure 4.12: Stress relaxation of PAAm hydrogel at thickness values. Of 5 mm, 7 mm, and 9.5 mm.

4.3.8 Fatigue

"When the load applied on the samples was kept at 180±10 N, variation in maximum strain 60±4% and stress 520±50 kPa could be observed (Figure 4.13(a)). Hysteresis in the first cycle of loading clearly showed the residual strain after unloading. When the sample was loaded, unloaded, and then reloaded during consecutive cycles, the same stress produces an increased strain, indicating a strain-softening of the hydrogel sample. Mullins effect has been considered as the major factor for the softening of the network of hydrogels over consecutive loading cycles [176]. This strain-softening may stem from the breakage of covalent bonds [120].

The breaking of most sacrificial bonds in the network of the hydrogel is irreversible. Such bond-breaking progresses cycle by cycle, and the stress-stretch curve keeps changing until it reaches a steady-state. This progressive damage over many cycles is called shakedown [79]. Since the network is significantly damaged in the steady-state after many cycles, the stress-strain hysteresis is relatively small, and the hydrogel can be assumed as elastic. The energy release rate is well defined in the steady-state, G = HW, where W is the area of the stress-stretch curve in the steady-state and H is the distance between the two jaws when the sample is undeformed [79]. During the

13,000th cycle, the difference between the energy release rates calculated from the loading and the unloading curves is 12%, while it is 33% during the initial cycle. The area within a hysteresis loop is energy dissipated during a cycle (usually in the form of heating or breaking of covalent bonds). This energy represents the plastic work from the cycle. The hysteresis loss of the first compressive cycle, rather different from the elastic behaviour of the subsequent cycles, resulted in sacrificing the covalent bonds of the PAAm network.

The hydrogel sample variation during fatigue cycles could be observed in Figure 4.13 (b). After the completion of each 1000 loading cycle, there was only a 1% loss of total weight, indicating that water loss can be neglected. This could be due to the 60% swelling hydrogel used in the testing. The presence of both solid skeleton and fluid phase support carrying loads in hydrogels. Due to the negligible water drain, the mechanical behaviour of the tested hydrogel can be described by using the theory of rubber elasticity or single-phase models of viscoelastic material" [167, pp.534-535].

According to IWGDF guidelines [54], after wearing a diabetic insole, the peak pressure should be less than 200 kPa. By considering the safety factor of 2, PAAm samples were tested under maximum stress of 400 kPa. The maximum number of fatigue cycles was increased up to 20 000 at this stress (Figure 4.14). The Foot is most at risk for re-ulceration in the first 20-30 days after healing when patients start to resume full walking activities [169]. The maximum number of steps walked by diabetic foot ulcer patient vary between 1461-2154 and the peak stress range between 240 kPa and 325 kPa [53]. Based on these facts the expected minimum number of fatigue cycles of 20 000 was satisfied by the SN PAAm hydrogel.

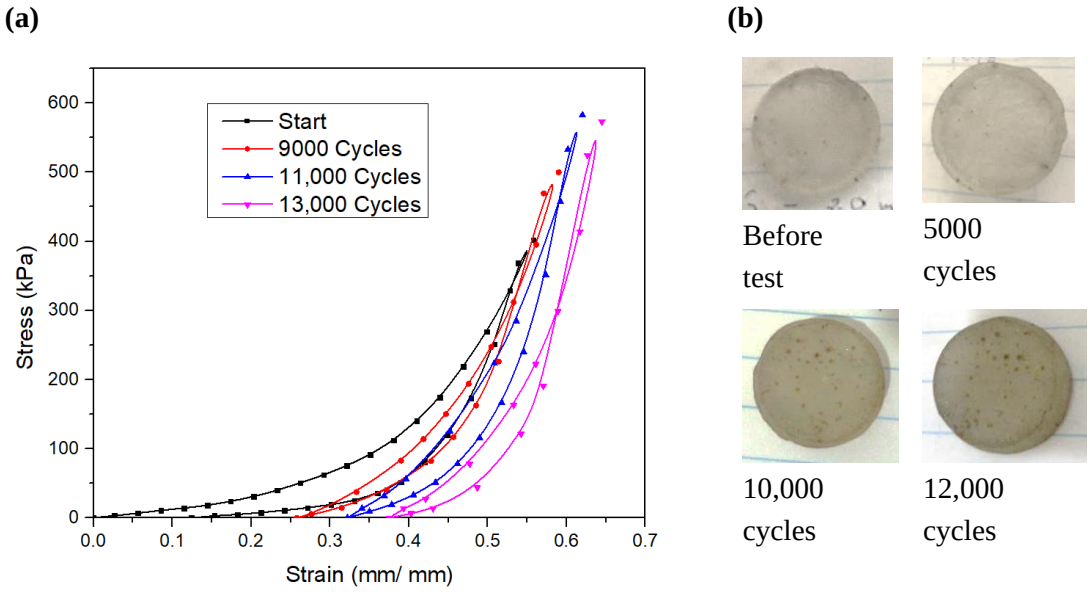

Figure 4.13: 1M AAm 1CL hydrogel compressive fatigue test. (a) Variation of stress with strain up to 13,000 cycles. at 200 mm/min crosshead speed and maximum stress of 550±50 kPa (b) Hydrogel sample physical appearance variation with the number of cycles.

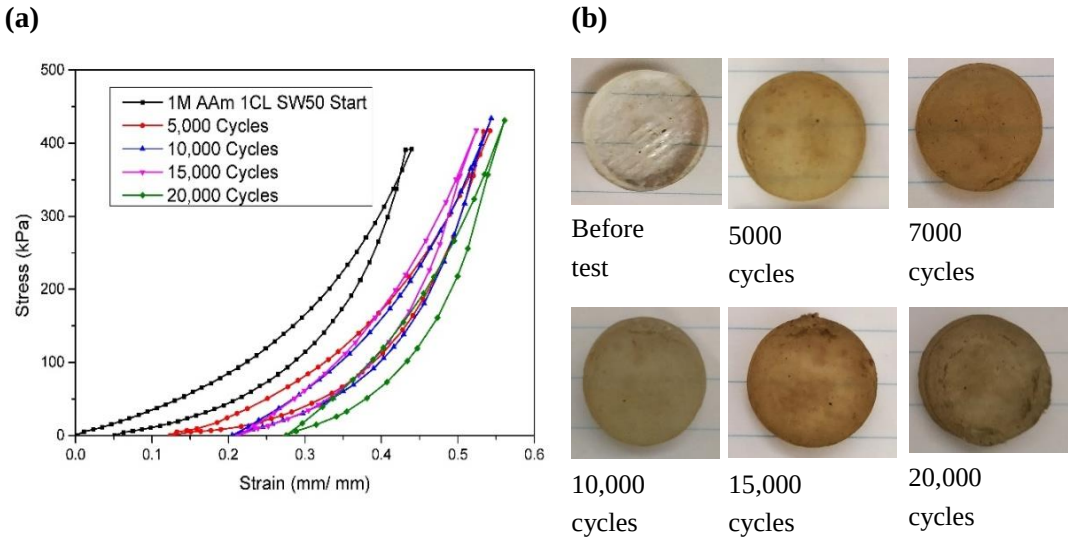

Figure 4.14: 1M AAm 1CL hydrogel compressive fatigue test (a) Variation of stress with strain up to 20,000 cycles at maximum stress of 425±25 kPa. (d) Hydrogel sample physical appearance variation with the number of cycles (undeformed diameter 20 mm and thickness 5 mm)

4.3.9 Temperature effect

A significant variation of average compressive stress and stiffness vs strain of PAAm hydrogels cannot be seen under 20°C, 30°C, and 40°C temperatures. The highest average stress and stiffness values of 362 kPa and 2.1 MPa at 0.5 strain were at 30°C (Figure 4.15 and Table 4.6). The swelling percentage of triplicated samples was measured before and after each test. The observed average weight reduction after the test was 0.1% and its impact on mechanical properties was negligible based on the results obtained at different swelling percentages in section 4.3.2.

The maximum and minimum values of the PAAm average curve vary by 30%, 15%, and 20% at 20°C, 30°C, and 40°C. The accuracy of the load cell of UTM, the variations in temperature distribution inside the oven, and the inhomogeneity of structure are the main factors affecting this variation in results.

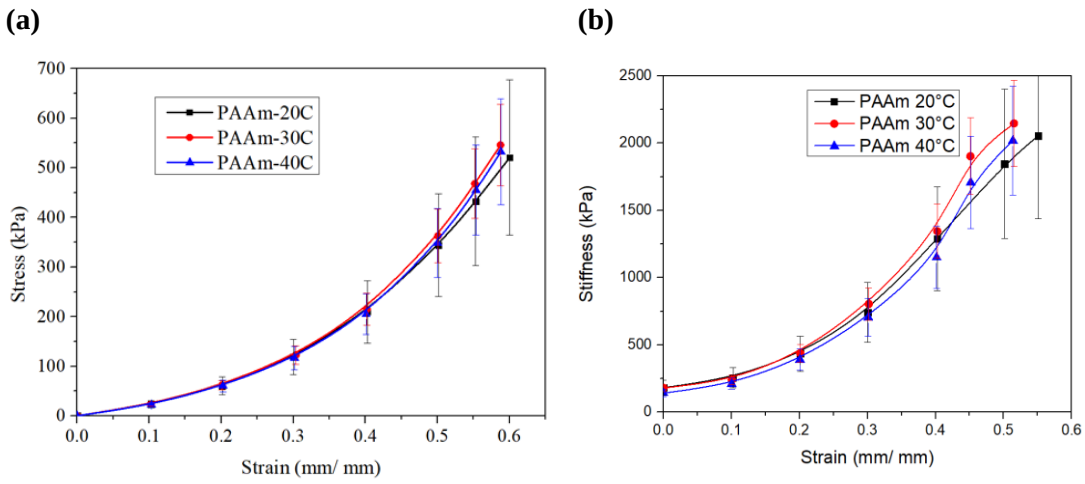

Figure 4.15: Variation of hydrogel compression properties under 20°C, 30°C and 40°C temperatures (a) (c) PAAm stress vs strain behaviour(d) PAAm stiffness variation with strain

Table 4.6: The stress and stiffness values at 0.5 strain for 20°C, 30°C, and 40°C temperatures

Temperature (°C)	Stress at 0.5 strain (kPa)	Stiffness at 0.5 strain (MPa)
20	344±30%	1.8±30%
30	362±15%	2.1±15%
40	348±20%	2.0±20%

4.3.10 Drying properties of PAAm hydrogels

The three 10 ml disk shape samples of PAAm hydrogels were observed for the reduction in weight at ambient conditions (dry bulb temperature 32±1°C, wet bulb temperature 27°C, and Relative Humidity 70%) The rate of weight reduction during the 2nd day (48 hrs) was 0.13 g/hr and this rate was reduced to 0.004g/hr in 5th day (120 hrs) (Figure 4.16).

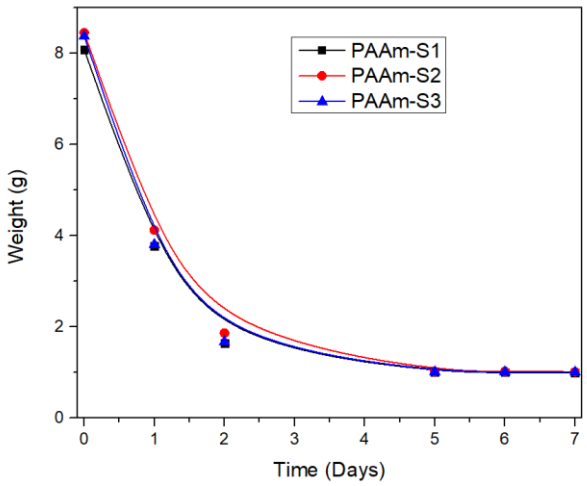

Figure 4.16: Drying rate of PAAm hydrogel at room temperature 30±1C and relative humidity 70±3%

4.3.11 Variation of dry weight with the initial volume of solution.

The PAAm hydrogel with dry weight variation with initial liquid volume showed almost linear behaviour with equation $y = 0.09297\,x - 0.0958$ (Figure 4.17). The variation of test results was 5%. This curve can be used to make hydrogel samples with different volumes and calculate the swelling percentage at each stage of drying. The drying of the PAAm hydrogel can be stopped at the desired swelling percentage based on the weight of the sample.

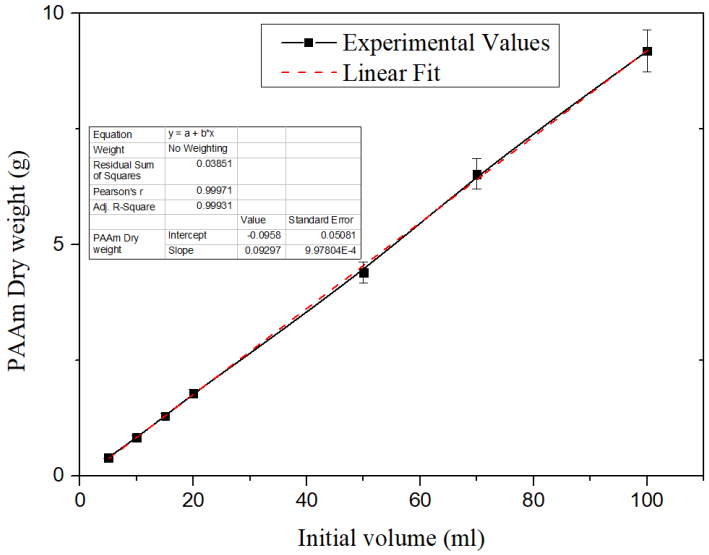

Figure 4.17: Variation of PAAm dry weight with initial solution volume.

4.3.12 Variation of PEG mol% in 1M AAm 1CL

The softening behaviour of 1M AAm 1CL was observed with the increase of PEG content from 0 to 0.15 mol %. The addition of 0.1mol % PEG showed the desired stiffness of 200 kPa at 0.5 strain (Figure 4.18)

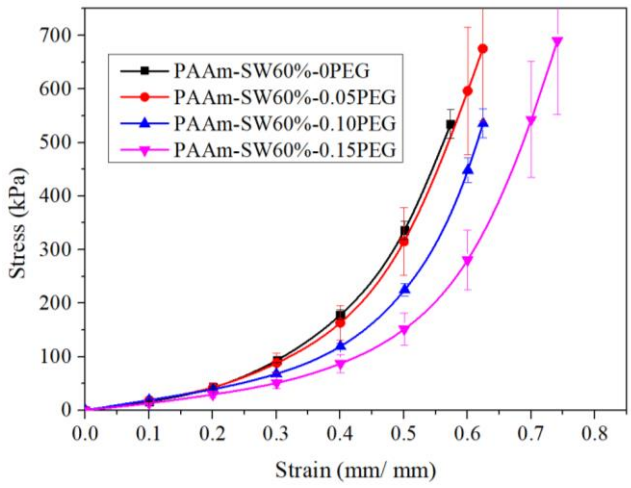

Figure 4.18: The variation of stress with strain for different concentrations of PEG

4.3.13 Fatigue property after adding PEG

The strain energy density of SN 1M AAm 1CL 0.1 PEG hydrogel was reduced and stiffness increased drastically during the first 100 cycles (Figure 4.19 (a)). The addition of PEG improved softness and damping properties and reduced the recovery rate after compression. The behaviour in the stress-strain curve became almost linear at the end of 100 cycles. The fatigue life was limited to 2000 cycles at the maximum stress of 400 kPa (Figure 4.19 (b) and (c)).

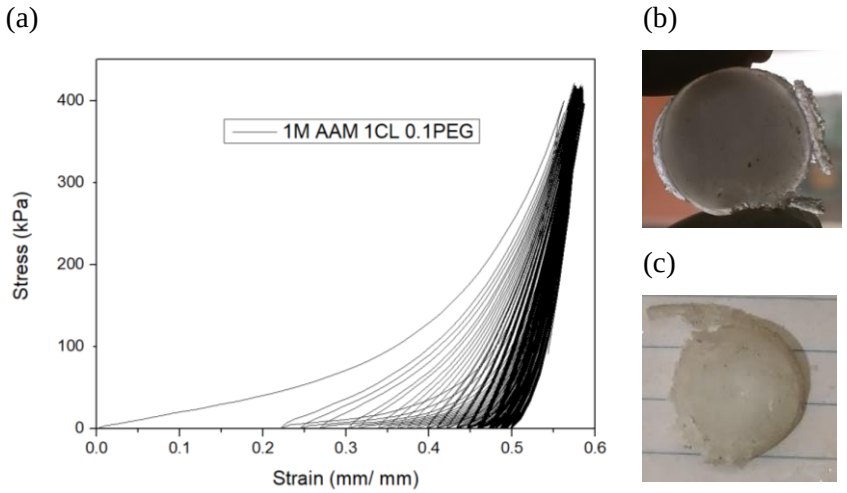

Figure 4.19: (a) The stress vs strain behaviour of 1M AAm 1CL 0.1 PEG under maximum stress of 400 kPa for 100 cycles (b) sample after 1000 cycles (b) sample after 2000 cycles

4.4 Comparison of properties of insole materials and hydrogels

4.4.1 Compression stress and stiffness

The stiffness of the sample increased with crosshead speed under constant swelling percentage. The sample tested at 100 mm/min showed maximum stress and compression module of 800 kPa and 3 MPa respectively at 58% strain and 62% swelling (Figure 4.20(a) and (b)).

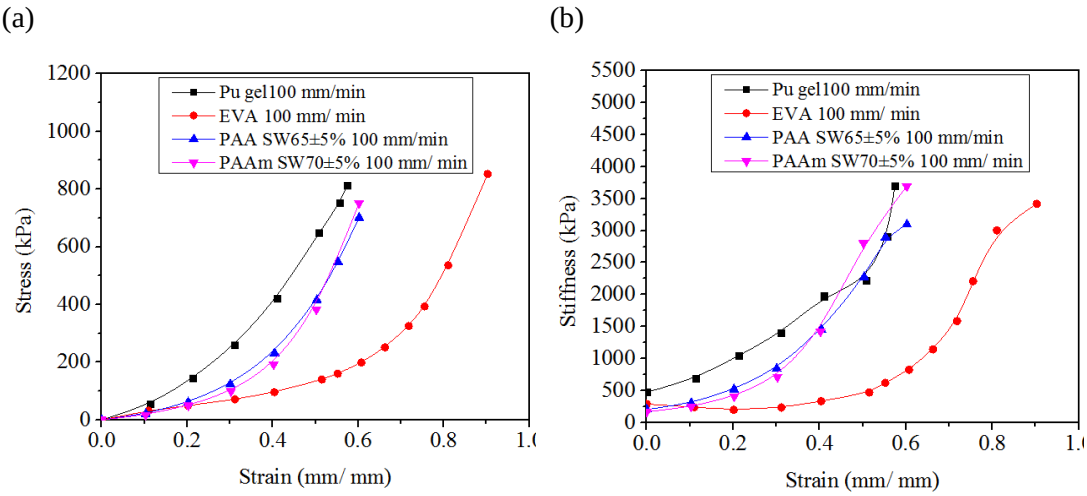

Figure 4.20: Compression behaviour of PU gel, EVA, DN PAA hydrogels, and SN PAAm hydrogels (a) Variation of stress with the strain (b) Variation of stiffness with strain.

4.4.2 Stress relaxation

Stress relaxation describes how polymers relieve stress under constant strain. All tested materials showed viscoelastic properties. The PU Gel, EVA, silicone, and PAAm hydrogel samples were tested for repeated stress relaxation (constant strain for 60 s, unloading for 40 s, and peak stress of 250 kPa) (Figure 4.21 (a) and (b)). The gradual increase in maximum constant strain in each cycle to maintain peak stress of 250 kPa (Figure 4.21 (a)) indicated the deterioration of material property in EVA and PU Gel. The reduction in stress at 10s from the first cycle to the 5^{th} cycle indicated the deterioration of stress relaxation ability of EVA and PU Gel materials (Table 4.7). The residual strain at the unloaded state indicates the shape memory of the material. The highest to lower shape memory was shown by EVA, PAAm PU gel, and Silicone. The gradual increase in strain value at the unloaded state indicates the fast deterioration of shape recovery property of EVA while PAAm and Silicone show superior shape recovery due to constant strain. The lowest stress value at the end of the relaxation period showed the superior viscoelastic property by PAAm hydrogel (Figure 4.21(b)).

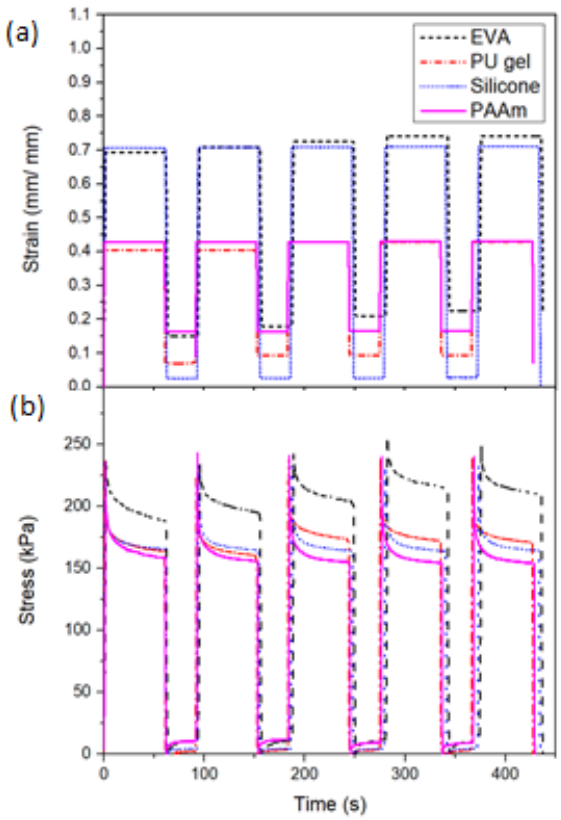

Figure 4.21: The repeated stress relaxation test conducted on EVA(St. error 1.1%), PU Gel (St. error 1.0%), Silicone (St. error 1.0%), and PAAm (St. error 2.1%) (a) Variation of strain with time (b) Variation of stress with time.

Table 4.7: Peak pressure reduction and increase in deformation with number of cycles

Material	Stress reduction in 10 s at 1st cycle (%)	Stress reduction in 10 s at 5th cycle (%)	Increase in strain from 1st to 5th cycle under strain (%)
EVA	13.6	11.6	6.8
PU Gel	25.9	24.8	5.9
Silicone	24.3	22.8	0.6
PAAm	27.1	31.7	0.2

4.4.3 Creep

The cyclic creep test under the constant stress of 200 kPa was conducted for EVA, PU gel, PAAm hydrogels (Standard error 3%), and Silicone materials (Figure 4.22(a)). The highest strain value was shown by EVA due to its low stiffness compared to other materials (Figure 4.22(b)). The sudden increase in the strain in EVA and PU gel at the start of the loading cycle shows the lower shock absorption ability compared to PAAm hydrogels and Silicone materials. The highest to lower creep recovery at the unloading period was shown by Silicone, PAAm, PU gel, and EVA respectively.

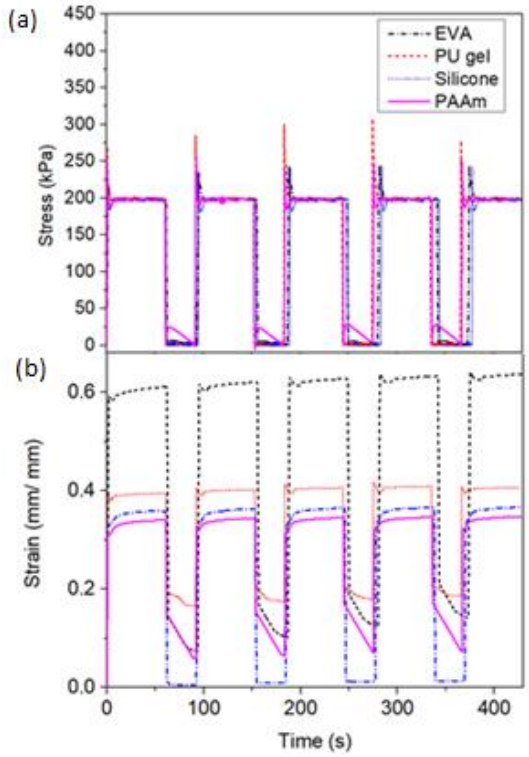

Figure 4.22: The repeat creep of EVA, PU gel, Silicone, and SN PAAm hydrogels (Standard deviation:0.011) (a) variation of stress with time (b) Variation of strain with time

4.4.4 Shear

The fracture shear stress and average shear modulus values of DN PAA hydrogel were 82±3% kPa at 0.84 strain and 74±3% kPa respectively. The PAAm hydrogel showed fracture shear stress of 83±3% kPa at the strain of 4 and an average shear modulus of 18±3% kPa (Figure 4.23). This result is compatible with the PAAm hydrogel shear modulus tested by Yeung et al [127]. This showed shear modulus variation between 10 Pa to 50 kPa for different compositions of AAm and MBA. Shear modulus of the subcalcaneal soft tissue range from 18 kPa to 124 kPa [42] indicating shear modulus of SN PAAm hydrogels giving protection for tissue damage due to lower shear modulus of 19.8 kPa (Table 4.8) by reducing initial effect before soft tissue deformation. The higher shear modulus of EVA material shows the inability to create a ball-bearing effect [56] on the foot during shear.

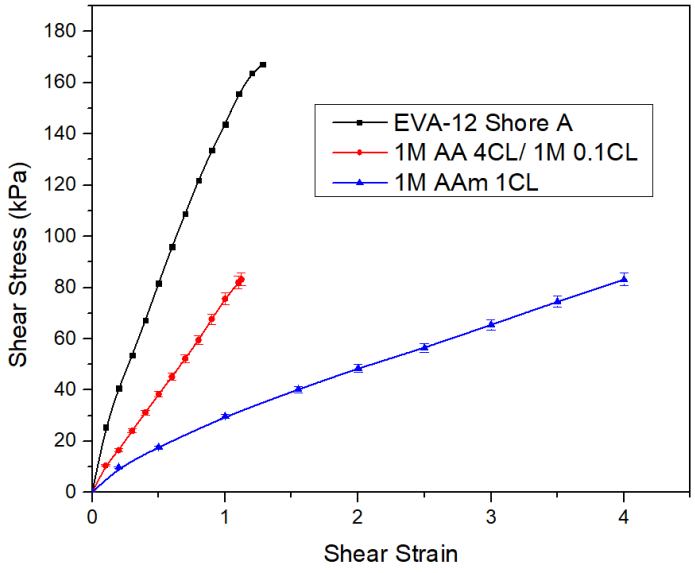

Figure 4.23: DN PAA (Swelling 60%)and SN PAAm (Swelling 50%) hydrogels shear stress variation with strain: Error percentage 3%, Crosshead speed 5 mm/min.

Table 4.8: Shear modulus of hydrogels and EVA

Material	Shear modulus (kPa)	The standard error (kPa)
EVA	128.7	4.1
PAA	72.0	0.63
PAAm	19.8	0.75

4.4.5 Rebound Resilience

The impact forces are applied on the insoles during heel strike heel-strike peak that occurs at the first stage of human stance. The rebound resilience of hydrogel was compared with EVA, Silicone rubber, and PU gel (Table 4.9). The lowest rebound height (highest shock absorption) was given by the SN PAAm hydrogel sample. It could be observed a 62% reduction in rebound resilience of 5 mm PAAm hydrogel compared to 5 mm EVA. The high viscous component of hydrogel contributed to absorbing high impact energy compared to other insole materials.

Table 4.9: Rebound resilience values comparison between hydrogel and insole materials

Material	Manufacturer	Thickness (mm)	Rebound resilience (%)	Hardness (Shore A)
EVA foam	DSI Samson Group, Colombo, Sri Lanka	4	32±1	20
EVA foam		5	34±1	12
EVA foam		6	38±1	20
EVA foam		10	55±1	10
Silicone	Oppo Medical Inc, USA.	5	35±1	7
PU gel	SIDAS, Voiron, France	4	35±1	5
PU gel		8	55±1	
DN PAA hydrogel	-	5±0.2	21±1	5
DN PAA hydrogel	-	7±0.2	23±1	
SN PAAm hydrogel	-	5±0.2	13±1	-
SN PAAm hydrogel	-	7.5±0.2	28±1	-

4.5 Pressure redistribution properties comparison with pressure insole readings

During the pressure insole test, a maximum 200 N constant load was applied using the universal testing machine (Figure 4.24). The no insole maximum stress of 698 ±10% kPa within the range of diabetic barefoot maximum stress [45] was reduced below recommended 200 kPa [54] when EVA and PAAm hydrogel insole was used. The PAAm hydrogel with 7 mm thickness showed an 11.5% reduction in mean peak pressure compared to the 7 mm thick silicone rubber insole. The comparison of 5 mm thickness EVA and PAAm showed that EVA material has a 9% lower mean peak pressure this is mainly due to the low hardness of EVA. When the thickness of the PAAm hydrogel was increased to 7 mm, the average peak pressure of PAAm showed a 1% lower value than EVA (Figure 4.25).

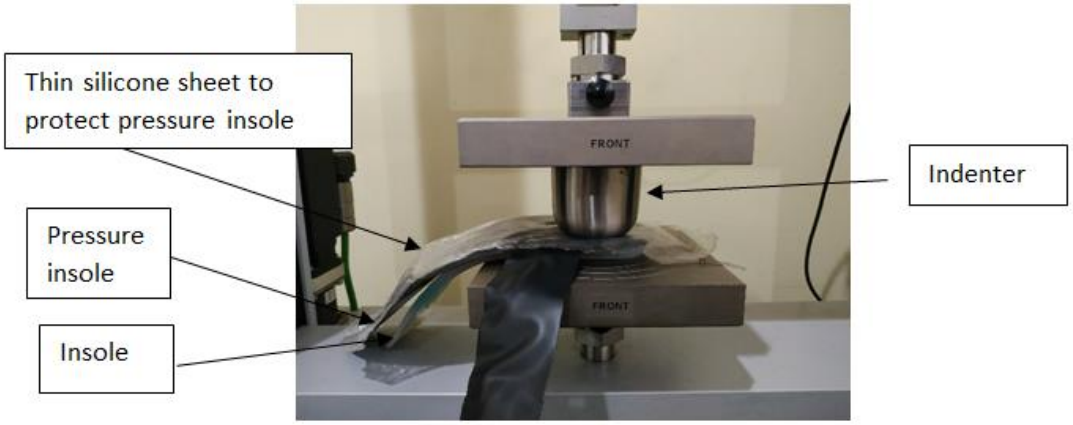

Figure 4.24: Testing different insole materials pressure distribution with Tactilus pressure sensor under the constant load of the indenter.

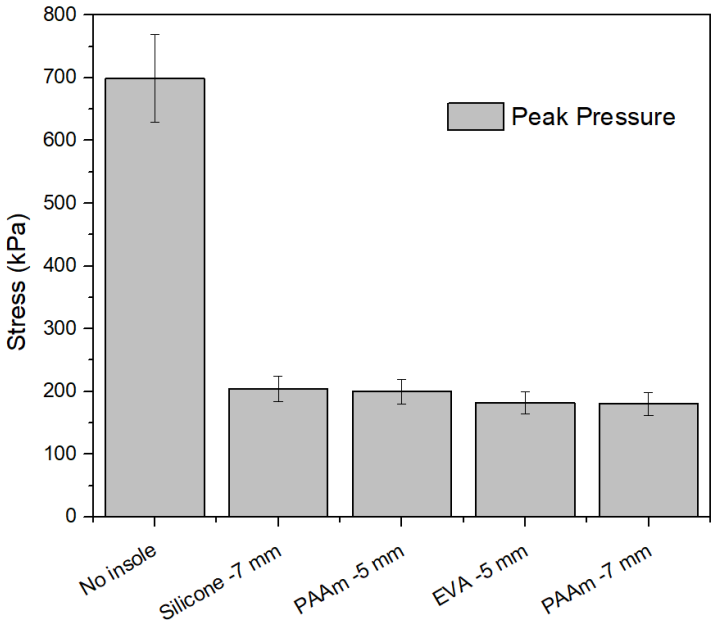

Figure 4.25: Variation of peak pressure of PAAm hydrogel and other insole materials.

4.6 Finite element analysis

4.6.1 Material model development

According to the similarity of the theoretical curve shown in Fig 2.4 (c) and the test results are shown in Fig 4.7, Fig 4.8, and Fig 4.9, stress-strain behaviour showed the hyperelastic nature. Further, the time-dependent stress-strain relationship of viscous material showed in (2.5) proved by the creep curves and stress relaxation curves shown in Fig 4.11and Fig 4.12 respectively. The behaviour of hydrogel showed an initial hyperelastic (large strain) followed by a time-dependent strain (assumed to be zero volume loss), under creep compression loading. Hence the PAAm hydrogel behaviour can be considered as hyper-viscoelastic. A similar model was used by Külcü [177] and Lei et al [178]. The model parameters were determined by fitting with the experimental results (Table 4.10) and the Ogden hyperelastic material model was selected based on stability and least deviation from the experimental curve. The FEA model was created as unconfined compression and the element type was CAX4H (4-node bilinear axisymmetric quadrilateral, hybrid, constant pressure). The hydrogel sample with 19.5±0.5 mm diameter and 5 mm thickness was compressed between two plates as

shown in Figure 4.27(a). The Ogden hyperelastic material model coefficients were calculated in Abaqus finite element analysis software [152] based on experimental test data.

The Ogden hyperelastic material model shows close agreement with the experimental stress-strain curve (Figure 4.26) indicating hyperelastic behaviour of the hydrogel sample. The Ogden hyperelastic model with N=3 parameters consisted of μ_1=3.47, α_1=5.03, μ_2=2.32, α_2=6.02, μ_3=1.25, α_3=2.82, D_1=0, D_2=0 and D_3=0.

The viscoelastic material model coefficients, g_i Prony =0.6, k_i Prony=0.4, and tau_i Prony=60, curve fit with stress relaxation curve indicating the viscoelastic behaviour of the sample (Figure 4.27(d)). The experimental average stress of 335.6 kPa matches the average FEA stress of 335.8 kPa (SD 95.85 kPa) when the friction coefficient was 0.4 (Figure 4.27 (b) and (c)).

Table 4.10: Experimental compression data used for FEA hyperelastic model

Strain	Stress (MPa)
0	0
0.1	0.017
0.2	0.0496
0.3	0.0983
0.4	0.1916
0.5	0.382
0.6	0.7508

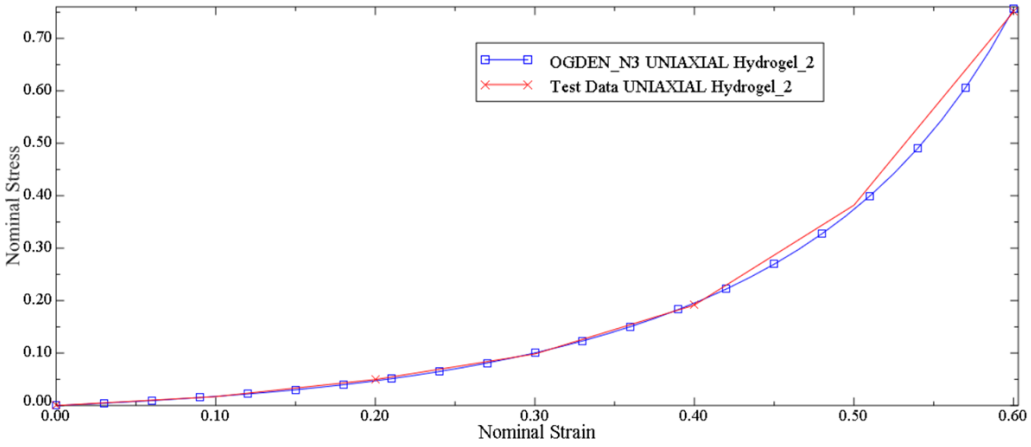

Figure 4.26: The Ogden hyperelastic N=3 and experimental curve fittings.

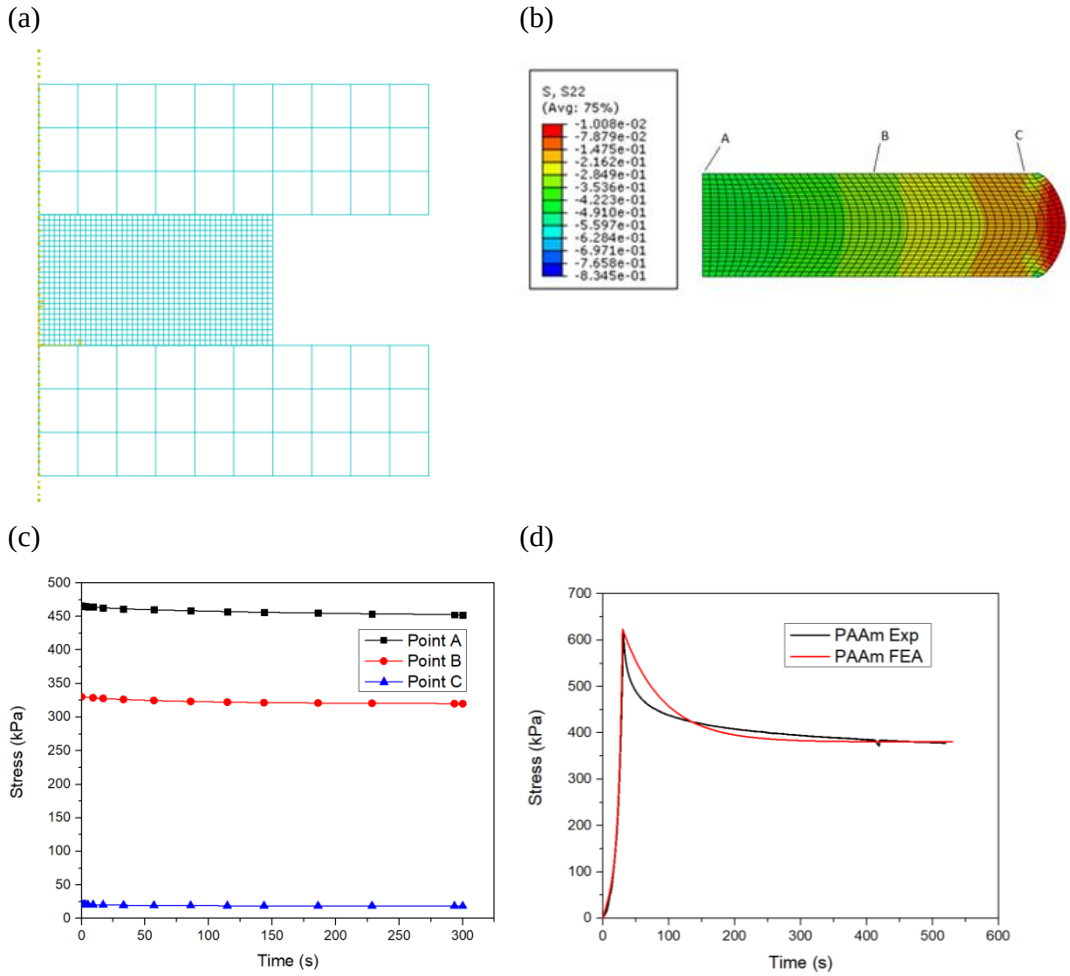

Figure 4.27: (a) the FEA model arrangement used in parameter identification (b) FEA results under constant load (c) Stress values at A, B, and C points. (d) Stress relaxation curves fitting to identify relaxation parameters.

4.6.2 Verification of FEA model with pressure insole readings and peak pressure variation with thickness

The top surface of hydrogel and indenter contact was considered as frictionless due to the smooth surface of stainless steel indenter contact with hydrogel surface and the bottom surface was rough due to bottom plate rough surface contact with hydrogel bottom surface (Figure 4.28(a)). Figure 4.28(b) shows the FEA model for vertical stress variation for a 5 mm PAAm hydrogel sample. The stress vs time curves of the FEA model and pressure insole results (accuracy 10%-Table A.1)) overlap each other showing validity of the FEA model (Figure 4.28(c)). The expected stress of below 200 kPa can be achieved when the thickness of the PAAm hydrogel sample was above 6

mm under a constant force of 200N. Significant reduction in peak pressure can be observed up to 8 mm. the thickness increase beyond 8 mm does not reduce peak pressure significantly and may cause unbalance of the foot (Figure 4.28(d)). An increase in thickness from 5 mm to 10 mm in steps of 1 mm results in a reduction in peak pressure by 6.3%, 5.2%, 7.1%, 1.8%, and 4.2% respectively (Table 4.11).

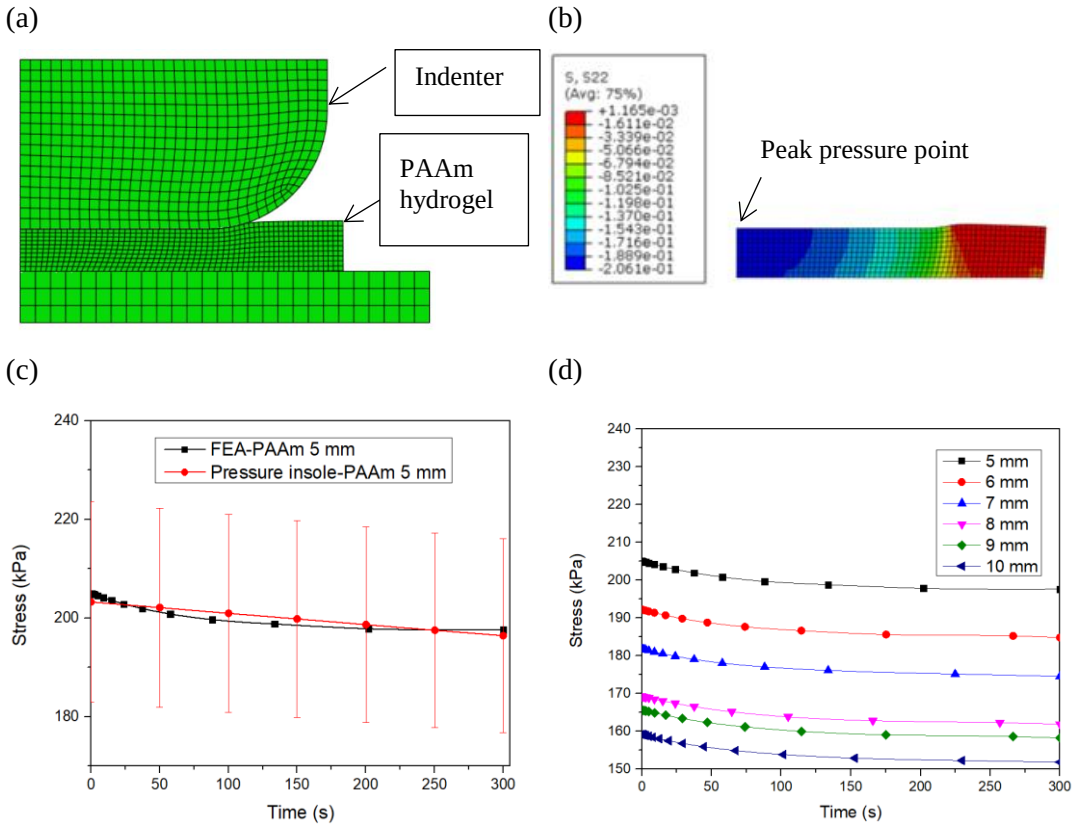

Figure 4.28: (a) FEA model to simulate pressure insole test arrangement. (b) FEA vertical pressure distribution for 5 mm thickness sample. (c) comparison of peak pressure variation with time for FEA model and pressure insole.

Table 4.11: Thickness and peak pressure values from FEA model

Thickness (mm)	Peak pressure (kPa)	Percentage reduction (%)
5	205	-
6	192	6.3
7	182	5.2
8	169	7.1
9	166	1.8
10	159	4.2

4.7 The thermal conductivity comparison

Warmer temperatures on soft tissue are prone to ulceration and the tissue resistance to breakdown is increased when cooled to 25°C to 28°C [179]. The low thermal conductive insulated diabetic footwear and repeated loading lead to high plantar tissue temperatures and an increased tendency to DFU. The faster gait resulted in higher temperature when EVA is used as insole material [180]. The comparison of Silicone EVA and PAAm hydrogel showed that PAAm hydrogel had the highest thermal conductivity (Table 4.12).

Table 4.12: Thermal conductivity of PAAm hydrogel, EVA, and Silicone rubber

Material	**Thermal conductivity (W/m .K)**	**Reference**
PAAm hydrogel	0.41 to 0.57 at 23% to 88% water content	[181]
Silicone rubber	0.20	[182]
EVA	0.11 to 0.13	[180]

Chapter 5

CONCLUSIONS

The overall aim of this project was the development and mechanical characterization of hydrogel-based insole material for diabetic feet based on experimental studies and finite element analysis models. The two types of hydrogels developed include double network polyacrylic acid (DN PAA) and single network polyacrylamide (SN PAAm) hydrogels. The compression strength of SN PAAM (900 kPa) was higher than the double network polyacrylic acid hydrogel (796 kPa). The fatigue cycles of DN PAA were limited to 3000 cycles compared to SN PAAm hydrogel which can withstand 20 000 cycles at maximum stress of 400 kPa. The non-linear stress vs strain curve in both PAA and PAAm hydrogels can be identified as hyper-elastic.

When the PAAm hydrogel samples were tested under friction, the desired stiffness of 155 kPa to 276 kPa at 50 % strain was achieved at 9.5 mm thickness but when the top and bottom surfaces were lubricated with silicone oil, the samples showed lowering stress to below 200 kPa and thickness independent stress values at a given strain.

The finite element results showed that the peak pressure reduction can be observed with the increase of thickness. The 5mm to 10 mm thickness PAAm hydrogel modelled in ABAQUS finite element software showed that peak pressure reduction below 200 kPa can be observed above 6 mm thickness. The recommended thickness of PAAm hydrogel was 8 mm for effective pressure distribution.

PAA, PAAm, SIDAS® PU gel, and EVA samples did not show any significant variation in stiffness with the crosshead speed of compression. This strain rate-independent elastic behaviour was probably due to the selection of high crosshead speeds between 10 mm/ min to 200 mm/ min but the stress relaxation curves showed

the viscoelastic nature. These materials can be considered as hyper-viscoelastic by considering both non-linear hyperelastic and viscoelastic behaviours.

The highest stress relaxation property was shown by PAAm hydrogels when compared with other insole materials. The repeated stress relaxation test showed deterioration of stress relaxation property in PUGel, silicone, and EVA material. The slowdown of shape recovery rate or residual permanent deformation of EVA material could be visible during the unloading cycle when compared with PAAm hydrogels. The constant strain value and lowest stress value at the end of the relaxation period prove the better recoverable and viscoelastic property of PAAm hydrogel. The creep test showed the better shock absorption property of PAAm hydrogel and Silicone rubber compared to EVA and PU gel at impulsive loading.

The maximum stress acting on diabetic foot is 200 kPa and the number of steps per day is 2000. The highest risk time for re-ulceration is the first 20-30 days after healing an ulcer. The SN PAAm is an insole material for diabetic feet capable of withstanding for more than 20 days under maximum stress conditions of diabetic feet by providing additional benefits of better pressure redistribution, suitable shear properties, and high thermal conductivity.

Future Perspectives

The improvement of fatigue strength and minimizing drying of PAAm hydrogel are the main two properties to be considered. Adding humectants such as glycerin, applying a coating or polymer seal on hydrogel are suggested as a solution for drying. The addition of glycerine would reduce the compression strength and fatigue life even though it prevents the drying of the hydrogel. On the other hand, the addition of polymer seals such as polyurethane sheath would improve the fatigue life. The combined solution of glycerine added hydrogel with sealing is suggested to be tested for strength and fatigue life as a future improvement.

The options for the improvement of fatigue life of SN PAAm hydrogel include recent research developments of adding nanoparticles such as montmorillonite nanoclay and cellulose. The tough hydrogels such as dually crosslinked single network

PAAm/ PVA hydrogels are suggested to be tested according to the procedure given in the thesis.

References

[1] L. Prompers, M. Huijberts and J. Apelqvist, “High prevalence of ischaemia, infection and serious comorbidity in patients with diabetic foot disease in Europe. Baseline results from the Eurodiale Study.,” *Diabetologia,* vol. 50, no. 1, p. 18–25., 2007.

[2] K. Bakker, J. Apelqvist and N. C. Schaper, “International Working Group on Diabetic Foot Editorial B. Practical guidelines on the management and prevention of the diabetic foot 2011. ;,” *Diabetes Metab Res Rev,* vol. 28, no. 1, p. 225–231, 2012.

[3] J. M. Andrew, M. Boulton, S. Robert, M. D. Kirsner and M. D. Loretta Vileikyte, “Neuropathic diabetic foot ulcers. ; (1):,” *New Eng J Med,* vol. 351, no. 1, p. 48–55, 2004.

[4] International Diabetetes Federation, “IDF Diabetes Atlas Ninth edition 2019,” 2019.

[5] A. Healy, R. Naemi and N. Chockalingam, “The effectiveness of footwear as an intervention to prevent or to reduce biomechanical risk factors associated with diabetic foot ulceration: A systematic review,” *Journal of Diabetes and its Complications,* vol. 27, no. 4, pp. 391-400, 2013.

[6] N. Pound, S. Chipchase, K. Treece, F. Game and W. Jeffcoate, “Ulcer-free survival following management of foot ulcers in diabetes,” *Diabetic Medicine,* vol. 22, no. 10, pp. 1306-1309, 2005.

[7] S. A. Bus, R. Waaijman, M. Arts, M. de Haart, T. Busch-Westbroek, J. van Baal and F. Nollet, “Effect of Custom-Made Footwear on Foot Ulcer Recurrence in Diabetes: A multicenter randomized controlled trial,” *Diabetes Care,* vol. 36, no. 12, pp. 4109-4116, 2013.

[8] T. Ziegler, “3D printing: customized insoles for diabetes patients,” fraunhofer, 2 Nov 2016. [Online]. Available: https://www.fraunhofer.de/en/press/research-news/2016/november/3d-printing--customized-insoles-for-diabetes-patients.html. [Accessed 27 Oct 2017].

[9] W. P. Chen, C. W. Ju and F. T. Tang, “Effects of total contact insoles on the plantar stress redistribution: a finite element analysis,” *Clinical biomechanics,* vol. 18, no. 6, p. S17–S24, 2003.

[10] S. A. Bus, “The Role of Pressure Offloading on Diabetic Foot Ulcer Healing and Prevention of Recurrence,” *Plastic and Reconstructive Surgery,* vol. 138, no. 3S, pp. 179S-187S, 2016.

[11] J. J. Holewski, K. M. Moss, R. M. Stess, P. M. Graf and C. Grunfeld, “Prevalence of foot pathology and lower extremity complications in a diabetic outpatient clinic,” *J Rehabil Res Dev,* vol. 26, no. 3, pp. 35-44, 1989.

[12] M. C. Hodge, T. M. Bach and G. M. Carter, “Orthotic management of plantar pressure and pain in rheumatoid arthritis,” *Clinical Biomechanics,* vol. 14, pp. 567-75, 1999.

[13] H. Kato, T. Takada, T. Kawamura, N. Hotta and S. Torii, “The reduction and redistribution of plantar pressures using foot orthoses in diabetic patients,” *Diabetes Research and Clinical Practice,* vol. 31, pp. 115- 118, 1996.

[14] J. S. Paton, “A comparison of customised and prefabricated insoles to reduce risk factors for neuropathic diabetic foot ulceration: a participant-blinded randomised controlled trial,” *Journal of Foot and Ankle Research,* 2012.

[15] S. A. Bus, R. Van Deursen, D. Armstrong, J. Lewis, C. Caravaggi and P. Cavanagh, “Footwear and offloading interventions to prevent and heal foot ulcers and reduce plantar pressure in patients with diabetes: a systematic review,” *Diabetes/Metabolism Research and Reviews,* vol. 32, pp. 99-118, 2016.

[16] L. Huppin, “A new look at orthotics for diabetics,” Sep 2012. [Online]. Available: https://podiatrym.com/pm/Huppin912.pdf. [Accessed 27 Oct 2017].

[17] M. Curryer and E. D. Lemaire, “Effectiveness of various materials in reducing plantar shear forces. A pilot study,” *Journal of the American Podiatric Medical Association,* vol. 90, no. 7, pp. 346-353, 2000.

[18] J. Paton, R. B. Jones, E. Stenhouse and G. Bruce, “The Physical Characteristics of Materials Used in the Manufacture of Orthoses for Patients with Diabetes,” *Foot & Ankle International,* vol. 28, no. 10, pp. 1057-1063, 2007.

[19] G. Campbell, E. Newell and M. McLure, “Compression testing of foamed plastics and rubbers for use as orthotic shoe insoles,” *Prosthet Orthot Int.,* vol. 6, no. 1, pp. 48-52, 1982.

[20] L. Huppin, 2020. [Online]. Available: https://podiatrym.com/pdf/2020/8/Huppin920web.pdf.

[21] O. Wichterle and D. Lím, “Hydrophilic gels for biological use,” *Nature,* vol. 185, p. 117–118, 1960.

[22] J. Kopeček and J. Yang, “Hydrogels as smart materials,” *Polym Int,* 2007.

[23] Q. Chen, H. Chen, L. Zhua and J. Zheng, “Fundamentals of double network hydrogels,” *Journal of Materials Chemistry B,* vol. 3, no. 18, pp. 3654-3676, 2005.

[24] N. A. Peppas, P. Bures, W. Leobandung and H. Ichikawa, “Hydrogels in pharmaceutical formulations,” *European Journal of Pharmaceutics and Biopharmaceutics,* vol. 50, no. 1, pp. 27-46, 2000.

[25] C. Fleck, “Why “Wet to Dry”?,” *The Journal of the American College of Certified Wound Specialists,* vol. 1, no. 4, pp. 109-113, 2009.

[26] V. Jones, J. E. Grey and K. G. Harding, “Wound dressings,” *BMJ,* vol. 332, no. 7544, pp. 777-780, 2006.

[27] Wounds International and Systagenix;, “ADAPTIC TOUCH® Non-Adhering Silicone Dressing: case studies,” 2013.

[28] E. Caló and V. V. Khutoryanskiy, “Biomedical applications of hydrogels: A review of patents and commercial products,” *European Polymer Journal,* vol. 65, pp. 252-267, 2015.

[29] C. Weller, “Interactive dressings and their role in moist wound management,” *Advanced Textiles for Wound Care,* pp. 97-113, 2009.

[30] W. R. Spence, R. D. Burk and J. W. J. Rae, “Gel support for prevention of decubitus ulcers,” *Arch Phys Med Rehabil.,* vol. 48, no. 6, pp. 283-288, 1967.

[31] J. Cheung and M. Zhang, “A 3-dimensional finite element model of the human foot and ankle for insole design,” *Archives of Physical Medicine and Rehabilitation,* vol. 86, no. 2, pp. 353-358, 2005.

[32] B. Kathirgamanathan, P. Silva and J. Fernandez, “Implication of obesity on motion, posture and internal stress of the foot: an experimental and finite element analysis,” *Computer Methods in Biomechanics and Biomedical Engineering,* vol. 22, no. 1, pp. 47-54, 2018.

[33] D. Caccavo and G. Lamberti, “PoroViscoElastic model to describe hydrogels' behavior,” *Materials Science and Engineering: C,* vol. 76, pp. 102-113, 2017.

[34] P. E. Chatzistergos, R. Naemi, A. Healy, P. Gerth and N. Chockalingam, “Subject Specific Optimisation of the Stiffness of Footwear Material for Maximum Plantar Pressure Reduction,” *Annals of Biomedical Engineering,* vol. 45, no. 8, pp. 1929-1940, 2017.

[35] C. C. Hsu et al., “Diabetic effects on microchambers and macrochambers tissue properties in human heel pads,” *Clinical Biomechanics,* vol. 24, no. 8, pp. 682-686, 2009.

[36] A. Gefen, “Plantar soft tissue loading under the medial metatarsals in the standing diabetic foot,” *Medical Engineering & Physics,* vol. 25, no. 6, pp. 491-499, 2003.

[37] M. H. Jahss et al, “Investigations into the Fat Pads of the Sole of the Foot: Anatomy and Histology,” *Foot & Ankle,* vol. 13, no. 5, pp. 233-242, 1992.

[38] B. Derby and R. Akhtar, Mechanical properties of aging soft tissues, Springer, 2014.

[39] Y. N. Wang, K. Lee and W. R. Ledoux, “Histomorphological Evaluation of Diabetic and Non-Diabetic Plantar Soft Tissue,” *Foot & Ankle International,* vol. 32, no. 8, pp. 802-810, 2011.

[40] C. Y. L. Chao, Y. Zheng and G. L. Y. Cheing, “Epidermal Thickness and Biomechanical Properties of Plantar Tissues in Diabetic Foot,” *Ultrasound in Medicine & Biology,* vol. 37, no. 7, pp. 1029-1038, 2011.

[41] S. Pai and W. R. Ledoux, “The compressive mechanical properties of diabetic and non-diabetic plantar soft tissue,” *Journal of Biomechanics,* vol. 43, no. 9, pp. 1754-1760, 2010.

[42] S. Pai and W. R. Ledoux, “The shear mechanical properties of diabetic and non-diabetic plantar soft tissue,” *Journal of Biomechanics,* vol. 45, no. 2, pp. 364-370, 2012.

[43] L. Fernández-Seguín, J. Diaz Mancha, R. Sánchez Rodríguez, E. Escamilla Martínez, B. Gómez Martín and J. Ramos Ortega, “Comparison of plantar pressures and contact area between normal and cavus foot,” *Gait & Posture,* vol. 39, no. 2, pp. 789-792, 2014.

[44] T. M. Owings et al, “Plantar pressures in diabetic patients with foot ulcers which have remained healed,” *Diabetic Medicine,* vol. 26, no. 11, pp. 1141-1146, 2009.

[45] M. Yavuz et al., “Plantar Shear Stress in Individuals With a History of Diabetic Foot Ulcer: An Emerging Predictive Marker for Foot Ulceration,” *Diabetes Care,* vol. 40, no. 2, pp. e14-e15, 2016.

[46] S. Stucke et al., “Spatial relationships between shearing stresses and pressure on the plantar skin surface during gait,” *Journal of Biomechanics,* vol. 45, no. 3, pp. 619-622, 2012.

[47] S. Wu, R. Crews and D. Armstrong, “The pivotal role of offloading in the management of neuropathic foot ulceration,” *Current Diabetes Reports,* vol. 5, no. 6, pp. 423-429, 2005.

[48] L. A. Lavery, J. G. Fleishli, T. J. Laughlin, S. A. Vela, D. C. Lavery and D. G. Armstrong, “Is postural instability exacerbated by off-loading devices in high risk diabetics with foot ulcers?,” *Ostomy Wound Manage,* vol. 44, no. 1, pp. 26-32, 1998.

[49] P. Chakraborty, S. Ray, D. Biswas, A. Baidya, R. Bhattacharjee, P. Mukhopadhyay, S. Ghosh, S. Mukhopadhyay and S. Chowdhury, “A Comparative Study Between Total Contact Cast and Pressure-Relieving Ankle Foot Orthosis in Diabetic Neuropathic Foot Ulcers,” *Journal of Diabetes Science and Technology,* vol. 9, no. 2, pp. 302-308, 2014.

[50] S. Bus, J. Ulbrecht and P. Cavanagh, “Pressure relief and load redistribution by custom-made insoles in diabetic patients with neuropathy and foot deformity,” *Clinical Biomechanics,* vol. 19, no. 6, pp. 629-638, 2004.

[51] A. Sarikhani, A. Motalebizadeh, S. Asiaei and B. K. D. Azad, “Studying Maximum Plantar Stress per Insole Design Using Foot CT-Scan Images of Hyperelastic Soft Tissues,” *Applied Bionics and Biomechanics,* vol. 2016, pp. 1-6, 2016.

[52] K. Mills, P. Blanch and B. Vicenzino, “Influence of Contouring and Hardness of Foot Orthoses on Ratings of Perceived Comfort,” *Medicine & Science in Sports & Exercise,* vol. 43, no. 8, pp. 1507-1512, 2011.

[53] A. Martinez-Santos, S. Preece and C. J. Nester, “Evaluation of orthotic insoles for people with diabetes who are at-risk of first ulceration,” *Journal of Foot and Ankle Research,* vol. 12, no. 1, 2019.

[54] N. C. Schaper, J. J. V. Netten, J. Apelqvist, S. A. Bus, R. J. Hinchlife and B. A. Lipsky, 2019. [Online]. Available: https://iwgdfguidelines.org/wp-content/uploads/2019/05/IWGDF-Guidelines-2019.pdf.

[55] J. P. Pollard, L. P. Le Quesne and J. W. Tappin, “Forces under the foot,” *Journal of Biomedical Engineering,* vol. 5, no. 1, pp. 37-40, 1983.

[56] W. R. Spence and M. N. Shields, “Prevention of blisters, callosities and ulcers by absorption of shear forces,” *Journal of the American Podiatric Medical Association,* vol. 58, no. 10, pp. 428-434, 1968.

[57] C. Leber and P. M. Evanski, “A comparison of shoe insole materials in plantar pressure relief,” *Prosthetics and Orthotics International,* vol. 10, no. 3, pp. 135-138, 1986.

[58] J. W. K. Tong and E. Y. K. Ng, “Preliminary investigation on the reduction of plantar loading pressure with different insole materials (SRP – Slow Recovery Poron®, P – Poron®, PPF – Poron®+Plastazote, firm and PPS – Poron®+Plastazote, soft),” *The Foot,* vol. 20, no. 1, pp. 1-6, 2010.

[59] O. Mohamed, K. Cerny, L. Rojek, K. Herbert, R. Turner and S. Waistell, “The Effects of Plastazote and Aliplast /Plastazote Orthoses on Plantar Pressures in Elderly Persons With Diabetic Neuropathy,” *JPO Journal of Prosthetics and Orthotics,* vol. 16, no. 2, pp. 55-63, 2004.

[60] D. J. Lott, M. K. Hastings, P. K. Commean, K. E. Smith and M. J. Mueller, “Effect of footwear and orthotic devices on stress reduction and soft tissue strain of the neuropathic foot,” *Clinical Biomechanics,* vol. 22, no. 3, pp. 352-359, 2007.

[61] W. T. Lo, K. L. Yick, S. P. Ng and J. Yip, “New methods for evaluating physical and thermal comfort properties of orthotic materials used in insoles for patients with diabetes,” *Journal of Rehabilitation Research and Development,* vol. 51, no. 2, pp. 311-324, 2014.

[62] R. Patwa, N. Saha and P. Saha, “Magnetic hydrogel based shoe insoles for prevention of diabetic foot,” *Journal of Magnetism and Magnetic Materials,* vol. 514, p. 167153, 2020.

[63] E. Kerman, “New Approach to Foot Orthotics Materials: Hydrogel Insoles,” The university of British Columbia, Okanagam, 2020.

[64] A. C. Faulí, C. L. Andrés, N. P. Rosas, M. J. Fernández, E. M. Parreño and C. O. Barceló, “Physical Evaluation of Insole Materials Used to Treat the Diabetic Foot,” *Journal of the American Podiatric Medical Association,* vol. 98, no. 3, pp. 229-238, 2008.

[65] A. Requena, 2008. [Online]. Available: http://biomechconsulting.com/wp-content/uploads/2016/11/BIOMECH-BI002.pdf.

[66] U. H. Tang et al, “Comparison of plantar pressure in three types of insole given to patients with diabetes at risk of developing foot ulcers – A two-year, randomized trial,” *Journal of Clinical & Translational Endocrinology,* vol. 1, no. 4, pp. 121-132, 2014.

[67] M. Yavuz et al., “Temperature as a predictive tool for plantar triaxial loading,” *Journal of Biomechanics,* vol. 47, no. 15, pp. 3767-3770, 2014.

[68] D. G. Armstrong, K. Holtz-Neiderer, C. Wendel, M. J. Mohler, H. .. Kimbriel and L. A. Lavery, “Skin Temperature Monitoring Reduces the Risk for Diabetic Foot Ulceration in High-risk Patients,” *The American Journal of Medicine,* vol. 120, no. 12, pp. 1042-1046, 2007.

[69] J. S. Wrobel et al, “A Novel Shear Reduction Insole Effect on the Thermal Response to Walking Stress, Balance, and Gait,” *Journal of Diabetes Science and Technology,* vol. 8, no. 6, pp. 1151-1156, 2014.

[70] R. A. Nardin, P. M. Fogerson, R. Nie and S. B. Rutkove, “Foot Temperature in Healthy Individuals,” *Journal of the American Podiatric Medical Association,* vol. 100, no. 4, pp. 258-264, 2010.

[71] S. Bagavathiappan et al., “Correlation between Plantar Foot Temperature and Diabetic Neuropathy: A Case Study by Using an Infrared Thermal Imaging Technique,” *Journal of Diabetes Science and Technology,* vol. 4, no. 6, pp. 1386-1392, 2010.

[72] N. Papanas, K. Papatheodorou, D. Papazoglou, C. Monastiriotis and E. Maltezos, “Foot Temperature in Type 2 Diabetic Patients with or without Peripheral Neuropathy,” *Experimental and Clinical Endocrinology & Diabetes,* vol. 117, no. 1, pp. 44-47, 2008.

[73] P. N. Reddy, G. Cooper, A. Weightman, E. Hodson-Tole and N. D. Reeves, “Walking cadence affects rate of plantar foot temperature change but not final temperature in younger and older adults,” *Gait & Posture,* vol. 52, pp. 272-279, 2017.

[74] M. Hall, D. G. Shurr, M. B. Zimmerman and C. L. Saltzman, “Plantar Foot Surface Temperatures with Use of Insoles,” *The Iowa Orthopaedic Journal,* vol. 24, pp. 72-75, 2004.

[75] J. Gong, Y. Katsuyama, T. Kurokawa and Y. Osada, “Double-Network Hydrogels with Extremely High Mechanical Strength,” *Advanced Materials,* vol. 15, no. 14, pp. 1155-1158, 2003.

[76] J. Hu, K. Hiwatashi, T. Kurokawa, S. Liang, Z. Wu and J. Gong, “Microgel-Reinforced Hydrogel Films with High Mechanical Strength and Their Visible Mesoscale Fracture Structure,” *Macromolecules,* vol. 44, no. 19, pp. 7775-7781, 2011.

[77] Q. Chen, H. Chen, L. Zhu and G. Zhen, “Engineering of Tough Double Network Hydrogels,” *Macromolecular Chemistry and Physics,* vol. 217, no. 9, pp. 1022-1036, 2016.

[78] J. Tang, J. Li, J. J. Vlassak and Z. Suo, “Fatigue fracture of hydrogels,” *Extreme Mechanics Letters,* vol. 10, pp. 24-31, 2017.

[79] R. Bai et al., “Fatigue fracture of tough hydrogels,” *Extreme Mechanics Letters,* vol. 15, pp. 91-96, 2017.

[80] R. Bai, J. Yang, X. P. Morelle, C. Yang and Z. Suo, “Fatigue Fracture of Self-Recovery Hydrogels,” *ACS Macro Letters,* vol. 7, no. 3, pp. 312-317, 2018.

[81] J. Thomas, A. Shuen, A. Lowman and M. Marcolongo, “The effect of fatigue on associating hydrogels for nucleus pulposus replacement,” in *2003 IEEE 29th Annual Proceedings of Bioengineering Conference,* Newark, NJ, USA, 2003.

[82] J. Hu et al., “Functional compressive mechanics and tissue biocompatibility of an injectable SF/PU hydrogel for nucleus pulposus replacement,” *Scientific Reports,* vol. 7, no. 1, 2017.

[83] J. Stammen, S. Williams, D. Ku and R. Guldberg, “Mechanical properties of a novel PVA hydrogel in shear and unconfined compression,” *Biomaterials,* vol. 28, no. 19, pp. 2987-2993, 2007.

[84] A. Bassi, "Dynamic modulus of rubber by impact and rebound measurements," *Polymer Engineering and Science,* vol. 18, no. 10, pp. 750-754,, 1978.

[85] H. Yoo and H. Kim, "Synthesis and properties of waterborne polyurethane hydrogels for wound healing dressings," *Journal of Biomedical Materials Research Part B: Applied Biomaterials,* vol. 85B, no. 2, pp. 326-333, 2008.

[86] R. Udayanandana, P. Silva and T. Gunasekara, "Mechanical properties of double network poly (Acrylic Acid) based Hydrogels for potential use as a biomaterial," in *2019 41st Annual International Conference of the IEEE Engineering in Medicine and Biology Society (EMBC),* Berlin, 2019.

[87] M. Zhong et al, "Dually cross-linked single network poly(acrylic acid) hydrogels with superior mechanical properties and water absorbency," *Soft Matter,* vol. 12, no. 24, pp. 5420-5428, 2016.

[88] A. Pal, A. Giri and A. Bandyopadhyay, "Influence of hydrodynamic size and zeta potential of a novel polyelectrolyte poly(acrylic acid) grafted guar gum for adsorption of Pb(II) from acidic waste water," *Journal of Environmental Chemical Engineering,* vol. 4, no. 2, pp. 1731-1742, 2016.

[89] S. Sharma, A. Dua and A. Malik, "Superabsorbent Polymer Gels based on Polyaspartic Acid and Polyacrylic Acid," *Journal of Material Science & Engineering,* vol. 5, no. 3, pp. 1-7, 2016.

[90] S. Mammadova et al, "Synthesis, Structure and Swelling Properties of Hydrogels Based on Polyacrylic Acid," *Asian Journal of Chemistry,* vol. 29, no. 3, pp. 576-580, 2017.

[91] J. E. Elliott, M. Macdonald, J. Nie and C. N. Bowman, "Structure and swelling of poly(acrylic acid) hydrogels: effect of pH, ionic strength, and dilution on the crosslinked polymer structure," *Polymer,* vol. 45, no. 5, pp. 1503-1510, 2004.

[92] B. Işık, "Swelling behavior and determination of diffusion characteristics of acrylamide-acrylic acid hydrogels," *Journal of Applied Polymer Science,* vol. 91, no. 2, pp. 1289-1293, 2003.

[93] M. Yin, M. Yao, S. Gao, A. P. Zang, H. Tam and P. A. Wai, "Rapid 3D Patterning of Poly(acrylic acid) Ionic Hydrogel for Miniature pH Sensors," *Advanced Materials,* vol. 28, no. 7, pp. 1394-1399, 2015.

[94] J. You et al., "Quaternized Chitosan/Poly(acrylic acid) Polyelectrolyte Complex Hydrogels with Tough, Self-Recovery, and Tunable Mechanical Properties," *Macromolecules,* vol. 49, no. 3, pp. 1049-1059, 2016.

[95] G. He et al., "Preparation and properties of quaternary ammonium chitosan-g-poly(acrylic acid-co-acrylamide) superabsorbent hydrogels," *Reactive and Functional Polymers,* vol. 111, pp. 14-21, 2017.

[96] M. I. Sujan et al., "Bi-functional silica nanoparticles for simultaneous enhancement of mechanical strength and swelling capacity of hydrogels," *RSC Advances,* vol. 10, no. 11, pp. 6213-6222, 2020.

[97] J. A. Wiersma, M. Bos and A. J. Pennings, "High strength poly(meth)acrylamide copolymer hydrogels," *Polymer Bulletin,* vol. 33, no. 6, pp. 615-622, 1994.

[98] E. A. Smith, S. L. Prues and F. W. Oehme, "Environmental Degradation of Polyacrylamides," *Ecotoxicology and Environmental Safety,* vol. 37, no. 1, pp. 76-91, 1997.

[99] J. Kroschwitz and H. Mark, "Encyclopedia of polymer science and engineering," New York, Wiley, 1985, p. 171.

[100] S. Ronken et al, "A comparison of healthy human and swine articular cartilage dynamic indentation mechanics," *Biomechanics and Modeling in Mechanobiology,* vol. 12, no. 2, pp. 243-248, 2012.

[101] J. Wang, L. Lou and J. Qiu, "Super-tough hydrogels using ionically crosslinked networks," *Journal of Applied Polymer Science,* vol. 136, no. 44, p. 48182, 2019.

[102] N. Orakdogen and O. Okay, "Correlation between crosslinking efficiency and spatial inhomogeneity in poly(acrylamide) hydrogels," *Polymer Bulletin,* vol. 57, no. 5, pp. 631-641, 2006.

[103] W. Funke, O. Okay and B. Joos-Muller, "Intramolecularly crosslinked macromolecules with a globular structure," *Advances in Polymer Science,* pp. 139-234, 1998.

[104] Scientific, Fisher, May 2007. [Online]. Available: https://fscimage.fishersci.com/msds/90858.htm. [Accessed 6 August 2020].

[105] I. Gupta, R. S. Tomar, A. K. Nagpal and R. Singhal, "Synthesis and characterization of poly(AAm-co-BMA-co-AAc) hydrogels: effect of acrylamide content on swelling behaviour," *Designed Monomers and Polymers,* vol. 9, no. 6, pp. 589-605, 2006.

[106] W. Y. Chiu, G. M. Carratt and D. S. Soong, "A computer model for the gel effect in free-radical polymerization," *Macromolecules,* vol. 16, no. 3, pp. 348-357, 1983.

[107] R. Chen et al., "Temperature-regulated flexibility of polymer chains in rapidly self-healing hydrogels," *NPG Asia Materials,* vol. 11, no. 1, 2019.

[108] B. H. Cipriano et al, "Superabsorbent Hydrogels That Are Robust and Highly Stretchable," *Macromolecules,* vol. 47, no. 13, pp. 4445-4452, 2014.

[109] S. B. Ross-Murphy and S. Todd, "Ultimate tensile measurements of filled gelatin gels," *Polymer,* vol. 24, no. 3, pp. 481-486, 1983.

[110] B. D. Johnson, D. Beebe and W. C. Crone, "Effects of swelling on the mechanical properties of a pH-sensitive hydrogel for use in microfluidic devices," *Materials Science and Engineering: C,* vol. 24, no. 4, pp. 575-581, 2004.

[111] P. J. Flory and J. Rehner, "Statistical Mechanics of Cross-Linked Polymer Networks I. Rubberlike Elasticity," *The Journal of Chemical Physics,* vol. 11, no. 11, pp. 512-520, 1943.

[112] K. Daizo, S. Yujiro, S. Kiyoshi, S. Masaji and O. Masahide, "method of drying a hydrogel". United states of America Patent US3290790A, 1964.

[113] I. Yazici and O. Okay, "Spatial inhomogeneity in poly(acrylic acid) hydrogels," *Polymer,* vol. 46, no. 8, pp. 2595-2602, 2005.

[114] M. M. Fitzgerald, K. Bootsma, J. A. Berberich and J. L. Sparks, "Tunable Stress Relaxation Behavior of an Alginate-Polyacrylamide Hydrogel: Comparison with Muscle Tissue," *Biomacromolecules,* vol. 16, no. 5, pp. 1497-1505, 2015.

[115] M. L. Oyen, "Mechanical characterisation of hydrogel materials," *International Materials Reviews,* vol. 59, no. 1, pp. 44-59, 2013.

[116] M. Shibayama, "Spatial inhomogeneity and dynamic fluctuations of polymer gels," *Macromolecular Chemistry and Physics,* vol. 199, no. 1, pp. 1-30, 1998.

[117] F. Schosseler, F. Ilmain and S. J. Candau, "Structure and properties of partially neutralized poly(acrylic acid) gels," *Macromolecules,* vol. 24, no. 1, pp. 225-234, 1991.

[118] M. Y. Kizilay and O. Okay, "Effect of Initial Monomer Concentration on Spatial Inhomogeneity in Poly(acrylamide) Gels," *Macromolecules,* vol. 36, no. 18, pp. 6856-6862, 2003.

[119] W. Zhang et al, "Fatigue of double-network hydrogels," *Engineering Fracture Mechanics,* vol. 187, pp. 74-93, 2018.

[120] R. E. Webber, C. Creton, H. R. Brown and J. P. Gong, "Large Strain Hysteresis and Mullins Effect of Tough Double-Network Hydrogels," *Macromolecules,* vol. 40, no. 8, 2007.

[121] T. Zhang, S. Lin, H. Yuk and X. Zhao, "Predicting fracture energies and crack-tip fields of soft tough materials," *Extreme Mechanics Letters,* vol. 4, pp. 1-8, 2015.

[122] R. S. Rivlin and A. G. Thomas, "Rupture of rubber. I. Characteristic energy for tearing," *Journal of Polymer Science,* vol. 10, no. 3, pp. 291-318, 1953.

[123] N. Zhang, Z. Pan, J. Lei and Z. Liu, "Effects of temperature on the fracture and fatigue damage of temperature sensitive hydrogels," *RSC Advances,* vol. 8, no. 54, pp. 31048-31054, 2018.

[124] G. J. Lake and A. G. Thomas, "The strength of highly elastic materials," *Proceedings of the Royal Society of London. Series A, Mathematical and Physical Sciences,* vol. 300, no. 1460, pp. 108-119, 1967.

[125] F. A. Morrison, Understanding Rheology, Don Mills: Oxford University Press, 2001.

[126] J. M. Zuidema, C. J. Rivet, R. J. Gilbert and F. A. Morrison, "A protocol for rheological characterization of hydrogels for tissue engineering strategies," *Journal of Biomedical Materials Research Part B: Applied Biomaterials,* vol. 102, no. 5, pp. 1063-1073, 2013.

[127] T. Yeung et al., "Effects of substrate stiffness on cell morphology, cytoskeletal structure, and adhesion," *Cell Motility and the Cytoskeleton,* vol. 60, no. 1, pp. 24-34, 2004.

[128] X. Zhao, N. Huebsch, D. J. Mooney and Z. Suo, "Stress-relaxation behavior in gels with ionic and covalent crosslinks," *Journal of Applied Physics,* vol. 107, no. 6, pp. 063509-1-5, 2010.

[129] Q. M. Wang, A. C. Mohan, M. L. Oyen and X. H. Zhao, "Separating viscoelasticity and poroelasticity of gels with different length and time scales," *Acta Mechanica Sinica,* vol. 30, no. 1, pp. 20-27, 2014.

[130] D. F. Williams, The Williams dictionary of biomaterials, Liverpool: Liverpool University Press, 1999.

[131] Y. Ikada, "Biocompatibility of hydrogels," in *Gels Handbook*, San Diego [u.a.], Academic Pr, 2001, pp. 388-407.

[132] B. V. Slaughter, S. S. Khurshid, O. Z. Fisher, A. Khademhosseini and N. A. Peppas, "Hydrogels in Regenerative Medicine," *Advanced Materials,* vol. 21, no. 32-33, pp. 3307-3329, 2009.

[133] D. N. Shah, S. M. Recktenwall-Work and K. S. Anseth, "The effect of bioactive hydrogels on the secretion of extracellular matrix molecules by valvular interstitial cells," *Biomaterials,* vol. 29, no. 13, pp. 2060-2072, 2008.

[134] M. F. Passos et al, "PHEMA Hydrogels Obtained by Infrared Radiation for Cartilage Tissue Engineering," *International Journal of Chemical Engineering,* vol. 2019, pp. 1-9, 2019.

[135] S. Jiang, S. Liu and W. Feng, "PVA hydrogel properties for biomedical application," *Journal of the Mechanical Behavior of Biomedical Materials,* vol. 4, no. 7, pp. 1228-1233, 2011.

[136] M. Parlato, S. Reichert, N. Barney and W. L. Murphy, "Poly(ethylene glycol) Hydrogels with Adaptable Mechanical and Degradation Properties for Use in Biomedical Applications," *Macromolecular Bioscience,* vol. 14, no. 5, pp. 687-698, 2014.

[137] X. Xu, A. K. Jha, D. A. Harrington, M. C. Farach-Carson and X. Jia, "Hyaluronic acid-based hydrogels: from a natural polysaccharide to complex networks," *Soft Matter,* vol. 8, no. 12, p. 3280–3294, 2012.

[138] D. Saraydın, S. Ünver-Saraydın, E. Karadağ, E. Koptagel and O. Güven, "In vivo biocompatibility of radiation crosslinked acrylamide copolymers," *Nuclear Instruments and Methods in Physics Research Section B: Beam Interactions with Materials and Atoms,* vol. 217, no. 2, pp. 281-292, 2004.

[139] M. V. Risbud and R. R. Bhonde, "Polyacrylamide-Chitosan Hydrogels: In Vitro Biocompatibility and Sustained Antibiotic Release Studies," *Drug Delivery,* vol. 7, no. 2, pp. 69-75, 2000.

[140] R. K. Roeder, "Chapter 3. Mechanical Characterization of Biomaterials," in *Characterization of Biomaterials*, Notre Dame, Elsevier Science, 2013, pp. 56-83.

[141] G. A. Holzapfel, "a continuum approach for engineering," in *Nonlinear solid mechanics*, Chichester,UK, John Wiley and Sons Ltd, 2000.

[142] T. van Vliet, "Large deformation and fracture behaviour of gels," *Current Opinion in Colloid & Interface Science,* vol. 1, no. 6, pp. 740-745, 1996.

[143] T. van Vliet, H. Luyten and P. Walstra, "Fracture and Yielding of Gels," *Food Polymers, Gels and Colloids,* pp. 392-403, 1991.

[144] X. Wang and W. Hong, "Delayed fracture in gels," *Soft Matter,* vol. 8, no. 31, pp. 8171-8178, 2012.

[145] M. A. Haque, T. Kurokawa and J. P. Gong, "Anisotropic hydrogel based on bilayers: color, strength, toughness, and fatigue resistance," *Soft Matter,* vol. 8, no. 31, p. 8008, 2012.

[146] W. Hong, X. Zhao, J. Zhou and Z. Suo, "A theory of coupled diffusion and large deformation in polymeric gels," *Journal of the Mechanics and Physics of Solids,* vol. 56, no. 5, pp. 1779-1793, 2008.

[147] C. Huang, V. C. Mow and G. A. Ateshian, "The Role of Flow-Independent Viscoelasticity in the Biphasic Tensile and Compressive Responses of Articular Cartilage," *Journal of Biomechanical Engineering,* vol. 123, no. 5, pp. 410-417, 2001.

[148] Y. Hu and Z. Suo, "Viscoelasticity and poroelasticity in elastomeric gels," *Acta Mechanica Solida Sinica,* vol. 25, no. 5, pp. 441-458, 2012.

[149] M. A. Biot, "Theory of Deformation of a Porous Viscoelastic Anisotropic Solid," *Journal of Applied Physics,* vol. 27, no. 5, pp. 459-467, 1956.

[150] X. Wang and W. Hong, "A visco-poroelastic theory for polymeric gels," *Proceedings of the Royal Society A: Mathematical, Physical and Engineering Sciences,* vol. 468, no. 2148, pp. 3824-3841, 2012.

[151] Y. Mao, S. Lin, X. Zhao and L. Anand, "A large deformation viscoelastic model for double-network hydrogels," *Journal of the Mechanics and Physics of Solids,* vol. 100, pp. 103-130, 2017.

[152] ABAQUS, "ABAQUS User's Manual, Version 6.14," Providence, RI, 2014.

[153] M. Shibayama and K. Nagai, "Shrinking Kinetics of Poly(N-isopropylacrylamide) GelsT-Jumped across Their Volume Phase Transition Temperatures," *Macromolecules,* vol. 32, no. 22, pp. 7461-7468, 1999.

[154] H. Y. Liu and X. X. Zhu, "Lower critical solution temperatures of N -substituted acrylamide copolymers in aqueous solutions," *Polymer,* vol. 40, no. 25, pp. 6985-6990, 1999.

[155] E. C. Muniz and G. Geuskens, "Compressive Elastic Modulus of Polyacrylamide Hydrogels and Semi-IPNs with Poly(N-isopropylacrylamide)," *Macromolecules,* vol. 34, no. 34, pp. 4480-4484, 2001.

[156] X. Hu et al., "Dynamics of Dual Networks: Strain Rate and Temperature Effects in Hydrogels with Reversible H-Bonds," *Macromolecules,* vol. 50, no. 2, pp. 652-659, 2017.

[157] D. Lemmon, T. Shiang, A. Hashmi, J. Ulbrecht and P. Cavanagh, "The effect of insoles in therapeutic footwear—A finite element approach," *Journal of Biomechanics,* vol. 30, no. 6, pp. 615-620, 1997.

[158] S. Goske, A. Erdemir, M. Petre, S. Budhabhatti and P. Cavanagh, "Reduction of plantar heel pressures: Insole design using finite element analysis," *Journal of Biomechanics,* vol. 39, no. 13, pp. 2363-2370, 2006.

[159] Z. Taha, M. Norman, S. Omar and E. Suwarganda, "A Finite Element Analysis of a Human Foot Model to Simulate Neutral Standing on Ground.," *Procedia Engineering,* vol. 147, pp. 240-245, 2016.

[160] S. Maas, B. Ellis, G. Ateshian and J. Weiss, "FEBio: Finite Elements for Biomechanics," *Journal of Biomechanical Engineering,* vol. 134, no. 1, p. p.011005, 2012.

[161] A. P. G. Castro, J. Yao, T. Battisti and D. Lacroix, "Poroelastic Modeling of Highly Hydrated Collagen Hydrogels: Experimental Results vs. Numerical

Simulation With Custom and Commercial Finite Element Solvers," *Frontiers in Bioengineering and Biotechnology,* vol. 6, 2018.

[162] C. Briody, B. Duignan, S. Jerrams and J. Tiernan, "The implementation of a visco-hyperelastic numerical material model for simulating the behaviour of polymer foam materials," *Computational Materials Science,* vol. 64, pp. 47-51, 2012.

[163] R. W. Ogden, "Large Deformation Isotropic Elasticity: On the Correlation of Theory and Experiment for Compressible Rubberlike Solids," *Proceedings of the Royal Society A: Mathematical, Physical and Engineering Sciences,* vol. 328, no. 1575, pp. 567-583, 1972.

[164] A. E. Forte, F. D'Amico, M. N. Charalambides, D. Dini and J. G. Williams, "Modelling and experimental characterisation of the rate dependent fracture properties of gelatine gels," *Food Hydrocolloids,* vol. 46, pp. 180-190, 2015.

[165] C. W. J. Oomens, M. Vijven and W. M. Peters, "Skin Mechanics," in *Biomechanics of Living Organs: Hyperelastic Constitutive Laws for Finite Element Modeling,* Academic press, 2017, pp. 347-357.

[166] A. E. Bowden and J. Bergstrom, "Computer Modeling and Simulation of UHMWPE," in *UHMWPE Biomaterials Handbook (Third Edition),* Elsevier Science Publishing Co Inc, 2016, pp. 753-771.

[167] R. Udayanandana, P. Silva and T. Gunasekara, "Compression Fatigue and Stress Relaxation Properties of Single Network Polyacrylamide Hydrogels," in *2019 Moratuwa Engineering Research Conference (MERCon),* Colombo, 2019.

[168] Y. Nho et al, "Poly(acrylic acid)/polyethylene glycol hygrogel prepared by using gamma-ray irradiation for mucosa adhesion," *Journal of the Korean Physical Society,* vol. 66, no. 1, pp. 17-21, 2015.

[169] M. J. Mueller et al, "Effect of Achilles tendon lengthening on neuropathic plantar ulcers. A randomized clinical trial," *The Journal of Bone and Joint Surgery-American Volume,* vol. 85, no. 8, pp. 1436-1445, 2003.

[170] J. Foto and J. Birke, "Evaluation of Multidensity Orthotic Materials Used in Footwear for Patients with Diabetes," *Foot & Ankle International,* vol. 19, no. 12, pp. 836-841, 1998.

[171] J. Yang, C. Shao and L. Meng, "Strain Rate-Dependent Viscoelasticity and Fracture Mechanics of Cellulose Nanofibril Composite Hydrogels," *Langmuir,* vol. 35, no. 32, pp. 10542-10550, 2019.

[172] C. Gamonpilas, M. N. Charalambides and J. G. Williams, "Determination of large deformation and fracture behaviour of starch gels from conventional and wire cutting experiments," *Journal of Materials Science,* vol. 44, no. 18, pp. 4976-4986, 2009.

[173] J. Zhang, C. R. Daubert and E. A. Foegeding, "Characterization of polyacrylamide gels as an elastic model for food gels," *Rheologica Acta,* vol. 44, no. 6, pp. 622-630, 2005.

[174] H. J. Naghash and O. Okay, "Formation and structure of polyacrylamide gels," *Journal of Applied Polymer Science,* vol. 60, no. 7, pp. 971-979, 1996.

[175] T. van Vliet and P. Walstra, “Large deformation and fracture behaviour of gels,” *Faraday Discussions,* vol. 101, p. 359, 1995.

[176] T. Lu, J. Wang, R. Yang and T. Wang, “A Constitutive Model for Soft Materials Incorporatioting Viscoelasticity and Mullins Effect,” *Journal of Applied Mechanics,* vol. 84, no. 2, pp. 021010-1-9, 2016.

[177] I. D. Külcü, “Characterization of stress softening and self-healing in a double network hydrogel,” *Results in Physics,* vol. 12, pp. 1826-1833, 2019.

[178] J. Lei, S. Xu, Z. Li and Z. Liu, “Study on Large Deformation Behavior of Polyacrylamide Hydrogel Using Dissipative Particle Dynamics,” *Frontiers in Chemistry,* vol. 8, 2010.

[179] A. Erson et al., “Temperature Regulating Shoes for Prevention of Diabetic Foot Ulcers,” *Diabetes,* vol. 67, no. Supplement 1, pp. 41-LB, 2018.

[180] Y. Shimazaki and K. Aisaka, “Novel Thermal Analysis Model of the Foot-Shoe Sole Interface during Gait Motion,” *Proceedings,* vol. 2, no. 6, p. 278, 2018.

[181] N. Tang et al., “Thermal Transport in Soft PAAm Hydrogels,” *Polymers,* vol. 9, no. 12, p. 688, 2017.

[182] Silicones, Endeavour, “Silicone rubber for shoe insole,” [Online]. Available: https://www.eeclsilicone.com/silicone-rubber-for-shoe-insole.html.

[183] W. H. Organization, “Global report on diabetes,” WHO Press, France, 2016.

[184] Y. He, F. Yang, H. Zhao, Q. Gao, B. Xia and J. Fu, “Research on the printability of hydrogels in 3D bioprinting,” *Scientific Reports,* vol. 6, no. 1, 2016.

[185] M. Nakamura, A. Kobayashi, F. Takagi, A. Watanabe, Y. Hiruma, K. Ohuchi, Y. Iwasaki, M. Horie, I. Morita and S. Takatani, “Biocompatible inkjet printing technique for designed seeding of individual living cells,” *Tissue Eng,* vol. 11, no. 11-12, pp. 1658-1666, 2005.

[186] J. Barron, B. Spargo and B. Ringeisen, “Biological laser printing of three dimensional cellular structures,” *Applied Physics A,* vol. 79, no. 4-6, pp. 1027-1030, 2004.

[187] I. Ozbolat and M. Hospodiuk, “Current advances and future perspectives in extrusion-based bioprinting,” *Biomaterials,* vol. 76, pp. 321-343, 2016.

[188] F. Yang, V. Tadepalli and B. Wiley, “3D Printing of a Double Network Hydrogel with a Compression Strength and Elastic Modulus Greater than those of Cartilage,” *ACS Biomaterials Science & Engineering,* vol. 3, no. 5, pp. 863-869, 2017.

[189] J. Wei, J. Wang, S. Su, S. Wang, J. Qiu, Z. Zhang, G. Christopher, F. Ning and W. Cong, “3D printing of an extremely tough hydrogel,” *RSC Adv.,* vol. 5, no. 99, pp. 81324-81329, 2015.

[190] H. Zimmermann, S. Shirley and U. Zimmermann, “Alginate-based encapsulation of cells,” *Past, present, and future", Current Diabetes Reports,* vol. 7, no. 4, pp. 314-320, 2007.

[191] J. Visser, F. Melchels, J. Jeon, E. Bussel, L. Kimpton, H. Byrne, W. Dhert, P. Dalton, D. Hutmacher and J. Malda, “Reinforcement of hydrogels using three-

dimensionally printed microfibres," *Nature Communications,* vol. 6, p. 6933, 2015.

[192] Z. Koutkalaki, P. Papagiannis, P. Azariadis, P. Papanikos, S. Kyratzi, D. Zissis, D. Lekkas and E. Xidias, "Towards a Foot Bio-model for Performing Finite Element Analysis for Footwear Design Optimization using a Cloud Infrastructure.," *Computer-Aided Design and Applications,* 2015.

[193] Y. Hsu, Y. Gung, S. Shih, C. Feng, S. Wei, C. Yu and C. Chen, "Using an Optimization Approach to Design an Insole for Lowering Plantar Fascia Stress—A Finite Element Study.," *Annals of Biomedical Engineering,* vol. 36, no. 8, pp. 1345-1352, 2008.

[194] T. Spirka, A. Erdemir, S. Ewers Spaulding, A. Yamane, S. Telfer and P. Cavanagh, "Simple finite element models for use in the design of therapeutic footwear," *Journal ofBiomechanics,* vol. 47, p. 2948–2955, 2014.

[195] S. A. Bus, M. Maas, P. R. Cavanagh, R. P. J. Michels and M. Levi, "Plantar Fat-Pad Displacement in Neuropathic Diabetic Patients With Toe Deformity: A magnetic resonance imaging study," *Diabetes Care,* vol. 27, no. 10, pp. 2376-2381, 2004.

[196] O. Okay, "Macroporous copolymer networks," *Progress in Polymer Science,* vol. 25, no. 6, pp. 711-779, 2000.

[197] J. Paton, R. B. Jones, E. Stenhouse and G. Bruce, "The Physical Characteristics of Materials Used in the Manufacture of Orthoses for Patients with Diabetes," *Foot & Ankle International,* vol. 28, no. 10, pp. 1057-1063, 2007.

[198] R. Cornock, S. Beirne, B. Thompson and G. Wallace, "Coaxial additive manufacture of biomaterial composite scaffolds for tissue engineering," *Biofabrication,* vol. 6, no. 2, p. 025002, 2014.

[199] B. Dhariwala, E. Hunt and T. Boland, "Rapid Prototyping of Tissue-Engineering Constructs, Using Photopolymerizable Hydrogels and Stereolithography," *Tissue Engineering,* vol. 10, no. 9-10, pp. 1316-1322, 2004.

[200] B. Fischer, A. Schulz, M. Gepp, J. Neubauer, L. Gentile and H. Zimmermann, "3D printing of hydrogels in a temperature controlled environment with high spatial resolution," *Current Directions in Biomedical Engineering,* vol. 2, no. 1, p. 109–112, 2016.

[201] O. Silas et al, "Thermal stiffening of hydrophobic association hydrogels," *Polymer,* vol. 145, pp. 374-381, 2018.

Appendices

Appendix A: The specifications of Tactilus pressure insole

Table A.0.1: The specifications of Tactilus pressure insole

Sensor Specifications	**Value**
Type of Sensor	High-Performance V-Series Sensor
Technology	Resistive
Pressure Range	0 - 30 PSI (0 - 2.1 kg/cm^2)
Number of sensing points	16 x 8 (128 sensing points) per foot
Overall Sensor size	Shoe sizes 9 US (36 EU)
Sensing Point Size	0.62 in x 0.44 in (1.6 cm x 1.1 cm)
Scan speed	Up to 300 Hz
Sensor thickness	50 mils (1.27 mm)
Communication	USB/WiFi
Accuracy	± 10%
Repeatability	± 2%
Hysteresis	± 5%
Non-linearity	± 1.5%
Recording software	Tactilus 4.1